BIOCHEMICAL AND STRUCTURAL STUDIES OF UNC119 AND PrBP/δ: TWO LIPID-BINDING PROTEINS NECESSARY FOR PROTEIN TRANSPORT IN PHOTORECEPTOR CELLS

by

Ryan Nicholas Constantine

A dissertation submitted to the faculty of
The University of Utah
in partial fulfillment of the requirements for the degree of

Doctor of Philosophy

Interdepartmental Program in Neuroscience

The University of Utah

August 2012

Copyright © Ryan Nicholas Constantine 2012

All Rights Reserved

The University of Utah Graduate School

STATEMENT OF DISSERTATION APPROVAL

The dissertation of **Ryan Nicholas Constantine**

has been approved by the following supervisory committee members:

Wolfgang Baehr	, Chair	**05/02/2012** Date Approved
Christopher Peter Hill	, Member	**05/02/2012** Date Approved
Jun Yang	, Member	**05/02/2012** Date Approved
Mary Theresa Lucero	, Member	**05/02/2012** Date Approved
Robert Edward Marc	, Member	**05/02/2012** Date Approved

and by **Kristen Keefe** , Chair of

the Department of **Neuroscience**

and by Charles A. Wight, Dean of The Graduate School.

ABSTRACT

The mammalian photoreceptor is a dynamic polarized cell, in which protein transport and translocation are continuously taking place. The ability of these cells to accurately and efficiently localize protein components is essential for survival and proper functioning. Post-biosynthesis protein transport from IS to OS and translocation of transducin from OS to IS and back again, in response to light and dark, respectively, test the transport systems in these cells. Additionally, localization of membrane-associated proteins offers a challenge, as lipidated proteins must move freely within the hydrophilic intracellular environment until reaching a destination membrane. As a result, photoreceptors are an ideal model for studying intracellular membrane-associated protein trafficking.

Chapter 1 reviews photoreceptor structure and describes the need for accurate and efficient transport mechanisms in these cells. Eukaryotic prenylation and acylation are examined providing context for discussing the biosynthesis, transport, and light-induced translocation of transducin. Lastly, UNC119, which interacts with and is critical in mediating transducin's translocation, is reviewed.

Chapter 2 focuses on the biochemical and structural characterization of the UNC119-transducin-α interaction. The co-crystal structure of UNC119-Lauroyl-GAGASAEEKH at 2.0Å resolution offers definitive evidence for this interaction. Wild-type and *Unc119*$^{-/-}$ mouse models in conjunction with *C. elegans unc-119* mutants provide *in vivo* evidence that UNC119 is required for G protein trafficking in sensory

neurons. These data provide the first detailed description of a specific UNC119 function offering insight into the mechanism underlying transducin light-induced translocation.

Chapter 3 touches on the generation of an UNC119-Tα-GMP•PNP complex, but moves away from light-induced translocation and describes the role PrBP/δ plays in post-biosynthesis transport of PDE6. A general review of PrBP/δ and PDE6 offers a basic foundation for understanding how these two proteins interact and what role this interaction plays. While efforts focused on generating protein crystals of a PrBP/δ-PDE6 complex were unsuccessful, collaboration with Ted Wensel's group yielded a cryo-EM reconstruction of the complex and its features and implications are discussed.

Chapter 4 concludes this work with discussions of the aforementioned findings and future directions that might prove useful in further understanding the role UNC119 plays in G protein trafficking and how the PDE6-PrBP/δ complex assembles.

TABLE OF CONTENTS

ACKNOWLEDGEMENTS

Chapter 2 of this dissertation is coauthored by Houbin Zhang, Sergey Vorobiev, Yang Chen, Jayaraman Seetharaman, Yuanpeng Janet Huang, Rong Xiao, Gaetano Montelione, Cecilia Gerstner, Wayne Davis, George Innana, Frank Whitby, Erik Jorgensen, Chris Hill, Liang Tong, and Wolfgang Baehr and has been published in *Nature Neuroscience.* I would like to thank all of the authors for their contributions.

Chapter 3 describes a preliminary cryo-EM reconstruction of a PrBP/δ-PDE6 complex. Ted Wensel, Feng He, and Zhixian Zhi, collaborators from Baylor College of Medicine, have done the microscopy work described in this chapter and I would like to thank them for their efforts and willingness to work towards a common goal.

I cannot thank my advisor, Wolfgang Baehr enough for all that he has done for me during my time as a student in his lab. I am grateful that he was willing to accept me into his lab despite the fact that my scientific interests were outside of his area of expertise. His willingness to generate a collaboration with Chris Hill for my benefit is a great example of how he truly cares about training his students. Wolfgang provided an ideal laboratory environment allowing independence, yet always leaving his door open should questions or concerns arise. I hope that in the future I have the good fortune of working with individuals as talented, bright, and selfless as Wolfgang.

I also have to wholeheartedly thank Chris Hill for being willing to work with Wolfgang and myself to provide an environment in which I could work toward achieving my goals as a graduate student. Chris was instrumental in my training and success and I

am grateful for his willingness to provide me with space in his laboratory and access to his equipment, reagents, and expertise. I would also like to thank my remaining committee members, Jun Yang, Robert Marc, and Mary Lucero for their advice and support.

I would also like to thank the Moran Eye Center for supporting me during my training.

I am especially grateful for the excellent collaborative laboratory environments in both the Baehr and Hill labs. Thank you to everyone that willingly offered advice and guidance and engaged me in provocative scientific discussions. In the Baehr Lab I would like to thank Houbin Zhang for starting the UNC119 project and being willing to share it with me. His help was always useful and really benefitted our project. I also need to thank Cecilia Gerstner as she was always selfless and constantly offered her help with the most unpleasant of tasks. In the Hill lab I would especially like to thank Frank Whitby for all of his guidance in helping me to learn the challenging concepts and techniques in x-ray crystallography.

Lastly, I would like to thank my family members. My parents, Joseph and Sandra Constantine, and my brother Jason Constantine have always supported my endeavors, regardless of where they have brought me. My wife Kerri and son Nathan have provided me with a much-appreciated outlet of happiness and support throughout my training, especially when experiments in the lab were particulalry challenging. They have continually encouraged me, been patient with me, and enabled me to keep life in perspective. Thank you Kerri and Nathan, I love you both.

CHAPTER 1

INTRODUCTION AND BACKGROUND

Photoreceptor Architecture

Rod and cone photoreceptors of the mammalian retina are named for the cylindrical or conical shape of their outer segments (OS), respectively. The mouse retina contains approximately 6 million rods (Jeon *et al*., 1998) and 200,000 cones (3% of rods), while the human retina contains 110 million rods and 6.4 million cones (see webvision (http://webvision.med.utah.edu/, part XIII)). Photoreceptors are polarized cells consisting of a photosensitive primary (non-motile) cilium corresponding to the outer segment (OS), (**Fig. 1.1**), an inner segment (IS), a cell body containing the nucleus and a synaptic terminal. In mouse, each rod outer segment contains ~800 membranous discs arranged in a vertical stack (Nickell *et al*., 2007). Each disc houses roughly 25,000 molecules of rhodopsin, 2,500 molecules of transducin and 250 molecules of PDE6. Although the rod OS discs appear to float independently of the plasma membrane (PM), which surrounds them, filamentous connections between the discs and PM have been observed (Roof and Heuser, 1982; Koerschen *et al*., 1995). In contrast, cone outer segments are primarily formed by multiple invaginations of the plasma membrane, but also contain some enclosed discs that are disconnected from the plasma membrane. A major structural difference between mouse photoreceptor cells is outer segment volume: the rod OS is roughly 4X larger than the cone OS (Carter-Dawson and LaVail, 1979), calculated at 36 and 10 attoliters, respectively (Avasthi et al., 2009). The inner segments contain the metabolic machinery necessary for protein synthesis and processing, including the endoplasmic reticulum (ER), the Golgi apparatus and trans-Golgi network (TGN), and mitochondria. The inner and outer segments are connected by a cilium (CC) through which newly synthesized proteins must pass. Photoreceptor cell bodies have nuclei that

Figure 1.1 Electron micrograph of a mouse rod, partial view. The outer segment (OS) is connected to the inner segment (IS) by a cilium through which newly synthesized polypeptides must traffic. CC, connecting cilium; bb, basal body; mt, microtubules.

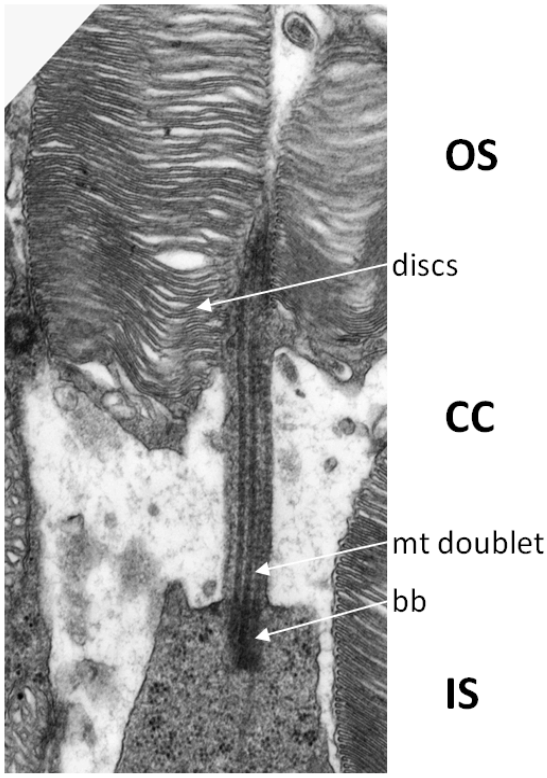
OS
discs
CC
mt doublet
bb
IS

make up the retinal outer nuclear layer (ONL). Information obtained via light reception is transmitted from the photoreceptor synaptic endings (spherules in rods, pedicles in cones) to second-order downstream neurons.

Photoreceptor Outer Segment Turnover

The pioneering work of Richard Young provided evidence that rod and cone outer segments are renewed approximately every ten days (Young, 1967; LaVail, 1976; Besharse and Hollyfield, 1979). Mechanisms that regulate disc membrane assembly at the proximal OS, concomitant disc shedding at the distal end of the OS, and phagocytosis of shed disc membranes by the adjacent retinal pigment epithelium (RPE) remain incompletely understood (Young and Bok, 1969; Anderson *et al*., 1978) (for review, see Nachury *et al*., 2010; Strauss, 2005). New discs are assembled at the base of the OS at a rate of 80 discs/day, which corresponds to ~ 1,000 rhodopsin molecules/min. Daily renewal of ~10% of the outer segment disk membranes requires both an extremely high rate of biosynthesis to replace OS proteins, as well as highly reliable transport and targeting pathways (Deretic *et al*., 2005; Sung and Tai, 2000; Deretic, 1998). Disc shedding at the apical end of the OS appears to be regulated by circadian processes (LaVail, 1980; LaVail and Ward, 1978), as rod discs are shed in the morning and cone outer segment discs at dusk (LaVail, 1980).

Phototransduction Component Lipidation

Protein prenylation. Protein prenylation is a common posttranslational modification in eukaryotic cells affecting up to 2% of all proteins expressed in mammalian cells, with this group of modified proteins having recently been referred to as

the “prenylome” (Nguyen *et al*., 2010). Prenyl side chains are synthesized in all living organisms via the mevalonate pathway and are attached to newly synthesized cytosolic proteins carrying a C-terminal CAAX box motif (C = cysteine, A = aliphatic amino acid, X = any amino acid) (Magee and Seabra, 2005; McTaggart, 2006). The C-terminal X determines the nature of the lipid chain in which leucine specifies geranylgeranylation (C20 chain) and all other residues result in farnesylation (C15 chain). The prenyl chain is attached to the cysteine of the CAAX via a thioether bond by cytosolic prenyl transferases (Zhang and Casey, 1996). Prenylated proteins dock to the endoplasmic reticulum (ER) and are further processed by the ER-associated enzymes (Gelb *et al*., 2006) ras converting enzyme 1 (RCE1) protease, which cleaves -AAX of the CAAX box and an isoprenyl cysteine carboxymethyl transferase (ICMT), which carboxymethylates the cysteine COOH (Winter-Vann and Casey, 2005) (**Fig. 1.2**). Both enzymes are essential for mouse development as deletion of either RCE1 or ICMT are embryonic lethal (Bergo *et al*., 2002; Bergo *et al*., 2001)**.**

Protein acylation. In addition to prenylation as described above, cellular proteins are commonly modified by the covalent attachment of long chain fatty acids that include, but are not limited to, palmitate (C16 chain) and myristoyl (C14 chain) groups. Despite differing by only two carbons, the biology of palmitate and myristoyl modifications are dissimilar. Palmitoylation is a posttranslational modification in which the fatty acid chain is reversibly (Resh, 1999) attached to either a cysteine, threonine, or serine residue on the protein via a thioester or ester bond (Olsen *et al*., 1985; Magee and Courtneidge, 1985; McIlhinney *et al*., 1985; Olsen and Spizz, 1986; Rose *et al*., 1984) (**Fig. 1.3**).

Figure 1.2 CAAX-Protein prenylation and processing (example: Gγ13). After prenylation in the cytosol, the protein docks at the ER and is processed by RCE1 protease that cleaves -AAX, and a S-adenosylmethionine-dependent methyltransferase (ICMT) that carboxymethylates cysteine.

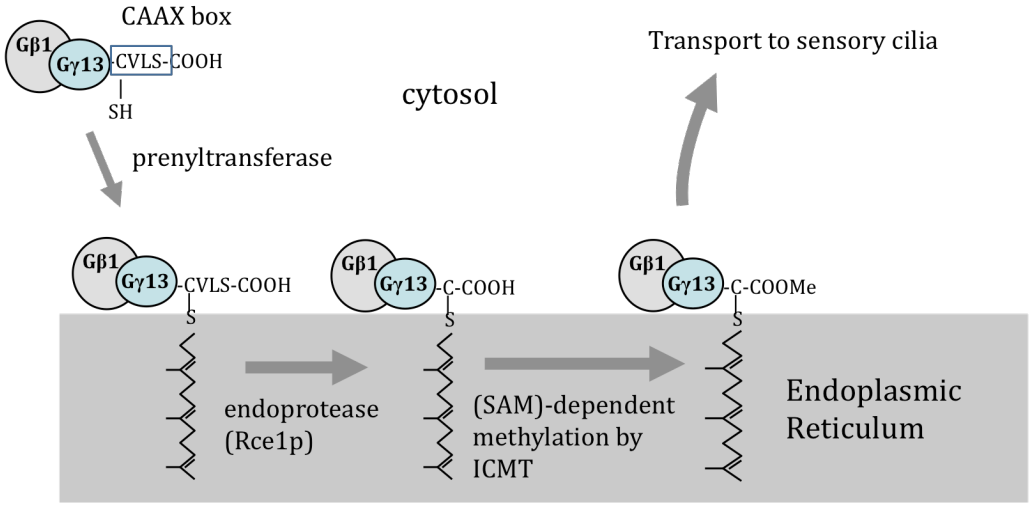
CAAX box
Gβ1
Gγ13
-CVLS-COOH
SH
cytosol
Transport to sensory cilia
prenyltransferase
Gβ1
Gγ13
-CVLS-COOH
S
endoprotease
(Rce1p)
Gβ1
Gγ13
-C-COOH
S
(SAM)-dependent
methylation by
ICMT
Gβ1
Gγ13
-C-COOMe
S
Endoplasmic
Reticulum

Figure 1.3 Palmitoylation (left panel) and myristoylation (right panel) linkages in eukaryotic proteins. **Left Panel**. Posttranslational fatty acid attachment (predominantly plamitate moieties) to cysteine, serine, or threonine via a thioester or ester bond. **Right Panel**. Co-translational attachment of myristoyl moieties on N-terminal glycine residues via amide bonds (Adapted from Towler and Gordon, 1988).

Palmitoylation

Thioester/Ester Bond

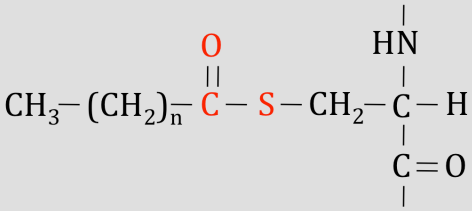

n = 12-16

N-myristoylation

Amide Bond

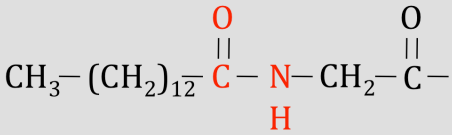

Myristoylation on the other hand is accomplished cotranslationally on amino terminal glycine residues by means of a non-reversible amide linkage (Olsen *et al*., 1985; Magee and Courtneidge, 1985; McIlhinney *et al*., 1985; Olsen and Spizz, 1986; Garber *et al*., 1985; Towler and Glaser, 1986) (**Fig. 1.3**). The temporal variation (co- vs. post-translational) of myristoyl and palmitoyl modifications coupled with residue preferences suggests that individual acyl moieties may indeed perform unique biological functions. The enzymes responsible for catalyzing myristoyl modifications and the resulting biological consequences are both most well understood and also most relevant to the work contained within and will thus be the focus of the remaining discussion of protein acylation. Myristoylated proteins exhibit diverse biological functions and can be found in a variety of cellular locales. However, N-myristoylation commonly mediates weak, reversible protein-protein or protein-membrane interactions (Farazi *et al*., 2001). The favorable properties of myristic acid relative to more abundant cellular fatty acids that led to its selection by the cell is not well understood. However, it has been postulated that its lower hydrophobicity relative to other longer fatty acid chains (stearic and palmitic acids) allows reversible membrane association (Franks and Lieb, 1986).

Myristoyl CoA:protein N-myristoyl transferase (NMT) is the enzyme responsible for myristoylation and due to the fact that this modification occurs cotranslationally, it has been proposed that NMT may exist as part of the ribosome complex (Olson and Spizz, 1986). However, more recent work using immunocytochemical characterization indicates that NMT is found predominantly in the cytosol, but can also be found attached to membranes and organelles (McIlhinney and McGlone, 1996). Characterization of NMT has been predominantly undertaken using yeast NMT and data shows that yeast

NMT is highly specific for myristoyl CoA (K_m ~ 0.4 uM) with significantly slower reaction velocities for acyl chains with shorter or longer lengths (Towler *et al*., 1987). Yeast NMT peptide substrate specificity has been studied extensively resulting in a series of criteria that can accurately be used to identify potential NMT substrates, which are described here: (a) glycine is absolutely required at position +1 (relative to the peptide initiator methionine); (b) position +2 prefers small uncharged residues and is intolerant of proline, charged residues, and aromatics; (c) all amino acids are permitted at positions +3 and +4; (d) serine is highly favored at position +5, but threonine, alanine, glycine, or cysteine are acceptable; (e) at position +6 all residues are acceptable except proline (Towler and Gordon, 1988; Farazi *et al*., 2001). The necessity of NMT is highlighted by the fact that a null *nmt1* allele in yeast results in recessive lethality and in *Drosophila melanogaster* is embryonic lethal (Duronio *et al*., 1989; Ntwasa *et al*., 2001). In immunocompromised human patients suffering from systemic fungal infections caused by either *Candida albicans* or *Cryptococcus neoformans*, a *NMT* null allele is lethal (Weinberg *et al*., 1995; Lodge *et al*., 1994).

Transducin Biosynthesis and Transport

The mechanisms underlying trafficking and ciliary targeting of heterotrimeric G proteins and G-protein coupled receptor (GPCR)-protein complexes in sensory neurons are largely unknown. Most details of this phenomenon derive from transfection of recombinant constructs in tissue culture (HEK293 cells, yeast) (for review, see Marrari *et al*., 2007). In the canonical model, Gα subunits carrying a myristoylation consensus sequence (Farazi *et al*., 2001) are acylated cotranslationally, and Gβ and Gγ subunits combine following biosynthesis and prenylation of Gγ. The field generally agrees that

Gαβγ heterotrimer formation is essential for targeting (Marrari *et al*., 2007), but it remains unclear as to how the complex traffics to the plasma membrane (PM). When $G\alpha_s$ and Gβγ were overexpressed in HEK cells, they targeted to the PM independent of the Golgi, most likely by diffusion. However, when a GPCR was co-expressed, PM targeting was Golgi-dependent, and both GPCR and G protein followed the classic secretory pathway (Dupre and Hebert, 2006). Therefore it appears that entire signaling complexes including GPCRs, G proteins, and target enzymes are assembled following biosynthesis and prior to PM targeting (Dupre *et al*., 2009; Dupre *et al*., 2007).

Transducin subunits are synthesized on free ribosomes in the inner segment cytosol (**Fig. 1.4**). Tα is acylated either cotranslationally or by an unidentified resident ER acyl transferase. Acylation of Tα is essential for membrane association and correct targeting to the outer segment, as recombinant Tα(G2A) remains cytoplasmic and does not target to the OS (Kerov *et al*., 2007). Tβ biosynthesis and folding require the chaperonin CCT and the co-chaperone PhLP1 (Lukov *et al*., 2005; Posokhova *et al*., 2011). Following release from CCT, Tβ combines with Tγ forming the obligate heterodimer Tβγ. Tγ is farnesylated in the cytosol by a soluble farnesyl transferase before or after heterodimer formation, which then docks to the ER for further processing (Marrari *et al*., 2007). Once at the ER, the prenylated C-terminus of Tγ (prenyl-CAAX) undergoes further processing, removing the three terminal amino acids (-AAX) and carboxymethylating the C-terminal cysteine to form prenyl-$COOCH_3$ (Hannoush and Sun, 2010) (**Fig. 1.2**). Genetic deletion of Tγ resulted in the degradation and mistargeting of Tα and Tβ, suggesting that heterotrimer formation is required for correct transducin

Figure 1.4 Transducin synthesis and processing. Tα is thought to be acylated cotranslationally, while Tγ is prenylated posttranslationally. Three transducin subunits combine at the ER to form a heterotrimeric G protein; CCT and PhLP are chaperones essential for correct folding of Tβ.

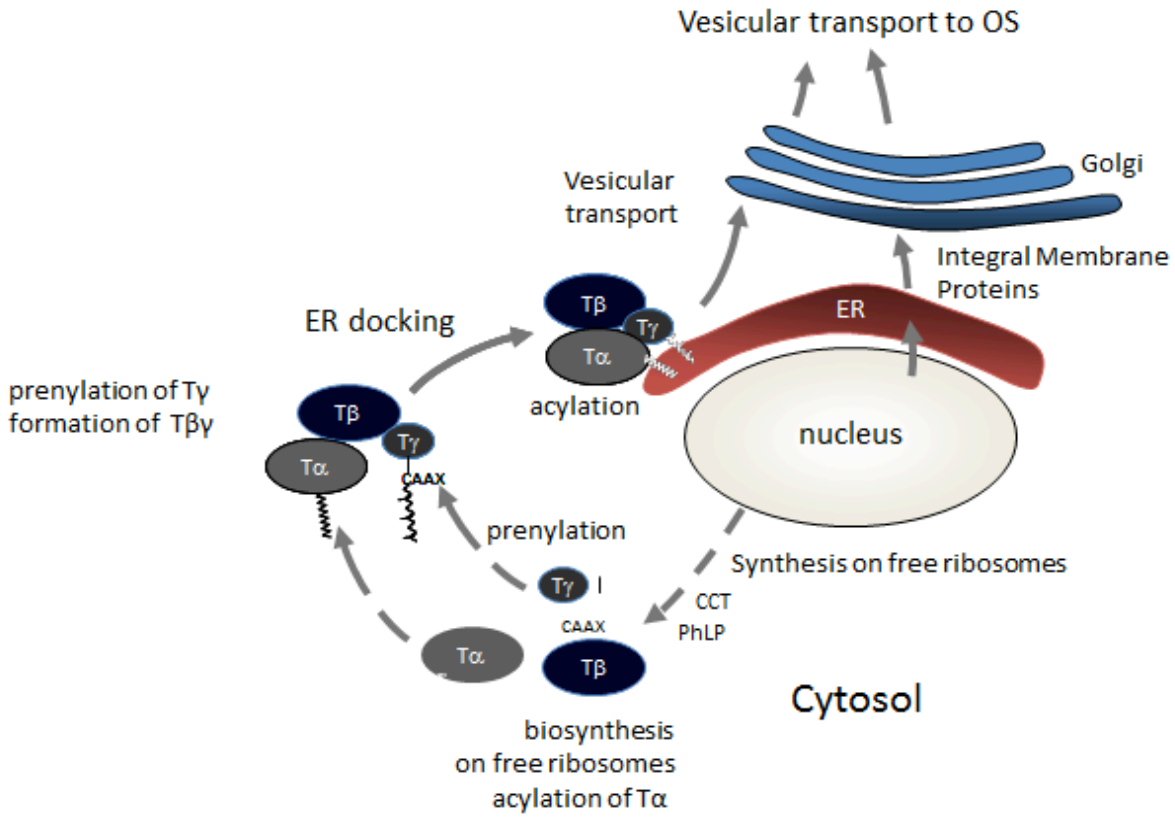
Vesicular transport to OS
Golgi
Vesicular transport
Integral Membrane Proteins
ER docking
Tβ
Tγ
Tα
ER
acylation
prenylation of Tγ
formation of Tβγ
nucleus
CAAX
prenylation
Synthesis on free ribosomes
CCT
PhLP
Cytosol
biosynthesis on free ribosomes
acylation of Tα

localization (Lobanova *et al*., 2008). It is presumed that membrane-associated transducin trafficks to the distal part of the inner segments by vesicular transport using molecular motors, most likely together with its GPCR, rhodopsin. However, trafficking of transducin subunits by diffusion to the outer segments has recently been proposed under specific conditions. Whether by active transport, passive diffusion or a combination of both, heterotrimeric transducin must be distributed efficiently as it is synthesized at a rate of approximately 200,000 heterotrimers/day/rod (80 discs are replaced daily, containing about 2,500* 80 molecules of transducin).

Light Induced Translocation

Light-activation of rhodopsin triggers GTP/GDP exchange on Tα causing $T\alpha^{GTP}$ and Tβγ to dissociate. Under persistent illumination, $T\alpha^{GTP}$ and Tβγ diffuse into the inner segment with a $t_{1/2}$ of 3-5 min for Tα and a $t_{1/2}$ of approximately 12 min for Tβγ (Calvert *et al*., 2006) (**Fig. 1.5**). Light-driven translocation results in approximately 80% of all transducin molecules moving from OS to IS (~1.6 million) in just minutes. The general consensus in the field remains that this enormous flux of molecules (1.5 million T / OS /10 min) can only occur by passive, three-dimensional diffusion. Upon arrival at the IS, $T\alpha^{GTP}$ hydrolyzes to $T\alpha^{GDP}$, which then recombines with Tβγ forming heterotrimeric $T\alpha^{GDP}\beta\gamma$ that associates with IS membranes. The precise membrane sink where the heterotrimer docks under persistent illumination is unknown, but likely candidates include the ER, Golgi and other intracellular membranes.

Upon resuming dark-adaptation, both Tα and Tβγ subunits return to the outer segments with a $t_{1/2}$ of ~2 hours. This relatively slow rate of return was suggested to

Figure 1.5 Schematic depicting the localization of Transducin in both dark and bright light conditions. In response to bright light, transducin translocates from the outer segment to the inner segment. The numbers to the left of the figure represent the percentages of transducin found in the outer segment in either dark or bright light conditions. OS, outer segment; IS, inner segment; N, nucleus; ST, synaptic terminal (Adapted from Calvert *et al*., 2006).

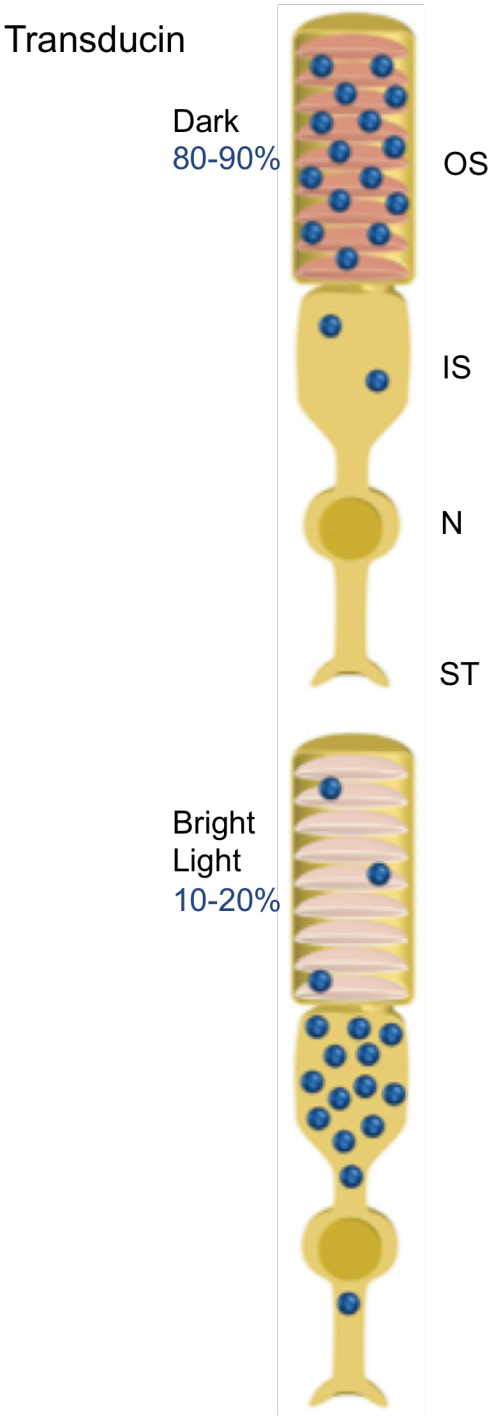
Transducin
Dark
80-90%
OS
IS
N
ST
Bright
Light
10-20%

occur by active transport using molecular motors (dynein). However, transducin has been shown to return to the outer segment in mouse eyecups depleted of ATP, without which molecular motors cannot function (Slepak and Hurley, 2008). For diffusion to occur, the heterotrimer would have to once again dissociate and then form soluble complexes with lipid-binding proteins enabling diffusion. Tβγ is known to associate with phosducin, which reduces its affinity for both Tα and rod OS membranes (Sokolov *et al*., 2004). Furthermore, it has been shown that the farnesyl group attached to Tγ may bind to PrBP/δ (PDE6δ), as Tβγ trafficking is impeded in Pde6δ$^{-/-}$ rods (Zhang *et al*., 2007). As a result, a significant problem remaining to be resolved was the mechanism underlying the discrepancies measured in the diffusion kinetics from OS to IS as compared to IS to OS, as a lipid-binding protein capable of solubilizing Tα had not yet been identified.

The PDE6D/UNC119 Supergene Family

Previous work in our lab identified PrBP/δ (for complete background see the Introduction in Chapter 3 of this thesis) as a prenyl binding protein essential for post-biosynthesis transport of prenylated components of the phototransduction cascade, specifically rhodopsin kinase (GRK1) and the α-sununit of cone phosphodiesterase (PDE6α') (Zhang *et al*., 2007). However, in a *PrBP/δ*$^{-/-}$ mouse model other prenylated proteins were transported appropriately following biosynthesis urging us to seek to identify another prenyl binding protein. UNC119 seemed to be a logical choice as *UNC119* and *PDE6D* constitute members of a new class of neural genes whose common function has been maintained through metazoan evolution. The mammalian *UNC119A/HRG4* gene encodes a widely expressed 27 kDa polypeptide (Higashide *et al*., 1996). By gene blasting, UNC119A homologs have been identified in all animals,

including unicellular protozoans such as *Paramecium* and *Tetrahymena*, unicellular parasites (*Trypanosome* and *Leishmania*), and plants (POC7 in *Chlamydomonas reinhardtii*). UNC119A has been identified in the basal body proteome of *C. reinhardtii* (Keller *et al*., 2009*)*, the flagellar rootlet of *Naegleria* (Chung *et al*., 2007), neurons of *C. elegans* (Maduro and Pilgrim, 1995) and in the mouse photoreceptor sensory cilium complex (Liu *et al*., 2007). In vertebrates, two UNC119 paralogs have been identified, most likely generated by gene duplication of an ancestral gene (**Fig. 1.6**). While background information about UNC119B will be provided for completeness, this work focuses primarily on UNC119A, which will be termed either UNC119 or UNC119A throughout.

UNC119A Discovery

UNC119A and UNC119B are comprised of 240 and 251 amino acids respectively, are ubiquitously expressed, and are closely related in sequence and gene structure (**Fig. 1.7**). The *unc-119* gene was initially discovered in *C. elegans* on the basis of a spontaneous mutation resulting in defects in chemosensation, locomotion, and feeding behavior (Maduro and Pilgrim, 1995). An *unc-119/LacZ* fusion construct was expressed predominantly in *C. elegans* neurons suggesting that the *unc-119* mutant phenotype is caused by a nervous system defect. Shortly thereafter, a human *UNC119A* ortholog termed Human Retina-specific Gene 4 (*HRG4*) was identified by subtractive cloning (Higashide *et al*., 1996). UNC119A/RG4 mRNA exhibited strong expression in retina with the protein localized to photoreceptor synapses (Higashide *et al*., 1998) and inner segments. The human *UNC119A* and *UNC119B* genes (**Fig. 1.7**) exhibit identical gene structures with each consisting of 5 exons (Higashide and Inana, 1999). *UNC119A*

Figure 1.6 Phylogram of PDE6D (PrBP/δ) and UNC119 paralogues. The four main branches are PDE6D, UNC119A, UNC119B, and the invertebrate Unc-119 branch. Only sequences from selected species are shown (from hundreds of genbank hits). PDE6D and UNC119 homologs are present throughout the animal kingdom, including unc-119 in plants (*Chlamydomonas reinhardtii*).

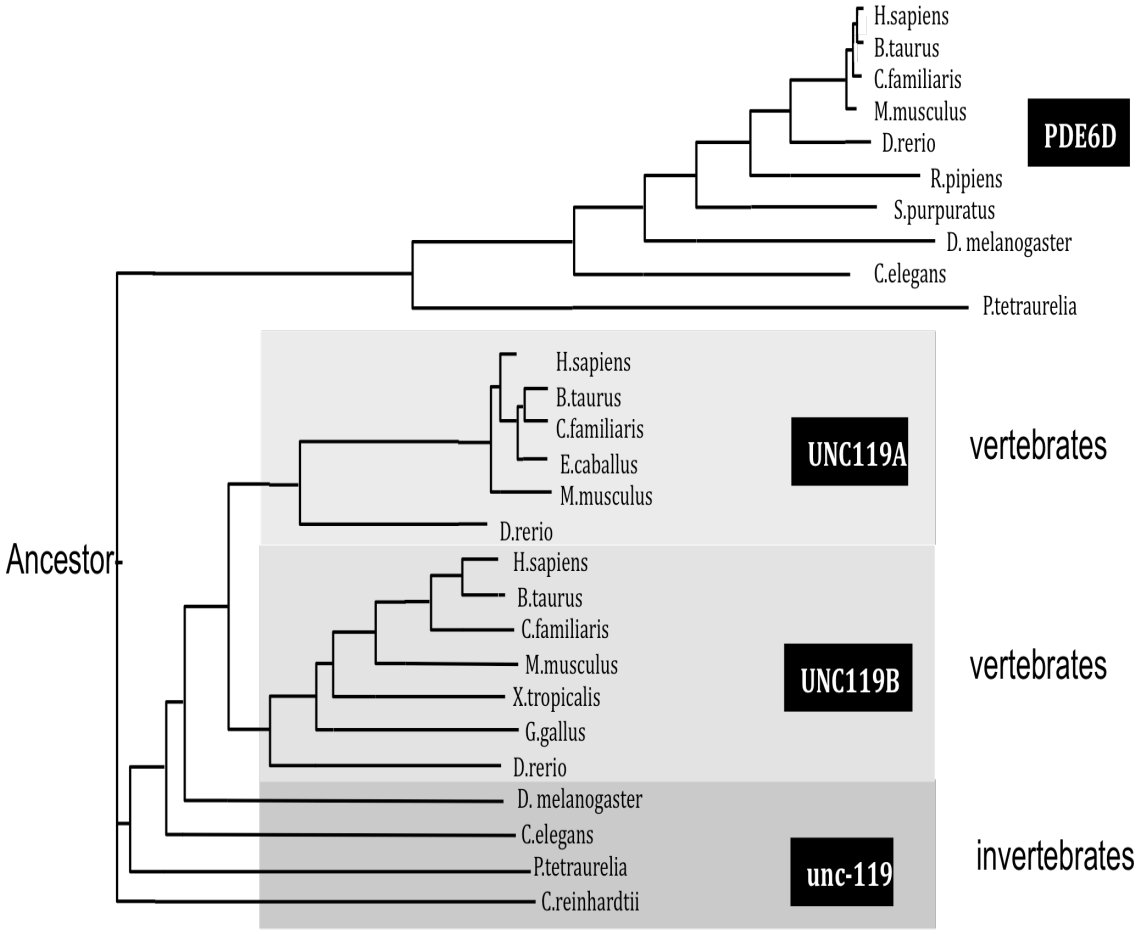
H.sapiens
B.taurus
C.familiaris
M.musculus
D.rerio
PDE6D
R.pipiens
S.purpuratus
D. melanogaster
C.elegans
P.tetraurelia
H.sapiens
B.taurus
C.familiaris
E.caballus
M.musculus
D.rerio
UNC119A
vertebrates
Ancestor
H.sapiens
B.taurus
C.familiaris
M.musculus
X.tropicalis
G.gallus
D.rerio
UNC119B
vertebrates
D. melanogaster
C.elegans
P.tetraurelia
C.reinhardtii
unc-119
invertebrates

Figure 1.7 UNC119 genes and proteins. **A**. Structure of UNC119 genes and gene products. Mutations associated with disease are noted in the UNC119 protein. Blue bars denote SH2- and SH3-interacting domains. **B**. Sequence alignment of UNC119 paralogs and PrBP/δ. Conserved residues are shown white on black background.

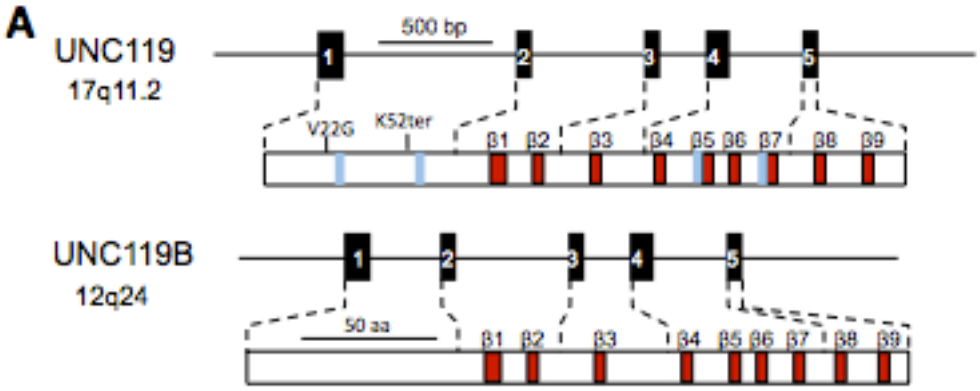

B

```
Unc119_hum      1 MKVKKGGGGAGTATESAPGPSGQSVAP----------IPQPPAESESGSE
unc119B_hum     1 ---MSGSNPKAAAAASAAGPGGLVAGKEEKKKAGGGVLNRLKARRQAPHH
Pde6d_hum       1 ----------------------------------------MSAKDE----

Unc119_hum     41 SEPD-AGPGPRPGPLQRKQPIGPEDVLGLQRITGDYLCSPEENIYKIDFV
unc119B_hum    48 AADDGVGAAVTEQELLALDTIRPEHVLRLSRVTENYLCKPEDNIYSIDFT
Pde6d_hum       7 ---------------------------------------RAREILRGFKLN

Unc119_hum     90 RFKIRDMDSGTVLFEIKKPPVSERLPINRR---DLDPNAGRFVRYQFTPA
unc119B_hum    98 RFKIRDLETGTVLFEIAKPCVSDQEEDEEEGGGDVDISAGRFVRYQFTPA
Pde6d_hum      19 WMNLRDAETGKLLWQGTEDLSVPGVEHEAR----------------VPKK

Unc119_hum    137 FLRLRQVGATVEFTVGDKPVNNFRMIERHYFRNQLLKSEDFHFGFCIPSS
unc119B_hum   148 FLRLRTVGATVEFTVGDKPVSNFRMIERHYFREHLLKNEDFDFGFCIPSS
Pde6d_hum      53 ILKCKAVSRELNFSS-TEQMEKFRLEQKVYFKGQCLEEWFFFGFEVIPNS

Unc119_hum    187 KNTCEHIYDFPPLSEELISEMIRHPYETQSDSFYFVDDRLVMEHNKADYSY
unc119B_hum   198 RNTCEHIYEFPQLSEDVIRLMIENPYETRSDSFYFVDNKLIMEHNKADYAY
Pde6d_hum     102 TNTWQSLIEAAGESQMKPASVLTG--NVIIETKFFDDDLLVSTSRVRLFY

Unc119_hum    237 SGTP
unc119B_hum   248 NGGQ
Pde6d_hum     150 V---
```

produces a splice variant in which the 3' most intron is retained, yielding a distinct C-terminal end (Swanson *et al*., 1998) lacking the β-sandwich structure. Both UNC119 paralogs exhibit significant sequence similarity with PrBP/δ (**Fig. 1.7**), particularly at the PrBP/δ C-terminal region, which in PrBP/δ forms a β-sandwich fold into which prenyl side chains can be inserted. A heterozygous stop codon in the *UNC119A* gene (K57ter) was linked to cone dystrophy in a single patient (Kobayashi *et al*., 2000a), a phenotype that was replicated in a transgenic mouse model expressing the murine *UNC119* gene with an identical stop codon (Kobayashi *et al*., 2000b). Furthermore, a G22V dominant negative mutation has been suggested to cause idiopathic CD4 lymphopenia (ICL), an immunodeficiency disorder associated with reduced T-cell stimulation (Gorska and Alam, 2012). The *UNC119B* gene was initially discovered by gene blasting and was first described in zebrafish (Manning *et al*., 2004).

UNC119A Interacting Proteins

Yeast two-hybrid screening and co-immunoprecipitation experiments have shown that UNC119A interacts with a large number of both related and unrelated polypeptides, including acylated G protein α-subunits, receptor-associated src-type tyrosine kinases, non-receptor protein kinases, small Arf-like GTPases (ARL proteins), the GTPase dynamin and the synaptic ribbon-associated protein RIBEYE (**Table 1.1**). Of the 17 known mammalian G-protein α-subunits, nine contain glycine as residue 2 (G2) and only seven of these contain a myristoylation consensus sequence. Both mouse rod and cone transducin (GNAT1 and GNAT2) α-subunits have been shown experimentally to interact with UNC119A. GNAT3 (gustducin, expressed in the gustatory system) is closely related in sequence and is therefore predicted to interact as well. ODR-3, a G protein present in

Table 1.1 UNC119 interacting partners. UNC119 interacts with acylated G protein α-subunits, src-type tyrosine kinases and the large GTPase dynamin, which are predicted to be myristoylated. In addition, UNC-119 interacts with a number of unrelated proteins such as small Arf-like GTPases, the Ca^{2+}-binding protein CaBP4, and RIBEYE. Column 1, interacting proteins; column 2, function (up and down arrows indicate activation or inhibition of enzyme activity); column 3, N-terminal sequence; column 5, pathways or cells; column 6, references.

UNC119A Interacting Partners

Molecule	Function	N-terminus	Pathway/Cells	Reference
Gnat1	Gα	MGAGASAE	Photoreceptor	(Zhang *et al*., 2011)
Gnat2	Gα	MGSGISAE	Photoreceptor	(Zhang *et al*., 2011)
ODR-3	Gα	MGSCQSNE	Olfaction	(Zhang *et al*., 2011)
GPA-13	Gα	MGCNFSSQ	Olfaction	(Zhang *et al*., 2011)
Dynamin	GTPase	MGNRGMEE	Endocytosis	(Gorska *et al*., 2006)
Lyn	srcTK↑	MGCIKSKR	Eosinophils	(Cen *et al*., 2003)
Hck	srcTK↑	MGGRSSC	Eosinophils	(Cen *et al*., 2003)
Lck	srcTK↑	MGCVSSN	T-cells	(Gorska *et al*., 2004)
Fyn	srcTK↑	MGCVQCKD	T-cells	(Gorska *et al*., 2004)
Abl	pTK↓	MGQQPGKV		(Vepachedu *et al*., 2009)
Arg	pTK↓	MGQQVGRV		(Vepachedu *et al*., 2009)
Rab11	GTPase	MGTRDDEY	Vesicular Transport	(Gorska *et al*., 2009)
Arl2	GDF	MGLLTILK	Vesicular Transport	(Kobayashi *et al*., 2003)
Arl3	GDF	MGLLSILR	Vesicular Transport	(Veltel *et al*., 2008b)
RP2	GAP	MGCCFFSK	Vesicular Transport	(Veltel *et al*., 2008a)
NPHP3		MGTASSLV	IMCD3 cilia	(Wright *et al*., 2011)
CYS1		MGSGSSR	IMCD3 cilia	(Wright *et al*., 2011)
C5orf30		MEVDINGD	IMCD3 cilia	(Wright *et al*., 2011)
CaBP4		MTTEQARQ	Synapse	(Haeseleer, 2008)
RIBEYE		MPVPSRHI	Synaptic Ribbon	(Alpadi *et al*., 2008)

C. elegans olfactory neurons has also been shown experimentally to interact directly with UNC119A (**Table 1.1**).

PrBP/δ and RhoGDI: Two Closely Related Prenyl Binding Proteins

The crystal structures of PrBP/δ and RhoGDI and with their cognate lipids inserted into the hydrophobic pocket have been determined at high resolution. Both exhibit β-sandwich folds in which a central cavity is capable of accommodating prenyl moieties (**Fig. 1.8A**). RhoGDIs are able to extract Rac, Rho and Cdc42 from cellular membranes and sequester them as a cytosolic complex, stabilizing the GDP-bound form and preventing GDP/GTP exchange (Garcia-Mata *et al*., 2011). One of the major differences between PrBP/δ and RhoGDI is that RhoGDI exhibits a strong functional preference for GDP-bound Rho GTPases, whereas PrBP/δ is able to solubilize both the GDP- and GTP-bound form of Ras, Rheb and Rap. PrBP/δ is considerably more promiscuous than RhoGDI and can interact with a variety of prenylated proteins expressed in photoreceptors. The loop connecting β-sheets β1 and β2 on PrBP/δ and RhoGDI is structurally very different despite the overall structural similarity of these proteins (**Fig. 1.8A**). This region is easily accessible in both structures and could therefore be involved in interacting with non-prenylated proteins. UNC119 shares a high degree of overall sequence similarity with Pr/BPδ, particularly in the C-terminal region, which folds into the β-sandwich structure responsible for lipid-binding (**Fig. 1.8B**).

G-protein Mistrafficking in *Unc119A*$^{-/-}$ Photoreceptors

The *Unc119a*$^{-/-}$ mouse shows no obvious retinal degeneration early in life (up to 6 months postnatally) (Ishiba *et al*., 2007), but accelerates by 17 months, and was complete

Figure 1.8 Comparison of RhoGDI and PrBP/δ structures and sequences. **A**. Structures of RhoGDI and PrBP/δ with lipid ligands inserted into the hydrophobic binding pocket. **B**. Sequence alignment of Human UNC119A, PrBP/δ, and RhoGDI. Only C-terminal residues of UNC119A (60-240) and RhoGDI (41-204) are shown. β-strands are depicted as large dark arrows for UNC119A. Identical residues are blue-shaded and similar residues gray-shaded.

A

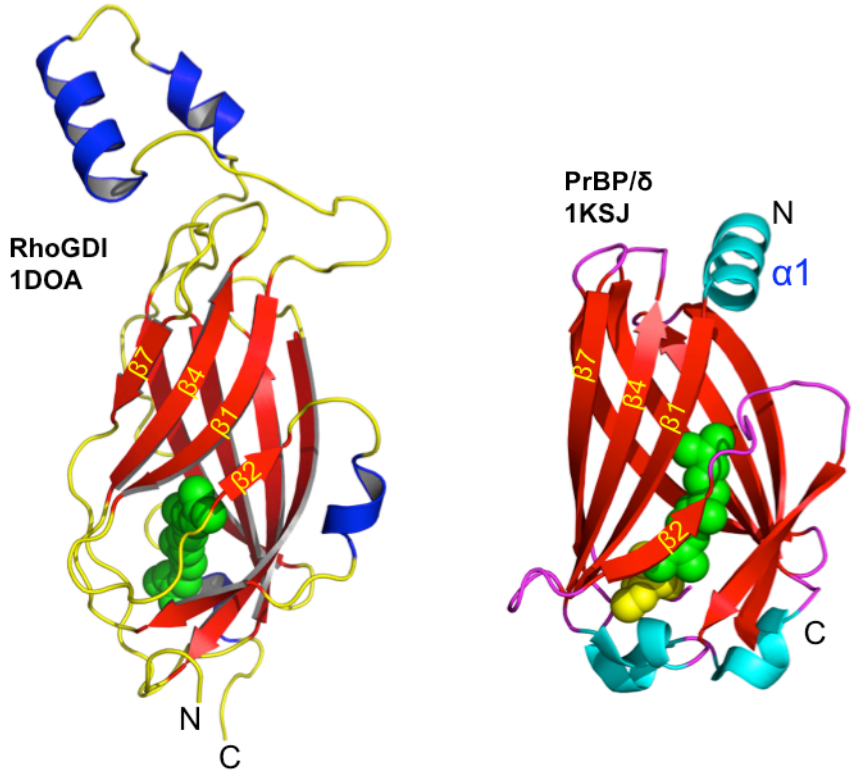
RhoGDI
1DOA
β7
β4
β1
β2
N
C
PrBP/δ
1KSJ
N
α1
β7
β4
β1
β2
C

B

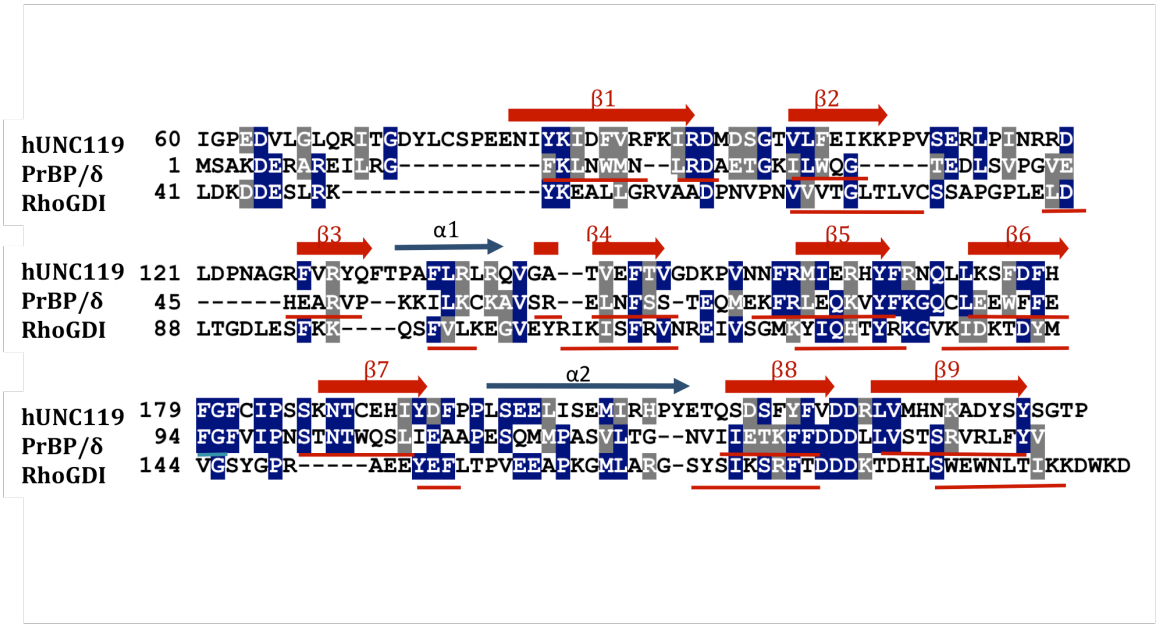
β1
β2
hUNC119 60 IGPEDVLGLQRITGDYLCSPEENIYKIDFVRFKIRDMDSGTVLFEIKKPPVSERLPINRRD
PrBP/δ 1 MSAKDERAREILRG----------FKLNWMN--LRDAETGKILWQG-----TEDLSVPGVE
RhoGDI 41 LDKDDESLRK----------YKEALLGRVAADPNVPNVVVTGLTLVCSSAPGPLELD
β3
α1
β4
β5
β6
hUNC119 121 LDPNAGRFVRYQFTPAFLRLRQVGA--TVEFTVGDKPVNNFRMIERHYFRNQLLKSFDFH
PrBP/δ 45 ------HEARVP--KKILKCKAVSR--ELNFSS-TEQMEKFRLEQKVYFKGQCLEEWFFE
RhoGDI 88 LTGDLESFKK----QSFVLKEGVEYRIKISERVNREIVSGMKYIQHTYRKGVKIDKTDYM
β7
α2
β8
β9
hUNC119 179 FGFCIPSSKNTCEHIYDFPPLSEELISEMIRHPYETQSDSFYFVDDRLVMHNKADYSYSGTP
PrBP/δ 94 FGFVIPNSTNTWQSLIEAAPESQMMPASVLTG--NVIIETKFFDDDLLVSTSRVRLFYV
RhoGDI 144 VGSYGPR-----AEEYEFLTPVEEAPKGMLARG-SYSIKSRFTDDDKTDHLSWEWNLTIKKDWKD

at 20 months. The slow progression of retinal degeneration may in part be attributable to the presence of UNC119B in photoreceptors, which may function in a redundant fashion. The detection of UNC119A in the mouse photoreceptor sensory cilium complex (Liu *et al*., 2007) suggests a possible role for UNC119A in cargo assembly, an argument that is further strengthened by the association of UNC119A with ARL3 and RP2 (retinitis pigmentosa protein 2), two proteins that localize to mouse and human cilia (Liu *et al*., 2007; Veltel *et al*., 2008a).

UNC119A in Zebrafish and *Drosophila*

The *Drosophila* nervous system expresses an UNC119A homolog termed DmUNC119A (Maduro *et al*., 2000). Expression of truncated DmUNC119A or human UNC119A (which maintains the conserved C-terminal region), under control of the unc-119 promoter was able to completely rescue the *C. elegans* unc-119 mutant phenotype (Maduro *et al*., 2000). The conserved C-terminus of UNC119A was shown to be required to rescue the mutant phenotype, but the N-terminus was determined to be dispensable. In zebrafish, an UNC119A homolog is required for normal development of the nervous system (Manning *et al*., 2004). Numerous neuronal defects, including absent or erroneously localized cell bodies, unbundled fascicles, errant axon pathways, and irregular axonal branching or unnecessary branching of motor neuron commissures result from morpholino oligonucleotide (MO)-mediated knockdown of the UNC119A protein (Manning *et al*., 2004). These "curly tail down" zebrafish exhibit a set of neuronal defects similar to those seen in *C. elegans* unc-119 mutants, any of which can be suppressed by expressing Unc-119 after embryonic development, demonstrating that

UNC-119 is required for the maintenance of the nervous system architecture (Knobel *et al*., 2001).

Summary and Goals

Photoreceptor survival and correct and accurate transmission of light-derived signals is highly dependent upon appropriate localization of the protein components that are required to satisfy these processes. Rod and cone cells are exquisitely dynamic and provide excellent models in which to study protein transport. In response to light, up to 80% of all transducin molecules translocate from the outer segment to the inner segment within minutes. Upon returning to the dark, transducin molecules must then efficiently make their way back to the outer segment in order to be correctly localized for the next light response. Likewise, massive protein movement takes place following protein biosynthesis in order to transport phototransduction components from the inner segment to the outer segment, a process that must take place continuously due to the rapid and constant turnover of outer segment discs. However, the transport of highly lipidated proteins throughout photoreceptor cells offers an additional challenge for these cells.

The main focus of this body of work was to first identify interacting partners of UNC119, characterize the interaction, and then determine the function of UNC119 in photoreceptor cells. The interaction of UNC119 with myristoylated Tα suggests that UNC119 functions as a chaperone involved in either the light-induced translocation of Tα or in post-biosynthesis transport. Gaining a full understanding of this interaction and identifying the function of UNC119 in photoreceptor cells will be addressed using a variety of experimental techniques. Characterizing the interaction between UNC119 and Tα will be accomplished through a series of pulldown experiments, isothermal titration

calorimetry, and most definitively by solving the co-crystal structure of UNC119 with a Tα-mimicking peptide. Furthermore, *Unc119* deletion in a mouse model and characterization of *C. elegans unc-119* mutants will help to elucidate the function of UNC119 in photoreceptors.

As an additional objective, which is the focus of Chapter 3 we aimed to further characterize the interaction between PrBP/δ and PDE6 at the molecular level by co-crystallizing and solving the structure of this protein complex. At present, we have successfully purified a PDE6-PrBP/δ complex, but have been unable to grow protein crystals. In collaboration with Ted Wensel's group at Baylor College of Medicine, we have used this purified complex to generate a preliminary cryo EM reconstruction that we hope will offer further insight into how both PrBP/δ and PDE6 function in photoreceptor cells.

References

Alpadi, K., Magupalli, V. G., Kappel, S., Koblitz, L., Schwarz, K., Seigel, G. M., Sung, C. H., and Schmitz, F. (2008). RIBEYE recruits Munc119, a mammalian ortholog of the Caenorhabditis elegans protein unc119, to synaptic ribbons of photoreceptor synapses. *J Biol. Chem.* 283:26461-26467.

Anderson, D. H., Fisher, S. K., Steinberg, R. H. (1978). Mammalian cones: disc shedding, phagocytosis, and renewal. *Invest Ophthalmol Vis Sci* 17:117-133.

Avasthi, P., Watt, C. B., Williams, D. S., Le, Y. Z., Li S., Chen, C. K., Marc, R. E., Frederick, J. M., Baehr, W. (2009). Trafficking of membrane proteins to cone but not rod outer segments is dependent on heterotrimeric kinesin-II. J Neurosci 29:14287-14298.

Bergo, M. O., Ambroziak, P., Gregory, C., George, A., Otto, J. C., Kim, E., Nagase, H., Casey, P. J., Balmain, A., Young, S. G. (2002). Absence of the CAAX endoprotease Rce1: effects on cell growth and transformation. *Mol Cell Biol* 22:171-181.

Bergo, M. O., Leung, G. K., Ambroziak, P., Otto, J. C., Casey, P. J., Gomes, A. Q., Seabra, M. C., Young, S. G. (2001). Isoprenylcysteine carboxyl methyltransferase deficiency in mice. *J Biol Chem* 276:5841-5845.

Besharse, J. C., Hollyfield, J. G. (1979). Turnover of mouse photoreceptor outer segments in constant light and darkness. *Invest Ophthalmol Vis Sci* 18:1019-1024.

Calvert, P. D., Strissel, K. J., Schiesser, W. E., Pugh, E. N., Jr., Arshavsky, V. Y. (2006). Light-driven translocation of signaling proteins in vertebrate photoreceptors. *Trends Cell Biol* 16:560-568.

Carter-Dawson, L. D., LaVail, M. M. (1979). Rods and cones in the mouse retina. I. Structural analysis using light and electron microscopy. *J Comp Neurol* 188:245-262.

Cen, O., Gorska, M. M., Stafford, S. J., Sur, S., and Alam, R. (2003). Identification of UNC119 as a novel activator of SRC-type tyrosine kinases. *J. Biol. Chem.* 278:8837-8845.

Chung, S., Kang, S., Paik, S., and Lee, J. (2007). NgUNC-119, Naegleria homologue of UNC-119, localizes to the flagellar rootlet. *Gene* 389:45-51.

Deretic, D., Williams, A. H., Ransom, N., Morel, V., Hargrave, P. A., Arendt, A. (2005). Rhodopsin C terminus, the site of mutations causing retinal disease, regulates trafficking by binding to ADP-ribosylation factor 4 (ARF4). *Proc Natl Acad Sci USA* 102:3301-3306.

Deretic, D. (1998). Post-Golgi trafficking of rhodopsin in retinal photoreceptors. *Eye 12* (Pt 3b):526-530.

Dupre, D. J., Hebert, T. E. (2006). Biosynthesis and trafficking of seven transmembrane receptor signalling complexes. *Cell Signal* 18:1549-1559.

Dupre, D. J., Robitaille, M., Rebois, R. V., Hebert, T. E. (2009). The role of Gbetagamma subunits in the organization, assembly, and function of GPCR signaling complexes. *Annu Rev Pharmacol Toxicol* 49:31-56.

Dupre, D. J., Baragli, A., Rebois, R. V., Ethier, N., Hebert, T. E. (2007). Signalling complexes associated with adenylyl cyclase II are assembled during their biosynthesis. *Cell Signal* 19:481-489.

Duronio, R. J., Towler, D. A., Heuckeroth, R. O., Gordon, J. I. (1989). Disruption of the yeast N-myristoyl transferase gene causes recessive lethality. *Science* 243:796-800.

Farazi, T. A., Waksman, G., Gordon, J. I. (2001). The biology and enzymology of protein N-myristoylation. *J Biol Chem* 276:39501-39504.

Franks, N. P., Lieb, W. R. (1986). Partitioning of long-chain alcohols into lipid bilayers: implications for mechanisms of general anesthesia. *Proc. Natl. Acad. Sci. USA* 83:5116-20.

Garber, E. A., Cross, F. R., Hanafusa, H. (1985). Processing of p60v-src to its myristylated membrane-bound form. *Mol. Cell. Biol.* 5:2781-88.

Garcia-Mata, R., Boulter, E., and Burridge, K. (2011). The 'invisible hand': regulation of RHO GTPases by RHOGDIs. *Nat. Rev. Mol. Cell Biol.* 12:493-504.

Gelb, M. H., Brunsveld, L., Hrycyna, C. A., Michaelis, S., Tamanoi, F., Van Voorhis, W. C., Waldmann, H. (2006). Therapeutic intervention based on protein prenylation and associated modifications. *Nat Chem Biol* 2:518-528.

Gorska, M. M. and Alam, R. (2012). A mutation in the human Uncoordinated 119 gene impairs TCR signaling and is associated with CD4 lymphopenia. *Blood* 6:1399-406.

Gorska, M. M., Cen, O., Liang, Q., Stafford, S. J., and Alam, R. (2006). Differential regulation of interleukin 5-stimulated signaling pathways by dynamin. *J Biol. Chem.* 281:14429-14439.

Gorska, M. M., Stafford, S. J., Cen, O., Sur, S., and Alam, R. (2004). Unc119, a novel activator of Lck/Fyn, is essential for T cell activation. *J Exp. Med.* 199:369-379.

Gorska, M. M., Liang, Q., Karim, Z., and Alam, R. (2009). Uncoordinated 119 protein controls trafficking of Lck via the Rab11 endosome and is critical for immunological synapse formation. *J. Immunol.* 183:1675-1684.

Haeseleer, F. (2008). Interaction and Colocalization of CaBP4 and Unc119 (MRG4) in Photoreceptors. *Invest Ophthalmol. Vis. Sci* 49:2366-2375.

Hannoush, R. N., Sun, J. (2010). The chemical toolbox for monitoring protein fatty acylation and prenylation. *Nat Chem Biol* 6:498-506.

Higashide, T., Murakami, A., McLaren, M. J., and Inana, G. (1996). Cloning of the cDNA for a novel photoreceptor protein. *J. Biol. Chem.* 271:1797-1804.

Higashide, T., McLaren, M. J., and Inana, G. (1998). Localization of HRG4, a photoreceptor protein homologous to Unc-119, in ribbon synapse. *Invest Ophthalmol. Vis. Sci* 39:690-698.

Higashide, T. and Inana, G. (1999). Characterization of the gene for HRG4 (UNC119), a novel photoreceptor synaptic protein homologous to unc-119. *Genomics* 57:446-450.

Ishiba, Y., Higashide, T., Mori, N., Kobayashi, A., Kubota, S., McLaren, M. J., Satoh, H., Wong, F., and Inana, G. (2007). Targeted inactivation of synaptic HRG4 (UNC119) causes dysfunction in the distal photoreceptor and slow retinal degeneration, revealing a new function. *Exp Eye Research* 84:473-485.

Jeon, C. J., Strettoi. E., Masland, R. H. (1998). The major cell populations of the mouse retina. *J Neurosci* 18:8936-8946.

Keller, L. C., Geimer, S., Romijn, E., Yates, J., III, Zamora, I., and Marshall, W. F. (2009). Molecular architecture of the centriole proteome: the conserved WD40 domain protein POC1 is required for centriole duplication and length control. *Mol. Biol. Cell* 20:1150-1166.

Kerov, V., Rubin, W. W., Natochin, M., Melling, N. A., Burns, M. E., Artemyev, N. O. (2007). N-terminal fatty acylation of transducin profoundly influences its localization and the kinetics of photoresponse in rods. *J Neurosci* 27:10270-10277.

Knobel, K. M., Davis, W. S., Jorgensen, E. M., and Bastiani, M. J. (2001). UNC-119 suppresses axon branching in C. elegans. *Development* 128:4079-4092.

Kobayashi, A., Higashide, T., Hamasaki, D., Kubota, S., Sakuma, H., An, W., Fujimaki, T., McLaren, M. J., Weleber, R. G., and Inana, G. (2000). HRG4 (UNC119) mutation found in cone-rod dystrophy causes retinal degeneration in a transgenic model. *Invest Ophthalmol. Vis. Sci* 41:3268-3277.

Kobayashi, A., Kubota, S., Mori, N., McLaren, M. J., and Inana, G. (2003). Photoreceptor synaptic protein HRG4 (UNC119) interacts with ARL2 via a putative conserved domain. *FEBS Lett.* 534:26-32.

Koerschen, H. G., Illing, M., Seifert, R., Sesti, F., Williams, A., Gotzes, S., Colville, C., Mueller, F., Dose, A., Godde, M., Molday, L., Kaupp, U. B., Molday, R. S. (1995). A 240 kDa protein represents the complete beta subunit of the cyclic nucleotide-gated channel from rod photoreceptor. pp 627-636.

LaVail, M. M. (1976). Rod outer segment disk shedding in rat retina: relationship to cyclic lighting. *Science* 194:1071-1074.

LaVail, M. M. (1980). Circadian nature of rod outer segment disc shedding in the rat. *Invest Ophthalmol Vis* Sci 19:407-411.

LaVail, M. M., Ward, P. A. (1978). Studies on the hormonal control of circadian outer segment disc shedding in the rat retina. *Invest Ophthalmol Vis Sci* 17:1189-3.

Liu, Q., Tan, G., Levenkova, N., Li, T., Pugh, E. N., Jr., Rux, J. J., Speicher, D. W., and Pierce, E. A. (2007). The proteome of the mouse photoreceptor sensory cilium complex. *Mol. Cell Proteomics.* 6:1299-1317.

Lobanova, E. S., Finkelstein, S., Herrmann, R., Chen, Y. M., Kessler, C., Michaud, N. A., Trieu, L. H., Strissel, K. J., Burns, M. E., Arshavsky, V. Y. (2008). Transducin gamma-subunit sets expression levels of alpha- and beta-subunits and is crucial for rod viability. *J Neurosci* 28:3510-3520.

Lodge, J. K., Jackson-Machelski, E., Toffaletti, D. L., Perfect, J. R., Gordon, J. I. (1994). Targeted gene replacement demonstrates that myristoyl-CoA: protein N-myristoyltransferase is essential for viability of Cryptococcus neoformans. *Proc. Natl. Acad. Sci. USA* 91:12008-12012.

Lukov, G. L., Hu, T., McLaughlin, J. N., Hamm, H. E., Willardson, B. M. (2005). Phosducin-like protein acts as a molecular chaperone for G protein betagamma dimer assembly. *EMBO J* 24:1965-1975.

Maduro, M. and Pilgrim, D. (1995). Identification and cloning of unc-119, a gene expressed in the Caenorhabditis elegans nervous system. *Genetics* 141:977-988.

Maduro, M. F., Gordon, M., Jacobs, R., and Pilgrim, D. B. (2000). The UNC-119 family of neural proteins is functionally conserved between humans, Drosophila and C. elegans. *J. Neurogenet.* 13:191-212.

Magee, A. I., Courtneidge, S. A., (1985). Two classes of fatty acid acylated proteins exist in eukaryotic cells. *EMBO J*. 4:1137-44.

Magee, T., Seabra, M. C. (2005). Fatty acylation and prenylation of proteins: what's hot in fat. *Curr. Opin. Cell Biol.* 17:190-196

Manning, A. G., Crawford, B. D., Waskiewicz, A. J., and Pilgrim, D. B. (2004). unc-119 homolog required for normal development of the zebrafish nervous system. *Genesis.* 40:223-230.

Marrari, Y., Crouthamel, M., Irannejad, R., Wedegaertner, P. B. (2007). Assembly and trafficking of heterotrimeric G proteins. *Biochemistry* 46:7665-7677.

McIlhinney, R. A., McGlone, K. (1996). Immunocytochemical characterization and subcellular localization of human myristoyl-CoA: protein N-myristoyltransferase in HeLa cells. *Exp. Cell Res.* 223(2):348-56.

McIlhinney, R. A., Pelly, S. J., Chadwick, J. K., Cowley, G. P. (1985). Studies on the attachment of myristic and palmitic acid to cell proteins in human squamous carcinoma cell lines: evidence for two pathways. *EMBO J*. 4:1145-52.

McTaggart, S. J. (2006). Isoprenylated proteins. *Cell Mol. Life Sci* 63, 255-267

Nachury, M. V., Seeley, E. S., Jin, H. (2010). Trafficking to the ciliary membrane: how to get across the periciliary diffusion barrier? *Annu Rev Cell Dev Biol* 26:59-87.

Nguyen, U. T., Wu, Y., Goodall, A., and Alexandrov, K. (2010). Analysis of protein prenylation in vitro and in vivo using functionalized phosphoisoprenoids. *Curr. Protoc. Protein Sci.* Chapter 14:Unit14.

Nickell, S., Park, P. S., Baumeister, W., Palczewski, K. (2007). Three-dimensional architecture of murine rod outer segments determined by cryoelectron tomography. *J Cell Biol* 177:917-925.

Ntwasa, M., Aapies, S., Schiffman, D. A., Gay, N. J. (2001). Drosophila embryos lacking N-myristoyltransferase have multiple developmental defects. *Exp. Cell Res.* 262:134-144.

Olsen, E. N., Spizz, G. (1986). Fatty acylation of cellular proteins. Temporal and subcellular differences between palmitate and myristate acylation. *J. Biol. Chem*. 261:2458-66.

Olson, E. N., Towler, D. A., Glaser, L. (1985). Specificity of fatty acid acylation of cellular proteins. *J. Biol. Chem*. 260:3784-90.

Posokhova, E., Song, H., Belcastro, M., Higgins, L., Bigley, L. R., Michaud, N.A., Martemyanov, K. A., Sokolov, M. (2011). Disruption of the chaperonin containing TCP-1 function affects protein networks essential for rod outer segment morphogenesis and survival. *Mol Cell Proteomics* 10:M110.

Resh, M. D. (1999). Fatty acylation of proteins: new insights into membrane targeting of myristoylated and palmitoylated proteins. *Biochim. Biophys. Acta* 1451, 1-16.

Roof, D. J., Heuser, J. E. (1982). Surfaces of rod photoreceptor disk membranes: integral membrane components. *J Cell Biol* 95:487-500.

Rose, J. K., Adams G. A., Gallione, C. J. (1984). The presence of cysteine in the cytoplasmic domain of the vesicular stomatitis virus glycoprotein is required for palmitate addition. *Proc. Natl. Acad. Sci. USA* 81:2050-54.

Slepak, V. Z., Hurley, J. B. (2008). Mechanism of light-induced translocation of arrestin and transducin in photoreceptors: interaction-restricted diffusion. *IUBMB Life* 60:2-9.

Sokolov, M., Strissel, K. J., Leskov, I. B., Michaud, N. A., Govardovskii, V. I., Arshavsky, V. Y. (2004). Phosducin facilitates light-driven transducin translocation in rod photoreceptors. Evidence from the phosducin knockout mouse. *J Biol Chem* 279:19149-19156.

Strauss, O. (2005). The retinal pigment epithelium in visual function. *Physiol Rev* 85:845-881.

Sung, C. H., Tai, A. W. (2000). Rhodopsin trafficking and its role in retinal dystrophies. *Int Rev Cytol* 195:215-267.

Swanson, D. A., Chang, J. T., Campochiaro, P. A., Zack, D. J., and Valle, D. (1998). Mammalian orthologs of C. elegans unc-119 highly expressed in photoreceptors. *Invest. Ophthalmol. Vis. Sci.* 39:2085-2094.

Towler, D. A., Eubanks, S. R., Towery, D. S., Adams, S. P., Glaser, L. (1987). Amino-terminal processing of proteins by N-myristoylation. Substrate specificity of N-myristoyl transferase. *J. Biol. Chem.* 262:1030-36.

Towler, D., Glaser, L. (1986). Acylation of cellular proteins with endogenously synthesized fatty acids. *Biochemistry* 25;878-84.

Towler, D. A., Gordon, J. I. (1988). The biology and enzymology of eukaryotic protein acylation. *Ann. Rev. Biochem.* 57:69-99.

Veltel, S., Gasper, R., Eisenacher, E., and Wittinghofer, A. (2008). The retinitis pigmentosa 2 gene product is a GTPase-activating protein for Arf-like 3. *Nat. Struct. Mol. Biol.* 15:373-380.

Veltel, S., Kravchenko, A., Ismail, S., and Wittinghofer, A. (2008). Specificity of Arl2/Arl3 signaling is mediated by a ternary Arl3-effector-GAP complex. *FEBS Lett.* 582:2501-2507.

Vepachedu, R., Karim, Z., Patel, O., Goplen, N., and Alam, R. (2009). Unc119 protects from Shigella infection by inhibiting the Abl family kinases. *PLoS. ONE* 4:e5211.

Weinberg, R. A., McWherter, C. A., Freeman, S. K., Wood, D.C., Gordon, J. I., Lee, S.C. (1995). Genetic studies reveal that myristoylCoA:protein N-myristoyltransferase is an essential enzyme in Candida albicans. *Mol. Microbiol.* 16:241-250.

Winter-Vann, A. M., Casey, P. J. (2005). Post-prenylation-processing enzymes as new targets in oncogenesis. *Nat Rev Cancer* 5:405-412.

Wright, K. J., Baye, L. M., Olivier-Mason, A., Mukhopadhyay, S., Sang, L., Kwong, M., Wang, W., Pretorius, P. R., Sheffield, V. C., Sengupta, P., Slusarski, D. C., and Jackson, P. K. (2011). An ARL3-UNC119-RP2 GTPase cycle targets myristoylated NPHP3 to the primary cilium. *Genes Dev.* 25:2347-2360.

Young, R. W. (1967). The renewal of photoreceptor cell outer segments. *J Cell Biol* 33:61-72.

Young, R. W., Bok, D. (1969). Participation of the retinal pigment epithelium in the rod outer segment renewal process. *J Cell Biol* 42:392-403.

Zhang, F. L., Casey, P. J. (1996). Protein prenylation: molecular mechanisms and functional consequences. *Annu Rev Biochem* 65:241-269.

Zhang, H., Li, S., Doan, T., Rieke, F., Detwiler, P. B., Frederick, J. M., Baehr, W. (2007). Deletion of PrBP/δ impedes transport of GRK1 and PDE6 catalytic subunits to photoreceptor outer segments. *Proc Natl Acad Sci USA* 104:8857-8862.

Zhang, H., Constantine, R., Vorobiev, V., Chen, Y., Seetharaman, J., Huang, Y. J., Xie, G., Montelione, G. T., Gerstner, C. D., Davis, M. W., Inana, G., Whitby, F. G., Jorgensen, E. M., Hill, C. P., Tong, L., and Baehr, W. (2011). UNC119 regulates G protein trafficking in sensory neurons. *Nature Neuroscience* 14:874-880.

CHAPTER 2

UNC119 IS REQUIRED FOR G PROTEIN TRAFFICKING IN SENSORY NEURONS[*]

[*] Reprinted with permission from Nature Neuroscience and The Nature Publishing Group Zhang, H. *et al*. UNC119 is required for G protein trafficking in sensory neurons. *Nature Neuroscience* 14, 874-880.

UNC119 is required for G protein trafficking in sensory neurons

Houbin Zhang[1,*], Ryan Constantine[1,2,*], Sergey Vorobiev[3], Yang Chen[3], Jayaraman Seetharaman[3], Yuanpeng Janet Huang[4], Rong Xiao[4], Gaetano T. Montelione[4], Cecilia D. Gerstner[1], M. Wayne Davis[5], George Inana[7], Frank G. Whitby[8], Erik M. Jorgensen[5,6], Christopher P. Hill[8], Liang Tong[3], and Wolfgang Baehr[1,5,9,#]

[1]*Department of Ophthalmology, University of Utah Health Science Center, Salt Lake City, UT 84132, USA*

[2]*Graduate Program in Neuroscience, University of Utah Health Science Center, Salt Lake City UT 84132, USA*

[3]*Department of Biological Sciences, Northeast Structural Genomics Consortium, Columbia University, New York, New York 10027, USA*

[4]*Center for Advanced Biotechnology and Medicine, Department of Molecular Biology and Biochemistry, Northeast Structural Genomics Consortium, Rutgers University, Piscataway, NJ 08854, USA*

[5]*Department of Biology and* [6]*Howard Hughes Medical Institute, University of Utah, 257 South 1400 East, Salt Lake City, Utah 84112, USA*

[7]*Bascom Palmer Eye Institute, University of Miami Miller School of Medicine, 1638 N.W., 10th Avenue, Miami, FL 33136, USA*

[8]*Department of Biochemistry, University of Utah School of Medicine, Salt Lake City, UT 84112-5650, USA.*

[9]*Department of Neurobiology and Anatomy, University of Utah Health Science Center, Salt Lake City UT 84132, USA*

*These authors contributed equally to this work

Running title: UNC119 and G protein trafficking

#Corresponding author: Wolfgang Baehr, Department of Ophthalmology, University of Utah Health Science Center, 65 N. Medical Dr, Salt Lake City, UT 84132 USA. Phone: 801-585-6643; fax: 801-585-1515; E-mail: wbaehr@hsc.utah.edu

Summary

UNC119 is widely expressed among vertebrates and invertebrates. Here we report that UNC119 recognized the acylated N-terminus of the rod photoreceptor transducin α-subunit (Tα) as well as *C. elegans* G proteins Odr-3 and Gpa-13. The crystal structure of human UNC119 at 1.95 Å resolution revealed an immunoglobulin-like β-sandwich fold. Pulldowns and isothermal titration calorimetry revealed a tight interaction between UNC119 and acylated Gα peptides. Co-crystallization of UNC119 with an acylated Tα N-terminal peptide at 2.0 Å revealed that the lipid chain is buried deeply into UNC119's hydrophobic cavity. UNC119 bound $T\alpha^{GTP}$ inhibiting its GTPase activity, thereby providing a stable UNC119-$T\alpha^{GTP}$ complex that is capable of diffusing from the inner segment back to the outer segment following light-induced translocation. UNC119 deletion in both mouse and *C. elegans* lead to G protein mislocalization. These results establish UNC119 as a novel Gα-subunit cofactor that is essential for G-protein trafficking in sensory cilia.

Introduction

Nonmotile primary cilia sensitive to external stimuli are found in both vertebrate and invertebrate sensory neurons. In mammalian photoreceptors or *C. elegans* olfactory cells, light receptors (rhodopsin) or odorant receptors, together with their G-proteins and associated signal transduction components transport to cilia by vesicular and

intraflagellar mechanisms. Defects in these trafficking pathways have been shown to impair signal transduction, ciliogenesis and cilia maintenance[1], often leading to severe disease. In both photoreceptors and odorant receptors, evidence shows that an ever increasing number of polypeptides is involved in vesicular trafficking and stabilizing intraflagellar transport, including components of the BBSome[2], Rab GTPases[3], Arf- and Arf-like GTPases[4] and prenyl binding proteins[5].

UNC119 is 27 kDa polypeptide identified in the basal body proteome of *C. reinhardtii*[6], the flagellar rootlet of *Naegleria*[7], neurons of *C. elegans*[8] and the mouse photoreceptor sensory cilium complex[9]. *unc-119* was first discovered in *C. elegans* on the basis of a spontaneous mutation affecting locomotion, feeding behavior and chemosensation[8]. Independently, a protein termed Retina Gene 4 (RG4) was discovered in the retina and recognized to be a *C. elegans unc-119* ortholog[10]. Although expressed in multiple tissues, UNC119 predominates in retinal photoreceptor inner segments and synaptic regions[11-13]. UNC119 has been shown to interact with several diverse proteins, including the Arf-like GTPases ARL2[14] and ARL3[15], the Ca^{2+}-binding protein CaBP4, a modulator of the voltage-gated Ca^{2+} channel Ca_v 1.4 present in rod and cone synapses[16] and the synaptic ribbon component RIBEYE[17] of photoreceptors. A heterozygous stop codon (K57ter) identified in the human *UNC119* gene of a patient with late-onset dominant cone dystrophy also produced dominant dystrophy in a transgenic mouse model[18].

Apart from the mammalian retina, UNC119 has been detected in leukocytes (eosinophils), T-cells, lung fibroblasts[19], the adrenal glands, cerebellum and kidney[11]. UNC119 has also been shown to activate Src-type tyrosine kinases associated with the

interleukin-5 receptor and the T-cell receptor by interacting with Src homology domains located in the N-terminal half of UNC119[20]. Widespread distribution of UNC119 in vertebrates, invertebrates and even flagellated protozoa suggests highly conserved and multiple functions throughout the animal kingdom.

Here we identify UNC119 as a novel lipid binding protein interacting with acylated N-termini of G-protein α subunits present in mouse photoreceptors and *C-elegans* olfactory neurons. The crystal structure at 1.95Å resolution reveals that UNC119 adopts an immunoglobulin-like β-sandwich fold. The N-terminal peptide of transducin-α (Tα) inserts deeply into the hydrophobic cavity formed by the β-sandwich fold of UNC119. Remarkably, the ligand enters the protein interior from the opposite side of that seen for structurally related proteins and the first six amino acid residues of the Tα peptide are deeply buried in the core making intimate contacts with UNC119. UNC119 knockouts demonstrate the requirement of UNC119 for G protein trafficking in animal models as diverse as mouse and *C. elegans*.

Results

The structure of human UNC119 at 1.95 Å resolution. The crystal structure of human UNC119 (residues 57-237) at 1.95 Å resolution (PDB ID 3GQQ) contains an immunoglobulin-like β-sandwich fold comprised of two β-sheets (**Figs. 2.1A,B**). The β-sheets, arranged in four antiparallel strands fold in a Greek key pattern (**Fig. 2.2A**), which is found in a large number of diverse proteins[21]. Strands β3- β4 and β7- β8 are linked by short α-helical loops (α1 and α2 in **Fig. 2.1A**). In the UNC119 structure, the two sheets

Figure 2.1 Crystal structure of human UNC119**.** (**A**) Ribbon representation of the structure of human UNC119 (residues 57-237). Nine β strands (β1-β9), shown in red, create two β-sheets that splay apart at one end to create an opening to the cavity at the center of the β-sandwich. The N- and C-termini are marked N and C, respectively. The structure of the loop 108-123 connecting strands β2 and β3 could not be resolved. (**B**) Structure of UNC119 viewed after a 90° rotation around the vertical axis.

Fig. 2.1
Zhang et al.

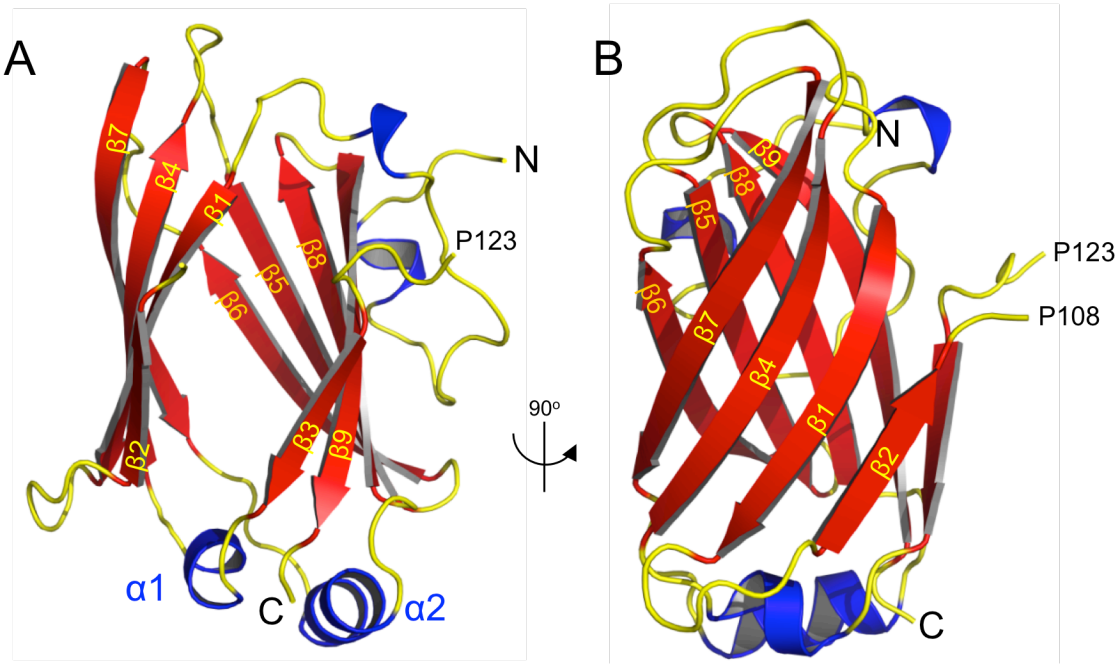

Figure 2.2 The Greek Key Motif in UNC119, RhoGDI and PrBP/δ
(**A**) Greek key motif of the β-sandwich fold common to the three structures. Blue arrows depict the strands that form one β-sheet, while gray arrows depict strands of the second β-sheet.
(**B**) Ribbon representation of the geranylgeranyl binding protein RhoGDI (1DOA) and the prenyl binding protein PrBP/δ (1KSH). RhoGDI is shown with Cys-geranylgeranyl of CDC42 present in its binding pocket. The presumed entrance to the hydrophobic pocket of PrBP/δ is indicated with an arrow (Hanzal-Bayer et al., 2002). Note that entrances to the hydrophobic pocket in UNC119 (**Fig. 2.3A,B**) and RhoGDI are located at the opposite edge of the β-sandwich fold. Figure created with PyMOL (www.pymol.org).
(**C**) Sequence Alignment of Human UNC119, PrBP/δ, and RhoGDI. Only C-terminal residues of UNC119 (60-240) and RhoGDI (41-204) are shown. β-strands are depicted as large red arrows for UNC119 and are underlined in red for PrBP/δ and RhoGDI. Identical residues are highlighted blue and similar residues gray.

Fig. 2.2
Zhang et al.

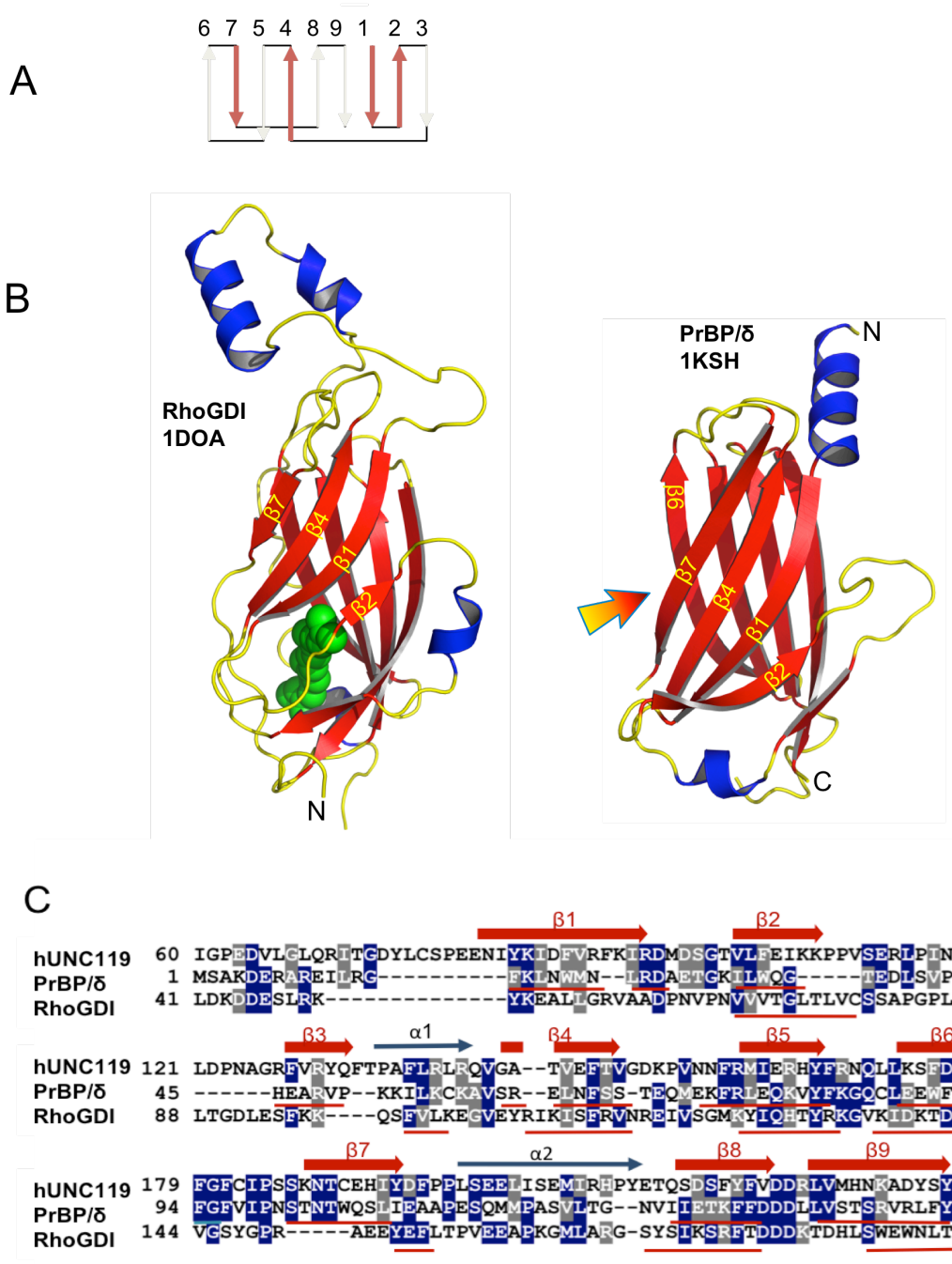

are splayed apart from each other at one edge of this β-sandwich, revealing a narrow, deep cavity penetrating the center of this structure (**Fig. 2.1A**). The atomic model is in agreement with the crystallographic data and expected stereochemistry (**Table 2.1**).

A search of the Protein Data Bank with the program DaliLite (http://www.ebi.ac.uk/Tools/dalilite/index.html) returned a large number of similar structures including PrBP/δ (*Z* score 12, 24% overall amino acid sequence identity with UNC119), and Rho-GDP dissociation inhibitor 1 (RhoGDI, *Z* score 9, 10% overall identity) (**Fig. 2.2B, 2.3A**). When restricted to the region that folds into β-sheets, UNC119 sequence similarity with PrBP/δ increased to 56% (**Fig. 2.2C**). PrBP/δ is a prenyl-binding protein that interacts with prenylated proteins participating in phototransduction[5], while RhoGDI regulates the function of the Rho GTPase CDC42[22]. Both proteins possess a hydrophobic pocket capable of accommodating farnesyl and geranylgeranyl chains[23, 24]. The aforementioned structural similarities suggested that UNC119 might be a lipid binding protein.

UNC119 interacts with the transducin α-subunit. To identify interacting partners of UNC119 in photoreceptors, we used the GST fusion protein pulldown technique followed by HPLC and tandem mass spectrometry (LC-MS/MS). From bovine retina lysates, we identified a polypeptide of approximately 40 kDa that specifically bound GST-UNC119 (asterisk, **Fig. 2.4A**). Sequence identification by LC-MS/MS yielded numerous peptides matching the rod Tα-subunit, and one matching cone Tα (**Fig. 2.4B**), both of which are involved in phototransduction. In the inactive state GDP is bound to Tα, permitting the interaction with Tβγ, yielding the heterotrimeric complex,

Table 2.1: UNC119 crystallographic data and refinement statistics

Data		
Crystal	HR3066a[a]	Au10pe
Space Group	$P2_12_12_1$	$P2_12_12_1$
Unit Cell Dimensions	a=77.89, b= 79.56, c=189.72	a=78.55, b=79.71 , c=189.59
Resolution (Å)	50.0 – 1.95	30.0 – 2.00
Resolution (Å) (high-resolution shell)	(2.02 – 1.95)	(2.07 – 2.00)
# Reflections measured		1,252,665
# Unique reflections	166,290	82,342
Redundancy	7.0	15.2
Completeness (%)	99.6 (100)	100 (100)
$\langle I/\sigma(I)\rangle$	26 (2.9)	11 (2.5)
Mosaicity (^{o})	0.37	1.1
Rsym[b]	0.088 (0.537)	0.116 (0.701)
Refinement		
Resolution (Å)	40.51 – 1.95	29.37 – 1.99
Resolution (Å) – (high-resolution shell)	(1.97 – 1.95)	(2.04 – 1.99)
# Reflections used for refinement	165,606	78,089
# Reflections in Rfree set	8,332	4,139
R[c]	0.191 (0.247)	0.200 (0.226)
Rfree[d]	0.214 (0.251)	0.250 (0.276)
RMSD: bonds (Å) / angles (°)	0.005 / 1.3	0.012 / 1.304
$\langle B\rangle$ (Å^2): GLL-1 residues/ # atoms	N/A	41 / 268
$\langle B\rangle$ (Å^2): UNC119 only / # atoms	33 / 8,265	29 / 8,299
$\langle B\rangle$ (Å^2): water molecules / # water	41 / 803	39 / 793
ϕ/ψ most favored (%)	99	97

Values in parenthesis refer to data in the high resolution shell.

[a] Friedel pairs were used in phasing crystal HR3066a.

[b] Rsym = $\Sigma|I-\langle I\rangle|/\Sigma I$ where I is the intensity of an individual measurement and $\langle I\rangle$ is the corresponding mean value.

[c] $R = \Sigma||Fo|-|Fc||/\Sigma|Fo|$, where $|Fo|$ is the observed and $|Fc|$ the calculated structure factor amplitude.

[d] Rfree is the same as R calculated with a randomly selected test set of reflections that were never used in refinement calculations.

Figure 2.3 Structural Alignment of UNC119 with PrBP/δ and RhoGDI
(**A**) UNC119 (red) aligned with PrBP/δ (blue). The Tα peptide is shown in dark gray and the acyl chain in green. Figure created with PyMOL (www.pymol.org).
(**B**) UNC119 (red) aligned with RhoGDI (cyan). The Tα peptide is shown in dark gray and the acyl chain in green. The geranylgeranyl chain of the GTPase CDC42 bound to RhoGDI is shown in light gray. Figures created with PyMOL (www.pymol.org).
(**C**) Electron density surrounding the Lauroyl-Tα peptide. View showing a simulated annealing Fo-Fc omit map contoured at 2.5 sigma (red mesh). Phases were calculated following deletion of the ligand, application of random shifts (0.1 A), and refinement of the resulting model. UNC119 residues that comprise the walls of the cavity are shown with yellow carbon atoms, the acyl chain is colored green, and residues that comprise the remainder of the Tα peptide are colored gray.

Fig. 2.3
Zhang et al.

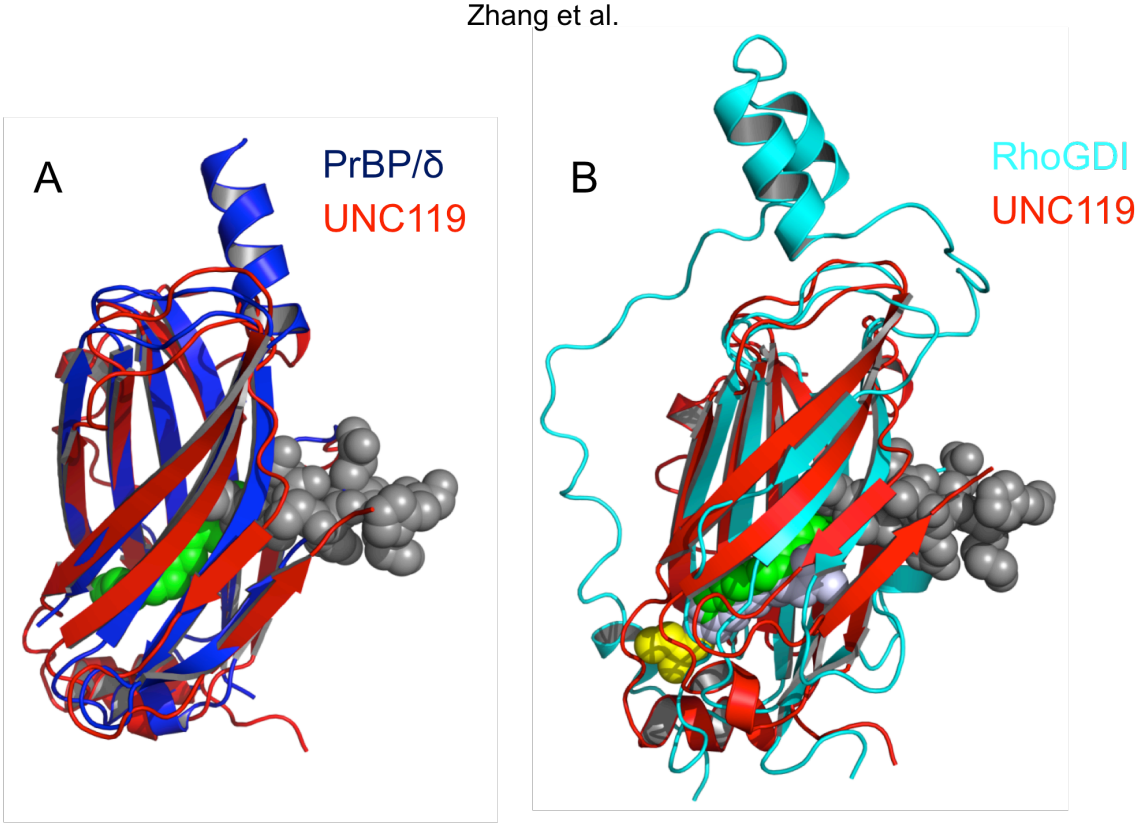

C

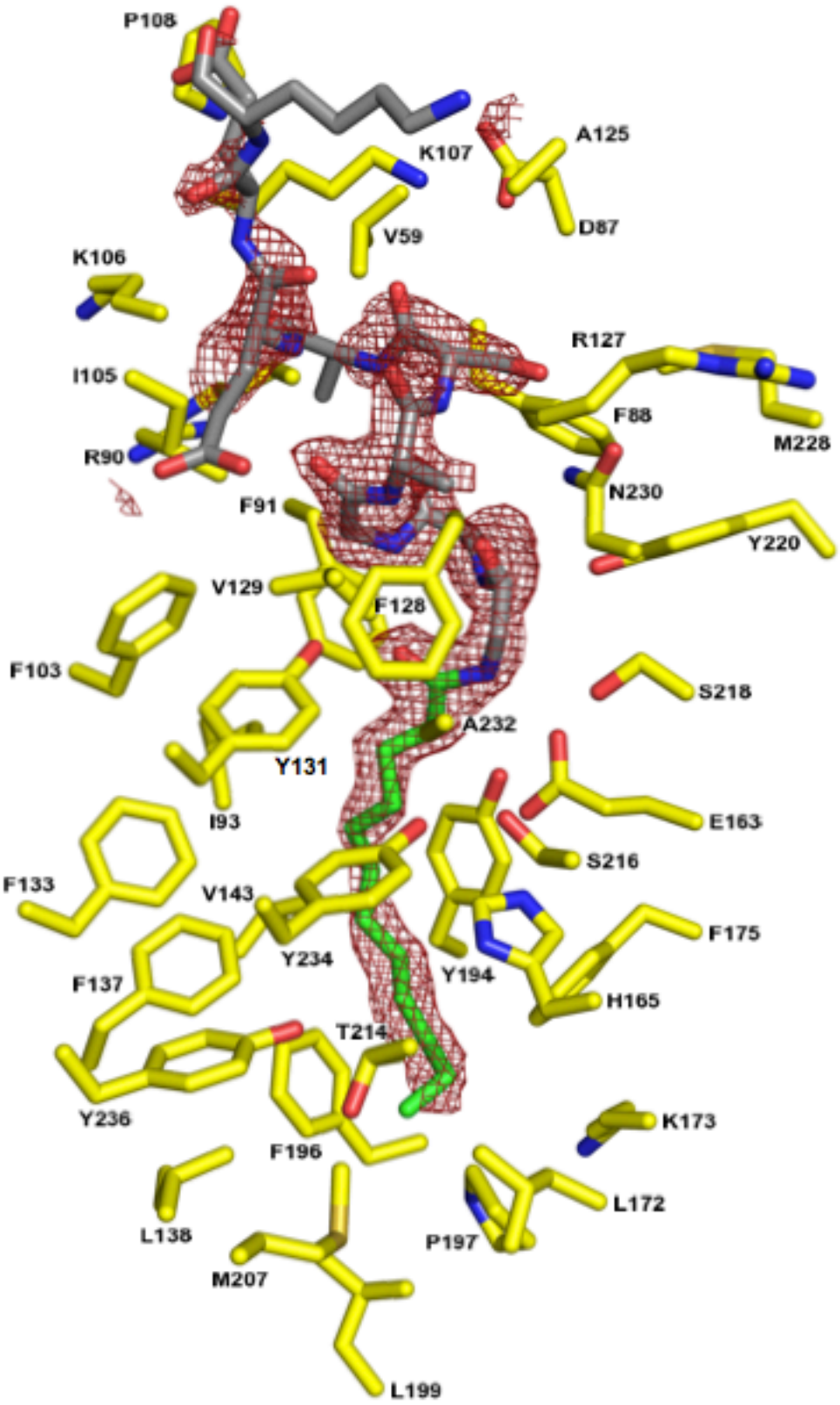
P108
K107
A125
D87
V59
K106
R127
I105
F88
M228
R90
N230
F91
Y220
V129
F128
F103
S218
A232
Y131
I93
E163
S216
F133
V143
F175
Y234
Y194
F137
H165
T214
Y236
K173
F196
L172
L138
P197
M207
L199

Figure 2.4 Interaction of UNC119 with Tα polypeptides. (**A**) Pulldown of rod and cone Tα with GST-UNC119 (representative Coomassie stained gel of four independent experiments). Bound polypeptides from bovine retina lysates were analyzed by SDS-PAGE. Lane 1, recombinant GST (G); Lane 2, pulldown with GST as a control (GC); Lane 3, GST-UNC119 pulldown (GU); Lane 4, GST-UNC119 fusion protein. An asterisk identifies the proteins pulled down by GST-UNC119. (**B**) Identification of peptides by LC-MS/MS. The 40 kDa polypeptides pulled down with GST-UNC119 were sequenced by LC-MS/MS. Identified peptide sequences, shown in red, were matched with rod and cone Tα. (**C**) GST-UNC119 pulldown of Tα from wild-type (lanes 1-4) and *Gnat1*$^{-/-}$ retina (lanes 5-8). Lanes 1,2,5,6, input; lanes 3,7, control pulldowns with GST; lanes 4,8, pulldowns with GST-UNC119. Acylated Tα is pulled down (lane 4), but not farnesylated Tγ (lane 8). (**D**) GST-UNC119 pulldown of Tα and Tα(G2A) expressed in HEK cells. Lanes 1–3, input; lanes 4–6, pulldowns. Lanes 1,4, HEK cells expressing bovine Tα; Lanes 2,5, HEK cells expressing bovine Tα(G2A); Lanes 3 and 6, mouse retina lysates. Blot was probed with anti-Tα antibody. Note that UNC119 does not interact with non-acylated Tα(G2A). (**E**) Specificity of retina lysate pulldowns. Lanes 1–3, mouse retina lysates (input); lanes 4–6, retina lysate pulldowns; lane 4, GST control; lane 5, 10 μg GST-UNC119 was added; lane 6, same as lane 5 but with 0.1% Triton X-100 and 0.1% NP-40 (DT) present in the binding buffer. Top panel, blot probed with anti-Tα. Bottom panel, same blot probed with anti-GCAP1 antibody. Note that myristoylated GCAP1 does not interact with GST-UNC119.

Fig. 2.4
Zhang et al.

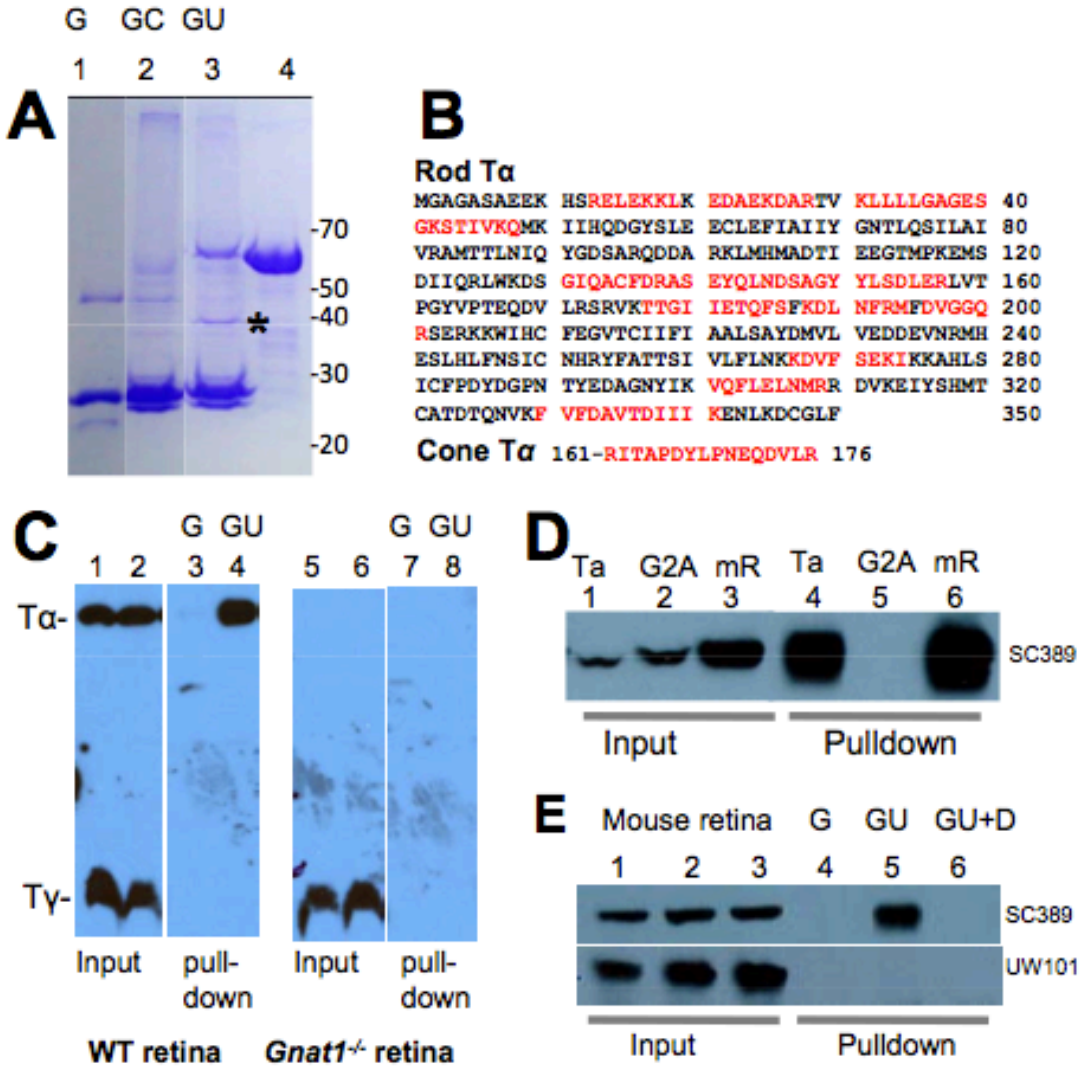

Tαβγ. To test whether UNC119 pulled down the heterotrimeric complex through its interaction with Tα, pulldowns were repeated using wild-type and *Gnat1*$^{-/-}$ (Tα knockout) mouse retina lysates (**Fig. 2.4C**). Immunoblots probed with anti-Tα and anti-Tγ antibodies showed that UNC119 interacts with Tα, but not with farnesylated Tγ (**Fig. 2.4C**, lane 4). Pulldowns were negative using *Gnat1*$^{-/-}$ retina lysates (**Fig. 2.4C**, lanes 7,8) confirming that UNC119 is not a prenyl binding protein.

The glycine residue at the N-terminus of rod Tα (G2) is heterogeneously acylated[25] carrying either C12:0, C14:1, C14:2, or C14:0 side chains, which play an important role in targeting Tα to the outer segment[26]. Due to the structural similarity among UNC119, PrBP/δ, and RhoGDI, we suspected that UNC119 would interact with the N-terminal acyl group of Tα. To test this hypothesis, G2 at the N-terminus of Tα was replaced with alanine, a mutation preventing Tα acylation. Recombinant Tα(G2A) did not interact with bovine GST-UNC119 in pulldown assays (**Fig. 2.4D**, lane 5) suggesting that the acyl side chain attached to G2 of Tα mediates the interaction with GST-UNC119. Furthermore, UNC119 failed to interact with N-myristoylated GCAP1 (**Fig. 2.4E**, lower panel) or recoverin (not shown), suggesting that the interaction with UNC119 requires some degree of specificity.

UNC119 is an acyl-binding protein. To independently confirm that UNC119 is a novel acyl-binding protein, a synthetic lauroylated (C12:0) peptide corresponding to the N-terminus of bovine Tα (2-GAGASAEEKH-11) was added to the pulldown assay. The acylated Tα peptide was able to competitively inhibit binding of Tα to UNC119 (**Fig. 2.5A**, lane 3), whereas the unacylated peptide had no effect (**Fig. 2.5A**, lane 4). These

Figure 2.5 UNC119 is an acyl-binding protein. (**A**) GST-UNC119 pulldowns and inhibition by an acylated N-terminal Tα peptide. Lane 1, retina lysate. Lanes 2–4, glutathione bead pellets of retina lysates that were incubated with GST-UNC119, in the absence of peptide (lane 2), the presence of lauroyl-GAGASAEEKH (lane 3), and in the presence of non-acylated GAGASAEEKH peptide (lane 4). Lanes 5-7, supernatants of 2–4. Note that lauroyl-GAGASAEEKH competes for binding (lane 3), but the non-acylated peptide did not (lane 4). (**B**) Isothermal titration calorimetry. Human UNC119 was titrated with G protein α-subunit N-terminal peptides. Red symbols, titration with N-terminal Tα peptide (lauroyl-GAGASAEEKH); black circles, titration with non-lauroylated GAGASAEEKH; green triangles, titration with myristoylated GAGASAEEKH; blue squares, titration with ODR-3 N-terminal peptide lauroyl-GSCQSNENSE. Lauroyl-GAGASAEEKH (red) and myristoyl-GAGASAEEKH (green) peptides were fit to a one-site model and bind with K_Ds of 0.54 μM ± 0.28 μM and 0.22 μM ± 0.14 μM, respectively. Lauroyl-ODR-3 (blue) binds more than one order of magnitude weaker (16.4 μM ± 3.0 μM). (**C**) Alignment of N-terminal peptides of mouse G protein α subunits, *C. elegans* G protein α-subunits GPA-13 and ODR-3, and Ca^{2+}-binding proteins GCAP1, GCAP2 and recoverin. Peptides lacking Gly at position 2 cannot be myristoylated, therefore interaction with UNC119 through an acyl chain does not extend to all subfamilies of Gα.

Fig. 2.5
Zhang et al.

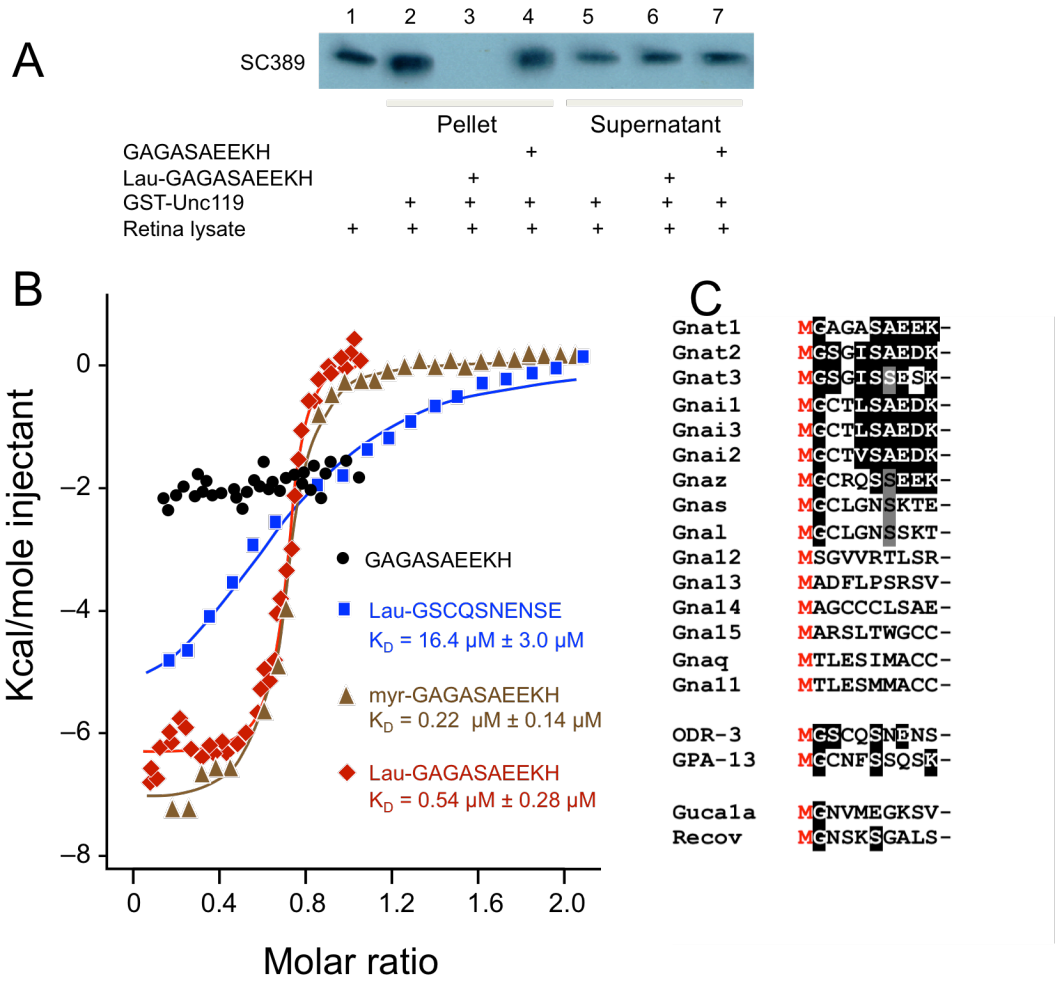

results support the requirement for the N-terminal acyl group as a mediator of the interaction between Tα and UNC119.

We then employed isothermal titration calorimetry (ITC) to determine the binding constant of acylated N-terminal G protein α-subunit peptides with UNC119 (**Fig. 2.5B**). ITC measures the binding enthalpy of two reactants enabling the resolution of two or more binding sites. We titrated the acylated N-terminal bovine Tα peptides and the acylated N-terminal *C. elegans* ODR-3 peptide (GSCQSNENSE). ODR-3 is expressed in *C. elegans* AWA, AWB, and AWC olfactory neurons and participates in chemosensory signal transduction (the *unc-119* null mutation was originally discovered in *C. elegans*)[8]. Microcalorimetry experiments showed that the unacylated Tα peptide does not interact with recombinant human UNC119, whereas lauroyl- and myristoyl-GAGASAEEKH each exhibited tight binding at a single site with K_Ds of approximately 0.54 μM ± 0.28 μM and 0.22 μM ± 0.14 μM, respectively (**Fig. 2.5B**). This dissociation constant is similar to those measured *in vitro* for farnesyl and geranylgeranyl side chains with PrBP/δ (0.7 μM, and 19 μM, respectively)[24]. UNC119 also bound the lauroylated N-terminal peptide derived from ODR-3, but did so by two orders of magnitude weaker than the lauroyl Tα peptide (K_D = 16.4 μM ± 3.0 μM), further implicating the N-terminal residues in binding specificity. Alignment of mouse N-terminal Gα peptides revealed that the *Gna11-15* and *Gnaq* subfamilies are not N-terminally acylated (**Fig. 2.5C**) indicating that the UNC119-Gα subunit interaction does not extend to all Gα subfamilies.

The UNC119 hydrophobic cavity is the lipid binding site. Interpretation of our structural and biochemical results suggested that the lipid inserts into the hydrophobic cavity at the center of the β-sandwich. The co-crystal structure of UNC119 with the

lauroylated Tα peptide at 2.0 Å (PDB ID: 3RBQ) showed that the pocket easily accommodates a lauroyl (C12) moiety (**Fig. 2.6**) in a very specific fashion as each molecule in the asymmetric unit of the crystal contains a similarly bound ligand (**Table 2.2** and **Fig. 2.7**). The cavity is lined predominantly by hydrophobic residues (mostly Phe and Tyr) that mediate the interaction with the lauroylated Tα peptide primarily via *Van der Waals* forces, consistent with properties of a lipid binding site (**Fig. 2.6C, 2.3C**). Remarkably, entrances to the lipid binding sites of PrBP/δ and RhoGDI (**Fig. 2.2B**) do not exist in UNC119, but instead are found on the opposite edge of the β-sandwich (**Figs. 2.6A,B, 2.3A,B**).

The lauroyl group and the first six residues of the Tα peptide are buried deeply within the hydrophobic pocket of UNC119 (**Figs. 2.6C, 2.3C)**, whereas peptide residues 7-10 make only peripheral contact with UNC119 and are poorly ordered. In general, the surrounding protein residues formed a surface that is highly complementary to the shape of the ligand, thereby rationalizing the high degree of conservation for the N-terminal residues of Tα and the contacting residues of UNC119. As expected for a hydrophobic environment, hydrogen bonding potentials were satisfied by specific interactions. The first six peptide residues lack polar side chains, with the exception of S6, which sits exposed to solvent. Most of the main chain groups participate in hydrogen bonds through the formation of a distorted 3_{10}-α helix by the first six residues of the peptide. Remaining buried polar groups of the peptide are coordinated by conserved UNC119 residues. The Y131 hydroxyl group hydrogen bonds with the lauroyl oxygen, E163 hydrogen bonds G2 NH, and Y220 coordinates A3 NH via a buried water molecule (**Fig. 2.6C**). This water molecule, along with E163 and Y220, constitute part of an extensive hydrogen-bonding

Figure 2.6 The lipid binding pocket of UNC119. (**A,B**) Two orientations of UNC119 co-crystallized with the acylated Tα peptide in the UNC119 hydrophobic cavity. The lauroyl chain is shown in green, and the ten amino acids of the peptide are modeled in dark gray. In B, UNC119 is viewed after a 90° rotation around the vertical axis and the individual β-strands are labeled β1-9 in yellow. (**C**) View of UNC119 residues and key water molecules interacting with the lauroyl-GAGASAEEKH ligand. The hydrogen-bonding network (black dashed lines) limits the depth to which the Tα peptide can penetrate UNC119. Hydrogen bonds were included if the average of the bond length for all six molecules in the asymmetric unit was 3.2 Å or less and satisfied appropriate hydrogen bonding stereochemistry. UNC119 residues are shown in yellow, the lauroyl chain is green and the attached residues are colored dark gray. Figures were created with PyMOL (www.pymol.org).

Fig. 2.6
Zhang et al.

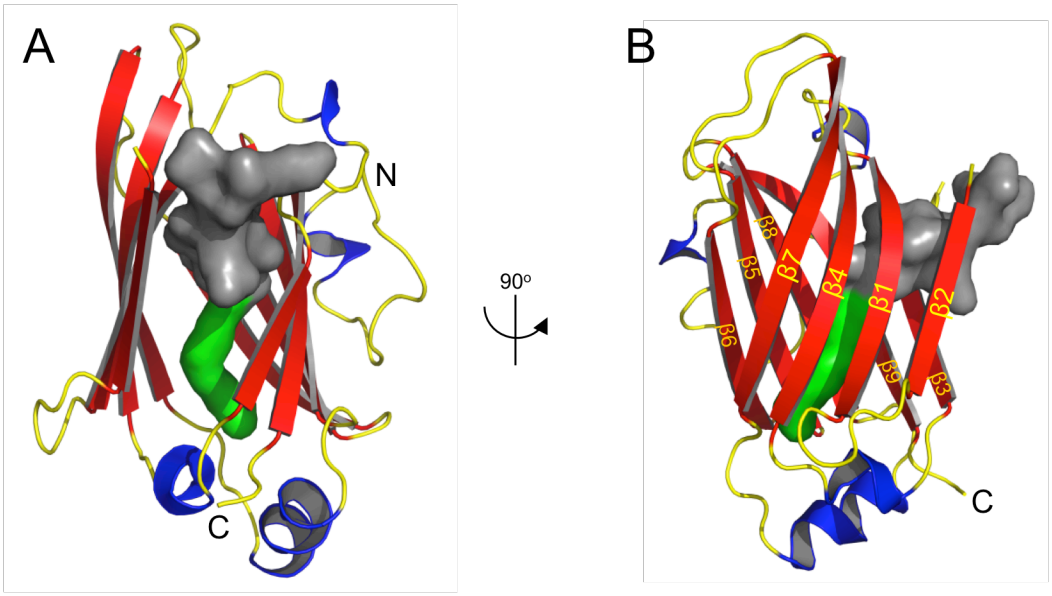

C

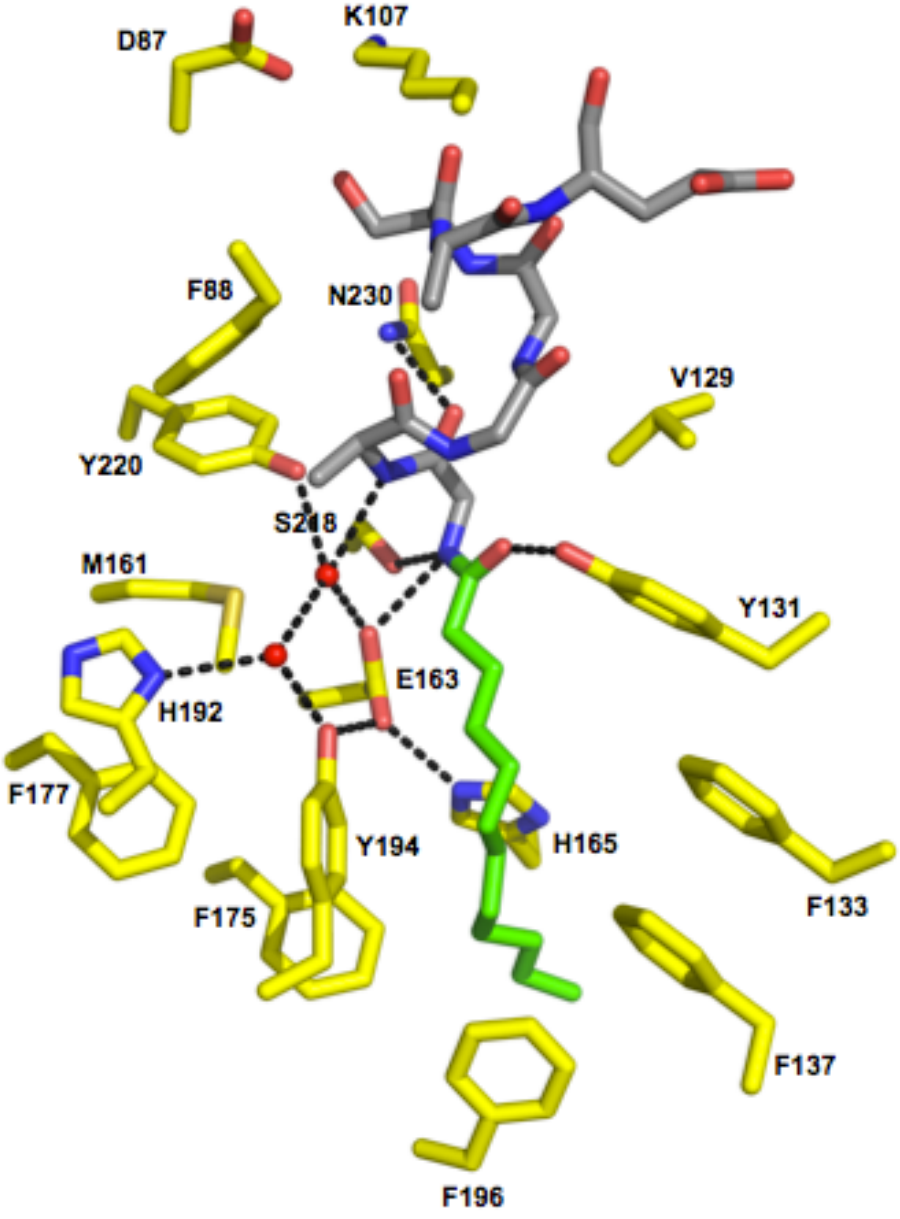
D87
K107
F88
N230
V129
Y220
S218
M161
Y131
E163
H192
F177
Y194
H165
F133
F175
F137
F196

Table 2.2. Comparison of the RMSD values for each of the six UNC119 chains and their associated ligands.
RMSD values are given for the overlap of all protein atoms in each chain, all atoms related to residue 501 (glycine and the attached lauroyl group), and the carbon-α trace for the peptide attached to the lauroyl group in each ligand.

Chains Overlapped	RMSD for all protein atoms	RMSD for residue 501[a]	RMSD of Cα trace[b]
B on A	0.373	0.252	0.190 (501-507)
C on A	0.459	0.315	0.180 (501-504)
D on A	0.320	0.284	0.182 (501-504)
E on A	0.449	0.370	0.323 (501-503)
F on A	0.458	0.635	0.424 (501-507)

[a]RMSD values calculated using all atoms on residue 501 with residue 501 defined as glycine plus the attached lauroyl group.
[b]Numbers in parentheses refer to residues on the ligand from which the RMSD values were calculated.

Figure 2.7. Overlap of the UNC119 carbon-α coordinates and associated ligands. The UNC119 carbon-α coordinates for each of the six molecules in the asymmetric unit were overlapped and are shown in red. In each of the molecules the lauroyl-GAGASAEEKH ligand is bound in very similar fashion. The acyl group of the ligand is shown in green and the ordered peptide residues of the ligand are colored gray. Figure created with PyMOL (www.pymol.org).

Fig. 2.7
Zhang et al.

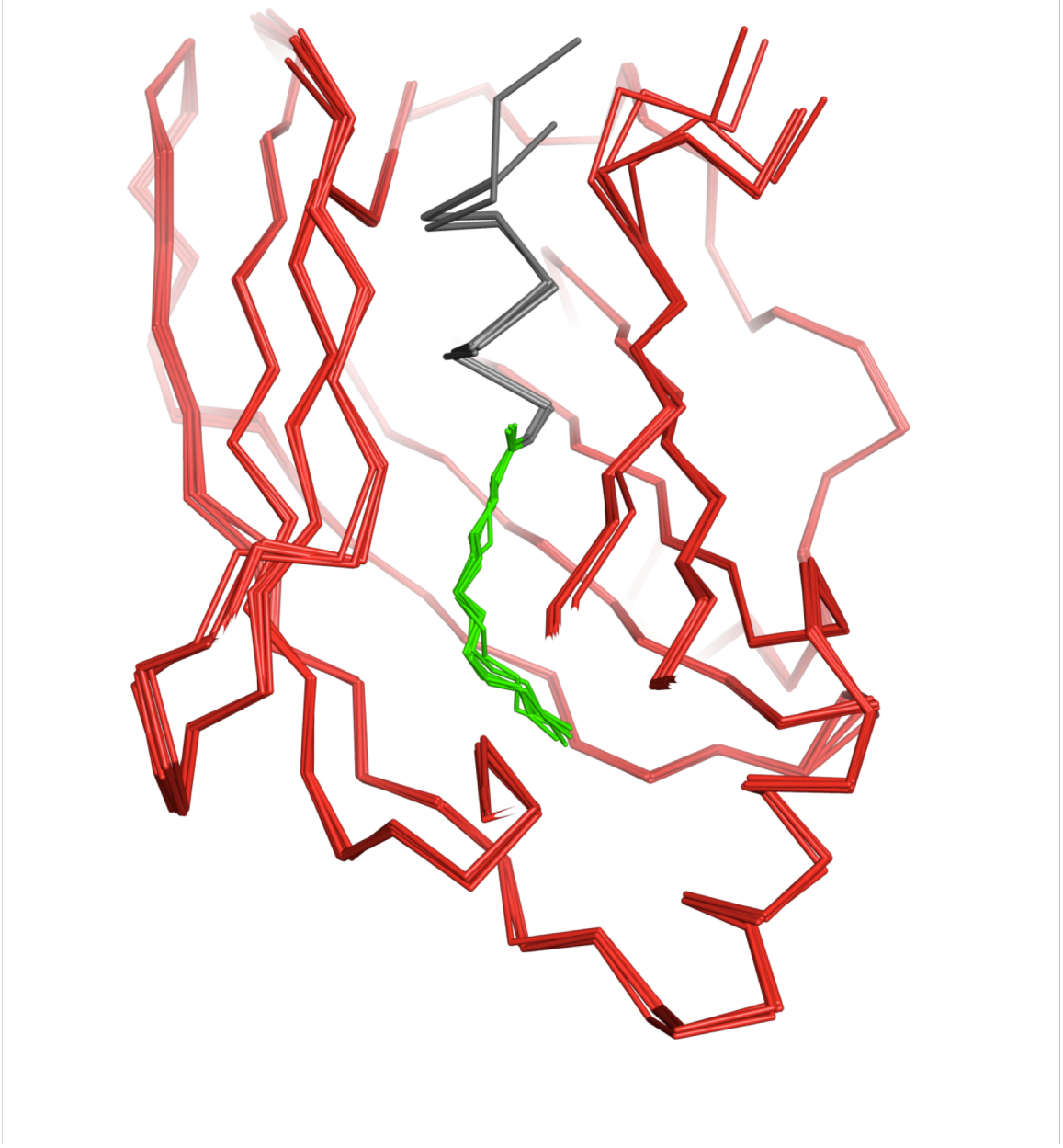

network that also includes H165, H192, Y194, S218, and one other water molecule. These interactions provide specific recognition of N-terminal groups that define the location of the peptide-acyl junction within the UNC119 cavity, thereby establishing the length of acyl chain that can be accommodated. We have also determined an isomorphous structure of UNC119 with the *C. elegans* ODR-3 lauroyl-GSCQSNENSE ligand (data not shown). This structure is superimposable with that of the Tα ligand but with a less-ordered peptide structure, consistent with the weaker binding affinity and absence of amino acid residues relevant for optimal binding.

Transducin-membrane interactions are regulated by GTP and UNC119. The co-crystal structure of UNC119 with the acylated Tα peptide implies that UNC119 may disrupt membrane association of Tα by inserting the acyl chain into its hydrophobic pocket. To investigate whether UNC119 facilitates dissociation of transducin from membranes under isotonic conditions where it is firmly membrane associated, we examined the extraction of Tα by UNC119 in the presence and absence of GTP. Tα could be extracted from rod outer segments (ROS) membranes by UNC119 only in the presence of GTP (**Fig. 2.8A**), suggesting that GTP/GDP exchange and disruption of TαTβγ are essential for dissociation.

To demonstrate that UNC119 does not extract $T\alpha^{GDP}T\beta\gamma$ from membranes, we investigated the interaction of UNC119 with $T\alpha^{GTP}$ and $T\alpha^{GDP}T\beta\gamma$. *In vitro*, association of $T\alpha^{GDP}T\beta\gamma$ to membranes can be disrupted in the dark by low salt (hypotonic) buffers in the absence of GTP[27]. In contrast, in the light, transducin is tightly bound to rhodopsin, requiring GDP/GTP exchange for disruption of the complex and membrane dissociation. $T\alpha^{GTP}$ and $T\alpha^{GDP}T\beta\gamma$ containing retinal lysates were prepared from light-adapted and

dark-adapted retina, respectively, and used for pulldown assays. Pulldowns indicated that UNC119 formed stable complexes only with $T\alpha^{GTP}$ (**Fig. 2.8B**, left panel), but not with $T\alpha^{GDP}T\beta\gamma$ (**Fig. 2.8B**, right panel), confirming that disruption of Tα from $T\alpha^{GDP}T\beta\gamma$ is necessary for the formation of the UNC119-$T\alpha^{GTP}$ complex.

To determine whether UNC119 binding to $T\alpha^{GTP}$ inhibits the GTPase activity of Tα, we measured GTP hydrolysis in a reconstituted system. Depleted ROS membranes containing rhodopsin exhibited very low GTPase activity originating from the remaining traces of transducin in the ROS membranes (**Fig. 2.8C**). The addition of transducin reconstituted GTPase activity yielding a K_{cat} of 1.5 moles $GTP_{hydrolyzed}$/mol transducin/min. However, Tα-GTPase activity was nearly completely inhibited in the presence of recombinant UNC119. Collectively, these results show that neither GTP nor UNC119 alone, was effective in solubilizing Tα from light-adapted membranes. The ability of UNC119 to extract $T\alpha^{GTP}$ from membranes and stabilize GTP suggests that UNC119 may play a key role in the light-induced translocation of transducin (see discussion).

UNC119 deletion in mouse affects transducin trafficking in photoreceptors. The *Unc119*$^{-/-}$ mouse shows no obvious retinal degeneration early in life, but develops a slowly progressing photoreceptor degeneration beginning 6 months postnatally[12]. In the dark-adapted *Unc119*$^{-/-}$ retina, Tα is partially retained in the inner segment and outer nuclear layer, while in the dark-adapted wild-type retina, Tα is detected almost exclusively in the outer segment (**Fig. 2.9A,B**). Transducin is thought to arrive at the outer segment by either vesicular transport[28] or passive diffusion[29], and UNC119 deletion appeared to have no effect on its localization.

Figure 2.8 UNC119 Interacts with Tα-GTP and Inhibits GTPase Activity. (**A**) Extraction of Tα from membranes by UNC119. Live mice were exposed to 10,000 lux/20 minutes driving transducin to the inner segments. Retina lysates in 1X PBS were incubated with either GST, mUNC119, GST and GTP, or mUNC119 and GTP, respectively. The soluble proteins (S) were separated from membrane-bound proteins (P) by centrifugation. Tα was detected by western blot using anti-Tα antibody. Tα elutes only in the presence of UNC119 and GTP. (**B**) Pulldown assays with light-adapted and dark-adapted mouse retinas. PBS/GTP supernatants from retinas of a light-adapted mouse (2,000 lux) and hypotonic supernatants from retinas of a dark-adapted mouse were used for pulldown assays, respectively. The proteins pulled down by GST or GST-UNC119 (pellet) and unbound proteins (supernatant) were analyzed by western blot using anti-Tα antibody. GST-UNC119 binds $T\alpha^{GTP}$ (left), but not $T\alpha^{GDP}T\beta\gamma$ (right). (**C**) GTPase activity of purified Tαβγ in the presence of ROS membranes. The activity of the reconstituted system (red line) corresponds to a rate of 1.5 mole GTP/min. Addition of BSA (light blue) has little effect, whereas addition of UNC119 (green) reduces the activity nearly to baseline. Baseline activity is caused by a low amount of Tαβγ still attached to the membranes (see inset). Inset, SDS-PAGE of purified native transducin (only Tα and Tβ subunits are shown), recombinant human UNC119 and depleted ROS membranes containing rhodopsin and a trace of transducin (only Tα is visible, Tβ co-migrates with rhodopsin).

Fig. 2.8
Zhang et al.

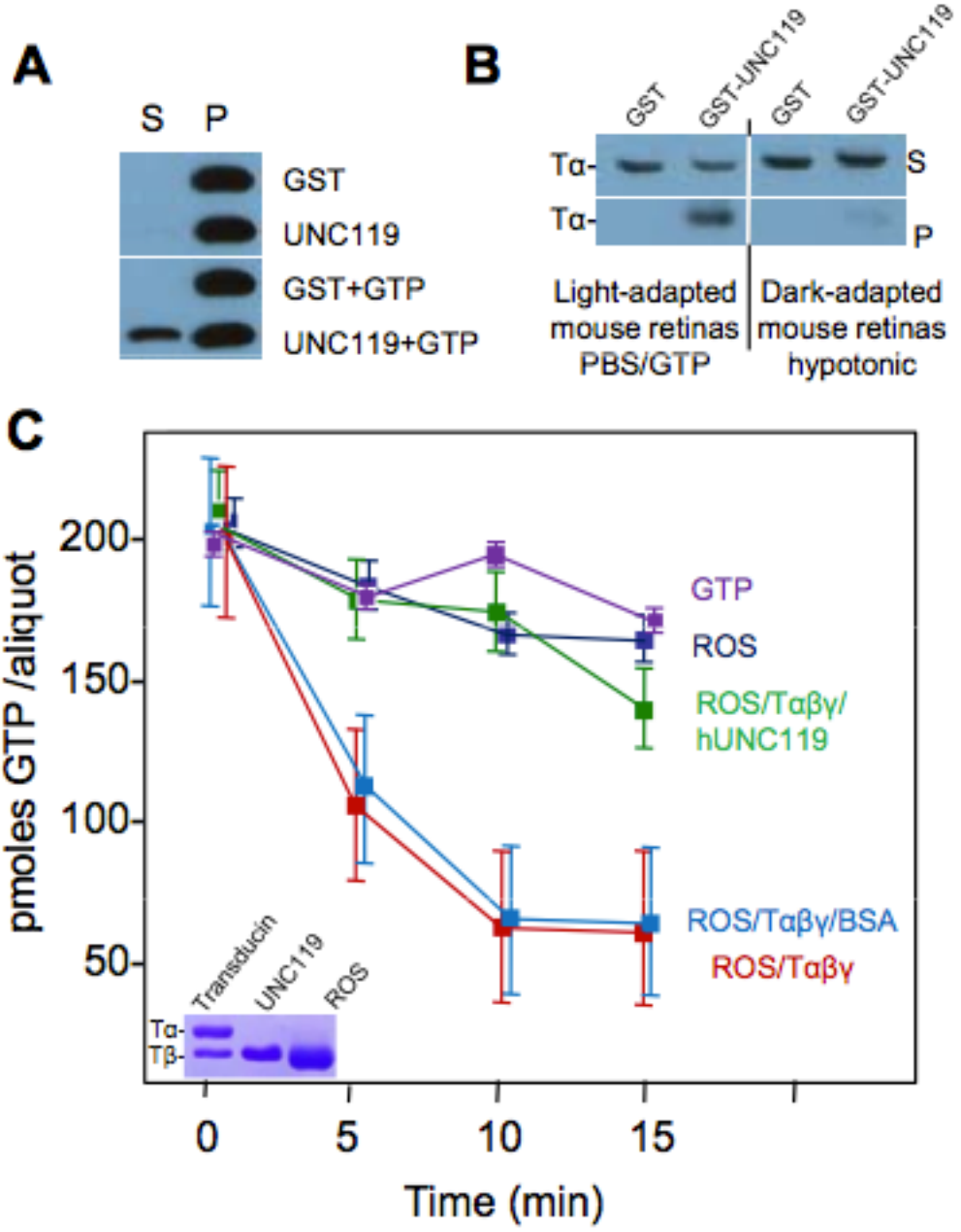

Figure 2.9 Slow Return of Transducin to the Outer Segment after Intense Light Exposure. (**A,B**) Localization of Tα (green) in dark-adapted wild-type and Unc119$^{-/-}$ retina. Mice were dark-adapted for at least 12 hours. Frozen sections were probed with anti-Tα antibody and FITC-linked secondary antibody. Note the presence of Tα in dark-adapted inner segments. (**C–J**) Mice were first exposed to intense light for 60 minutes, then dark-adapted for 0-24 hours. Frozen sections were probed with anti-Tα and FITC-linked secondary antibody. Note that Tα slowly returns to the wild-type outer segment, but is blocked in part from returning to the *Unc119*$^{-/-}$ outer segment. OS, outer segment; IS, inner segment; ONL, outer nuclear layer. (**K**) Quantification of inner segment fluorescence at 0, 3, 6, and 24 hours after start of dark-adaptation. Fluorescence signal was quantified using ImageJ software. Each bar included three independent measurements. Error bars denote means ± SD

Fig. 2.9
Zhang et al.

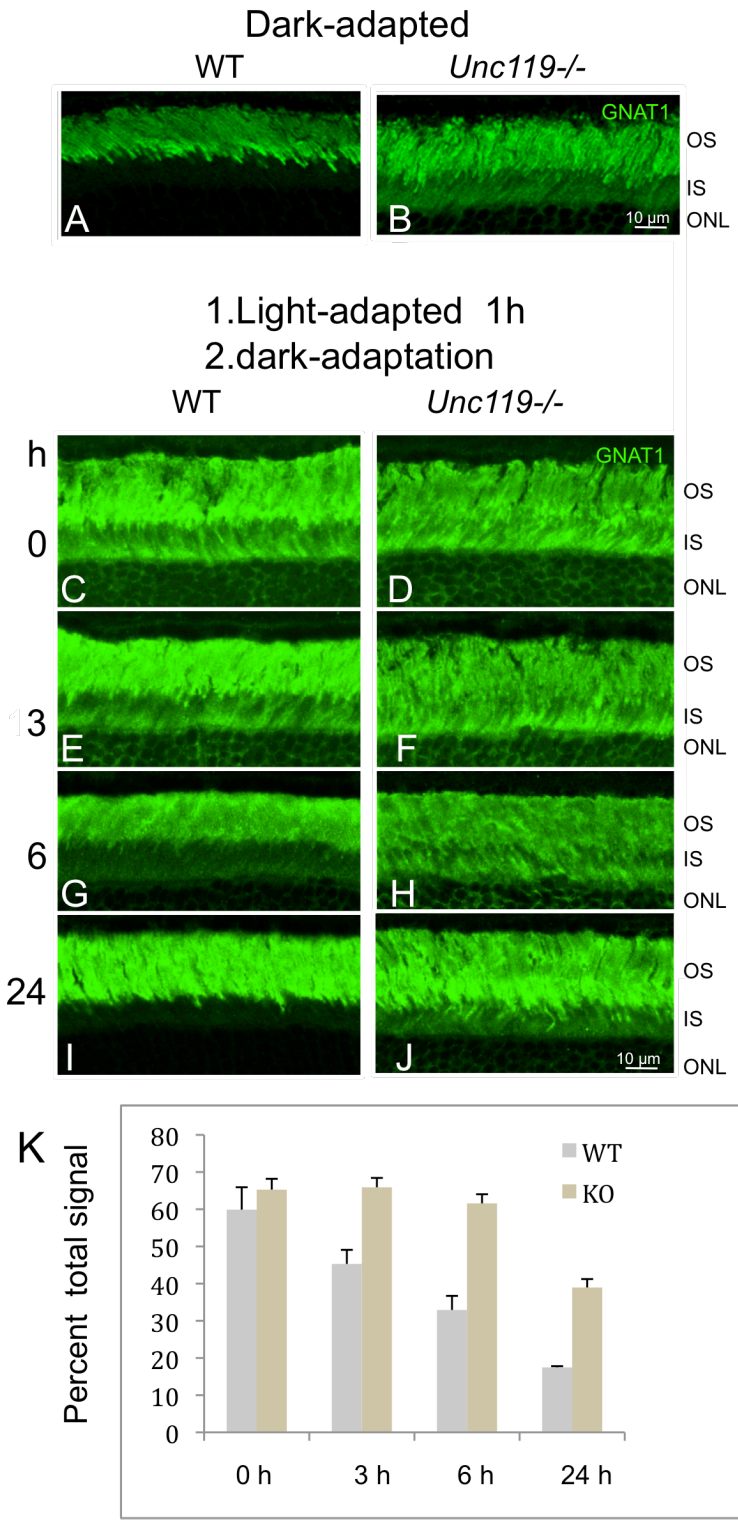

A fascinating property of transducin is its observed translocation to the inner segment in-bulk during intense light exposure as part of a light-adaptation and desensitization mechanism. Under intense light, $T\alpha^{GTP}$ and Tβγ translocate individually to the inner segment within minutes[30, 31] by diffusion[32]. Both Tα and Tβγ return to the outer segments in hours during prolonged dark-adaptation[30], presumably by restricted diffusion[29], as transducin does return to outer segments in eyecups depleted of ATP, which is required for molecular motor-driven transport. To determine the effect of UNC119 deletion on the return of transducin by diffusion, we exposed wild-type and *Unc119*$^{-/-}$ mice to intense light for 60 min followed by prolonged dark-adaptation (0-24 hours) (**Fig. 2.9C–K)**. Return of Tα was nearly complete in wild-type photoreceptors after three hours of dark-adaptation, yet a significant amount of Tα remained associated with *Unc119*$^{-/-}$ inner segment membranes following prolonged dark-adaptation (**Fig. 2.9F,H,J**). The partial efficacy of UNC119 deletion on Tα mislocalization and the resulting slow degeneration may be attributable to redundant UNC119 isoforms (see discussion).

Trafficking of ODR-3 and GPA-13 in *C. elegans* olfactory neurons requires UNC119. Originally discovered in *C. elegans*, *unc-119* mutants exhibit a complex phenotype, including defects in chemosensation, altered feeding behavior, inability to form dauer larvae[8] and excessive branching of motor neuron commissures[33]. We suspected G-protein participation in polypeptide trafficking to olfactory cilia and investigated the consequences of the *unc-119* deletion in *C. elegans* olfactory neurons. Although several G proteins participate in chemosensory signal transduction, ODR-3, predicted to be acylated at G2, is required to mediate signal transduction in AWA and

AWC sensory neurons[34]. ODR-3 is localized predominantly to the cilia, with only trace amounts found in the dendrites and cell bodies[35]. Immunolabeling of wild-type (**Figs. 2.10A, 2.11A**) and *unc-119* mutant worms (**Figs. 2.10B, 2.11B**) with antibody directed against ODR-3 revealed mislocalization of ODR-3 in the *unc-119* mutant worms. Correspondingly, while GPA-13 was present in the cilia of both wild-type (**Figs. 2.10C, 2.11C**) and *unc-119* mutant (**Figs. 2.10D, 2.11D**) ADF, ASH and AWC chemosensory neurons[35] , it was down-regulated and mislocalized in the mutant worm.

Reduced amounts of ODR-3 and GPA-13 present in the cilia of mutant worms could arise indirectly from abnormal neuronal morphology. To exclude this possibility, transgenic worms specifically expressing GFP in AWA, AWB or AWC neurons were crossed onto the *unc-119* mutant background. Ciliated endings of AWA and AWB neurons in *unc-119* mutants (**Fig. 2.11F,H**) were identical to wild-type (**Fig. 2.11E,G**), but the shape of the AWC sensory ending in *unc-119* mutants (**Fig. 2.11J**) was slightly different from wild-type (**Fig. 2.11I**). As the ciliary morphology of AWC neurons in the *unc-119* mutant was normal, however, it seems improbable that the decreased ODR-3 and GPA-13 protein levels observed in *unc-119* mutants were caused by disrupted cellular integrity.

To determine whether expression of transgenic, wild-type *unc-119* could restore G protein stability in amphid neurons, GFP::UNC-119 driven by the *gpa-13* promoter was introduced into *unc-119* mutant worms. GFP::UNC-119 expression was found in three pairs of amphid sensory neurons--presumably ADF, ASH and AWC (**Fig. 2.10E,G**). Labeling with anti-GPA-13 antibody showed an increase in GPA-13

Figure 2.10 Mislocalization of the G proteins ODR-3 and GPA-13 in a *C. elegans unc-119(ed3)* mutant. (**A–D**) Wild-type(A,C) and *unc-119* mutant (B,D) *C. elegans* were stained with an anti-ODR-3 (A,B) and anti GPA-13 (C,D) antibody. Mislocalization of ODR-3 and GPA-13 to the olfactory cell bodies and axons is evident in *unc-119* mutants. (**E–H**) Cell-specific rescue of *unc-119* in *C. elegans* restores GPA-13 and ODR-3 localization. The *unc-119* gene fused with GFP was driven by the *gpa-13* promoter in ADF, ASH and AWC in *unc-119* mutants. The transgenic (E,G) and *unc-119* mutant control (**F,H**) were labeled with GPA-13 (E,F**)** or ODR-3 antibodies (G,H).

Fig.2.10
Zhang et al.

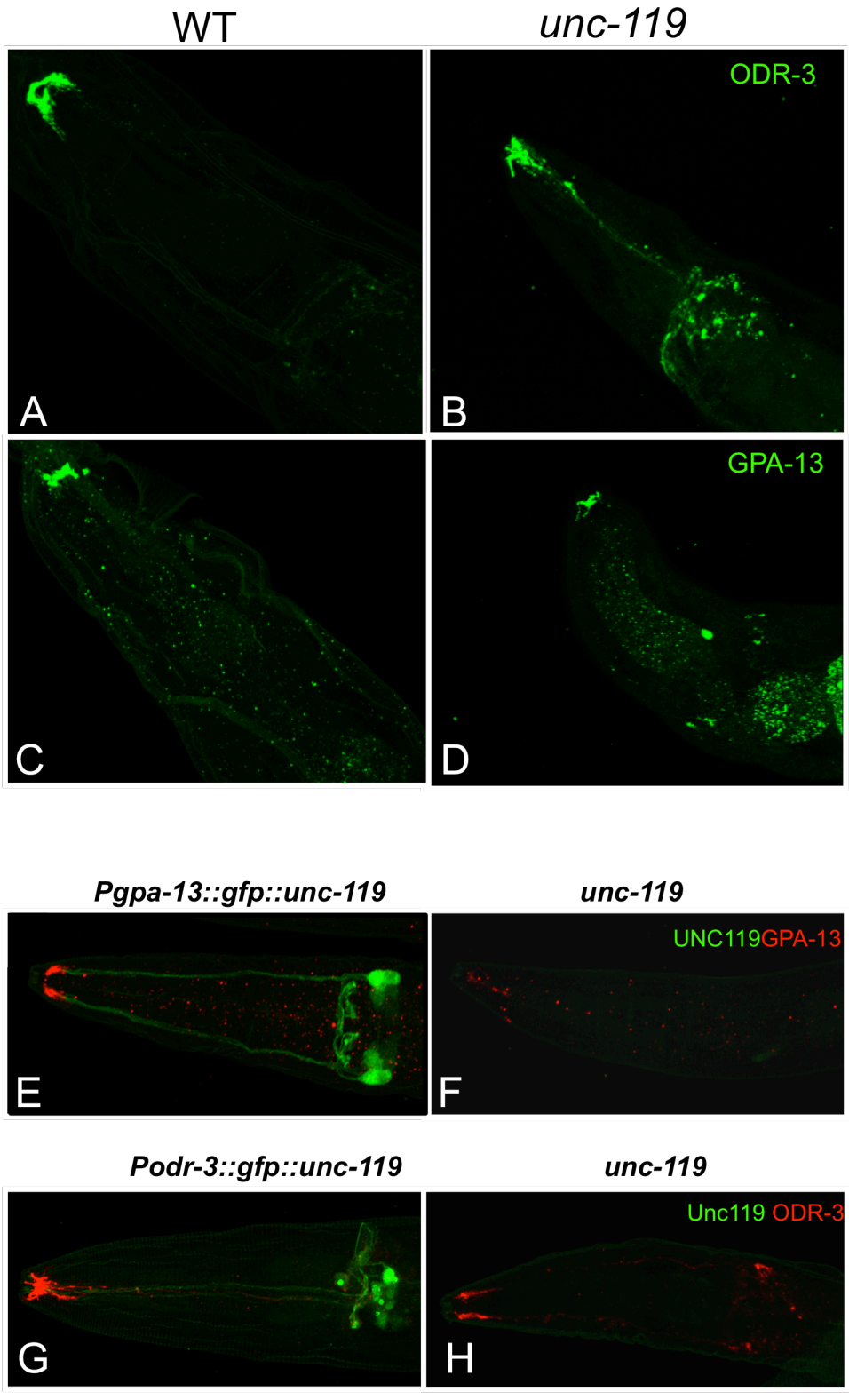

Figure 2.11. ODR-3 and GPA-13 Trafficking Defects in Mutant *C. elegans* Olfactory Neurons.
A-D, localization of ODR-3 (A, B) and GPA-13 (C,D) in wild-type (A,C) and *unc-119* mutant (B,D) *C. elegans* olfactory neurons. In wild-type neurons, ODR-3 and GPA-13 (green) traffic normally to the olfactory cilia. In mutant neurons, the G protein subunits are mislocalized (B, ODR-3) or exhibit decreased expression (D, GPA-13).
E-J, structural Integrity of AWA, AWB and AWC Cilia in *unc-119 C. elegans* and restoration of ODR-3 and GPA-13 Localization. GFP was specifically expressed in AWA neurons (E,F), AWB neurons (G,H), and AWC neurons (I,J) of wild-type (left column) and *unc-119* mutant (right column) *C. elegans* worms. Reporter constructs were odr-10::gfp for AWA, str-1::GFP for AWB, and str-2::GFP for AWC. The structural integrity of these neurons is not compromised in the mutant (F,H,J) when compared to WT (E,G.I). Please note that transgene *kyIs140* in the *unc-119* mutant background only expressed GFP in one of the two AWC neurons (**Fig. S3I,J**), while some of the transgenic worms expressed GFP in both AWC neurons (unpublished data). Similar phenomena have been reported for other mutants [1].

Fig. 2.11
Zhang et al.

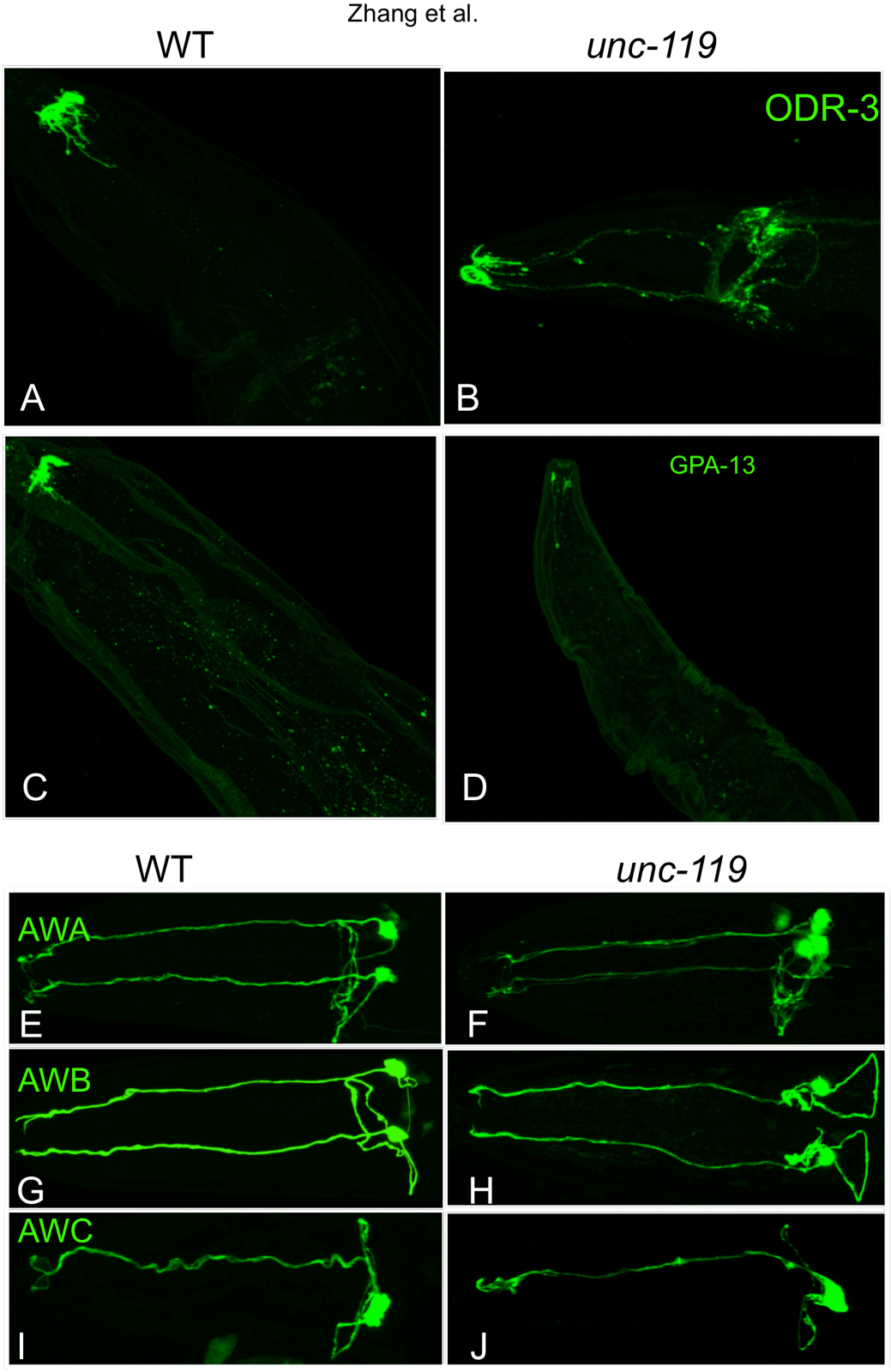

immunoreactivity in the cilia of the transgenic worms (**Fig. 2.10E**) relative to nontransgenic *unc-119* mutants (**Fig. 2.10F**). Because ODR-3 is also expressed in ADF, ASH and AWC neurons, transgenic worms were also labeled with anti-ODR-3 antibody. Increased levels of ODR-3 were also detected in the cilia of transgenic worms (**Fig. 2.10G**) relative to nontransgenic *unc-119* mutant worms (**Fig. 2.10H**). Transgenic expression of supplemental UNC-119 in these neurons was capable of restoring the wild-type phenotype.

Discussion

The immunoglobulin β-sandwich fold demonstrated by the crystal structure of human UNC119 is similar to that seen in PrBP/δ (PDB ID:1KSH)[23] and RhoGDI (PDB ID:1DOA)[22]. PrBP/δ is a prenyl binding protein and an important cofactor in the transport of prenylated proteins in photoreceptors[5]. RhoGDI extracts C-terminally geranylgeranylated Rac, Rho, and CDC42 from membranes providing a hydrophobic environment for their prenyl anchors in its pocket, thereby trapping these small G proteins in their inactive GDP bound form[22]. The β-strands of PrBP/δ and UNC119 align nicely when the two structures are superimposed (**Fig. 2.3A**), while the β-strands of RhoGDI and UNC119 are more divergent (**Fig. 2.3B**). Important differences are seen in the UNC119 structure. The entrance through which the lipid enters the hydrophobic pocket in RhoGDI (and presumably PrBP/δ) is located at the opposite edge of the β-sandwich fold. The opening of the UNC119 pocket is completely occupied by the first six amino acids of Tα with the acyl chain deeply inserted into the cavity. These data, along with the extensive interactions that limit the depth to which the Tα peptide can penetrate the UNC119 cavity (**Figs. 2.6C, 2.3A,B**), support the assertion that interaction specificity

with lipidated proteins is based in part upon the amino acid sequence immediately adjacent to the posttranslational modification.

UNC119 and G protein trafficking. G-protein subunits are either co-translationally acylated or acylated by an unidentified ER-resident acyl transferase. Acylated Gα and prenylated Gβγ most likely combine to form heterotrimeric G proteins at the ER[28]. Our results (**Fig. 2.9B**) show that the deletion of UNC119 in mouse leads to partial retention of transducin in the inner segment even after complete dark-adaptation, leaving post-biosynthesis transport largely intact. The partial effect seen in the *UNC119*$^{-/-}$ mouse is likely due to the redundancy of UNC119 isoforms. UNC119B, encoded by the *UNC119B* gene located on human chromosome 5 (*UNC119* is on chromosome 17) is 61% similar and 52% identical to UNC119 and like GST-UNC119, GST-UNC119B pulls down Tα from bovine retina lysate (RC and WB, unpublished results).

In contrast to vertebrates, the *C. elegans* genome harbors only one UNC119 gene. Accordingly, *unc-119* null mutant phenotypes are more severe and UNC-119 deletion affects both neuronal and non-neuronal cells resulting in a complex phenotype. We focused on olfactory neurons as defects in chemosensation have been reported in unc-119 worms[8]. *C. elegans* relies on its 11 pairs of amphid neurons to detect odorants and soluble molecules[36]. These sensory neurons are polarized ciliated cells with an overall morphology similar to vertebrate photoreceptors. *unc-119* deletion in the worm results in the mislocalization and mistargeting of the G proteins ODR-3 and GPA-13, which are expressed in AWA, AWB, and AWC as well as in ASH and ADF amphid cells (**Fig. 2.10B,D**). Proper localization of ODR-3 and GPA-13 was restored by expressing transgenic UNC119 under the control of their intrinsic promoters (**Fig. 2.10E,G**).

Interestingly, ODR-3, GPA-13 and Tα share only 27% overall sequence identity, with sequence similarity at the N-terminal 50 amino acids being very limited. The ODR-3 N-terminal peptide shares only three of ten amino acids with the Tα peptide (**Fig. 2.5C**), resulting in a lower affinity interaction with human UNC119 as shown by isothermal titration calorimetry (**Fig. 2.5B**).

Light-induced translocation of transducin by diffusion. Light-activation of rhodopsin triggers GTP/GDP exchange on Tα causing $T\alpha^{GTP}$ and Tβγ to dissociate and traffic to the inner segment by passive diffusion with a $t_{1/2}$ of 3-5 min for Tα and a $t_{1/2}$ of approximately 12 min for Tβγ[32]. Tβγ is known to associate with phosducin, which reduces its affinity for both Tα and rod outer segment membranes[37]. Upon return to the dark, both Tα and Tβγ subunits return to the outer segments in hours in wild-type mice. This same phenomenon has previously been described in eyecups depleted of ATP, without which, molecular motors do not function [29]. Therefore, a model in which "restricted" diffusion is responsible for the return of Tα and Tβγ to the outer segments is plausible.

We propose that the restriction is provided by an enzymatically switchable sink in the inner segments. We determined that UNC119 elutes Tα bound to membranes only in the presence of GTP (**Fig. 2.8B**), suggesting that the dissociation of $T\alpha^{GTP}$ and Tβγ is essential for UNC119/$T\alpha^{GTP}$ complex formation. Upon arrival at the inner segment following light-induced translocation (**Fig. 2.12A**), transducin subunits are presumed to recombine after Tα's intrinsic GTPase activity hydrolyzes GTP, permitting heterotrimeric transducin to dock to inner segment membranes which are devoid of rhodopsin. In the absence of the guanine exchange factor rhodopsin (**Fig. 2.12B**), GTP/GDP exchange is

Figure 2.12 Light-induced translocation of transducin and retun to the outer segement

(**A**) Schematic depiction of transducin translocation. Under intense light, $T\alpha^{GTP}$ and $T\beta\gamma$ translocate separately to the inner segment and following GTP hydrolysis, associate with inner segment membranes as a heterotrimer $T\alpha^{GDP}\beta\gamma$. Following GDP/GTP exchange, which is very slow in the absence of rhodopsin, $T\alpha^{GTP}$ is eluted from the membrane by the acyl-binding protein UNC119. $T\beta\gamma$ elutes and associates with a prenyl binding protein, either PrBP/δ or phosducin[37]. Both Tα/UNC119 and Tβγ/PrBP diffuse freely and reassociate with a destination membrane after GTP hydrolysis. The destination membrane could be the cell membrane at the distal inner segment where IFT cargo is assembled or one of many outer segment disks. (**B**) Kinetic analysis of return to the OS. In the absence of a GEF (rhodopsin), solubilization of Tα governed by GDP/GTP exchange is slow ($k= 10^{-4}$/sec)[38], and is most likely the rate limiting step for the return of transducin. Likewise, the hydrolysis of $T\alpha^{GTP}$ is slow ($k=0.025\ sec^{-1}$) in the absence of GAP, but not rate-limiting. GDP/GTP exchange maintains a rate constant of 0.0001/sec, resulting in only 0.01% of Tα solubilised per second[38], or one-third of Tα/hour, which explains the slow return to the outer segment.

Fig. 2.12
Zhang et al.

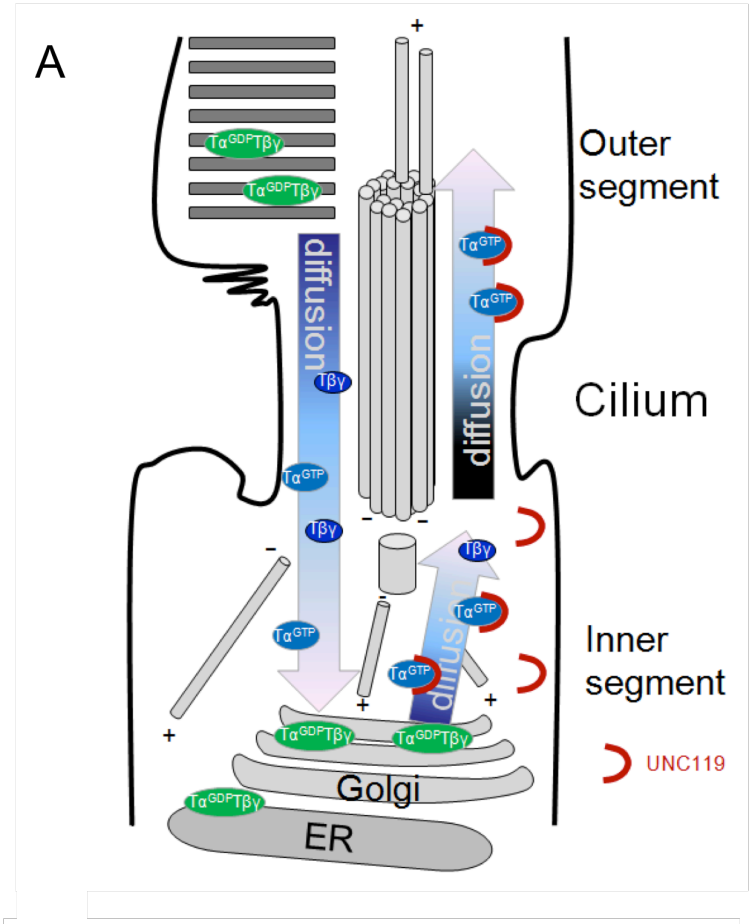

very slow (rate constant 10^{-4}/sec)[38]. Both the GTP requirement for Tα extraction from membranes and the slow rate constant suggest that this event is the rate-limiting step for return to the outer segment (**Fig. 2.12B**). The rate constant dictates that it will take approximately 10^4 seconds (166 minutes) for transducin to return to the outer segment, which agrees with experimentally observed return rates[31, 32]. Upon solubilization of the UNC119/Tα-GTP complex, it likely diffuses passively through the inner segment and connecting cilium, depositing Tα directly at discs in the outer segment. Following $T\alpha^{GTP}$ solubilization, PrBP/δ may extract Tβγ, whose transport to the outer segment is severely affected in a PrBP/δ deletion model [5]. An alternate candidate for interaction with Tβγ is phosducin, deletion of which affects light-driven translocation of Tβγ to the inner segment[37]. The detection of UNC119 in the mouse photoreceptor sensory cilium complex[9] suggests a possible role for UNC119 in cargo assembly and IFT, an argument that is further strengthened by the association of UNC119 with ARL3 and RP2 (retinitis pigmentosa protein 2), both of which localize to mouse and human cilia[9, 15].

Our data provide evidence for UNC119 functioning as a novel lipid binding protein as well as a necessary component in G protein trafficking. UNC119, along with G proteins, is distributed in virtually all living organisms from unicellular flagellated amoeba to mammals. Thus, our data in both mouse and *C. elegans* will likely prove helpful in elucidating mechanisms involved in membrane protein transport in the sensory systems of other species.

Protein Data Base Accession

UNC119: PDB 3GQQ
UNC119/lauroyl-GAGASAEEKH: PDB 3RBQ

Acknowledgments

We thank Randy Abramowitz and John Schwanof for access to the X4A beamline at NSLS; G. DeTitta of Hauptman Woodward Research Institute for crystallization screening. This work was supported by National Institute of Health grants EY08123 (WB), EY019298 (WB), EY014800-039003 (NEI core grant), EY10848 (GI), by the Howard Hughes Medical Institute (EJ) and by NIH Grant NS034307 (EJ), by a grant from the Protein Structure Initiative of the National Institutes of Health (U54 GM074958), by the University of Utah Macromolecule Crystallography Core Facility, by a Center Grant of the Foundation Fighting Blindness, Inc., (Columbia MD), to the University of Utah, and unrestricted grants to the Departments of Ophthalmology at the University of Utah from Research to Prevent Blindness (New York. N.Y.). WB is a recipient of a Research to Prevent Blindness Senior Investigator Award.

Author Contributions

HZ generated pull-down/light-induced translocation results and is responsible for *C.elegans* immunostaining and imaging; RC generated ITC results; RC, FGW and CPH generated human UNC119/acylated Tα-peptide co-crystals and solved the structure; SV, YC, JS, YJH, RX, GTM, and LT determined the human UNC119 structure; RC, CDG, and WB isolated ROS membranes, transducin and determined GTPase activity; MWD and EMJ generated transgenic C. elegans mutants; GI generated the Unc119 knockout mouse; HZ, RC, CPH, LT and WB wrote the manuscript.

Online Methods

Animals. Mice were maintained in a 12:12 h dark-light cycle. The animals' care was approved and maintained in accordance with institutional guidelines (IACUC) and the ARVO Statement for the Use of Animals in Ophthalmic and Vision Research. To dark-adapt, the mice were placed in the dark for 12 hours or more. For light-adaptation, the pupils of the mice were dilated with 1% Tropicamine and the mice were illuminated by 2,000 lux for 25 minutes. Following light-adaptation, mice were returned to the dark for 1.5, 3, 6 or 24 hours. *Unc119*$^{-/-}$ mice were from the colony of GI [12]. *Gnat1*$^{-/-}$ animals were obtained from Dr. Janis Lem.

***C. elegans* Strains.** Strains were maintained using standard methods. Strains were obtained from Caenorhabditis Genetics Center, Morris Maduro, and Piali Sengupta. Stably integrated strains used in this work were *oyIs[P(odr-10)::gfp] V* for examining AWA neurons, *lin-15(n765ts) X kyIs104[str-1::GFP, lin-15(+)] X* for examining AWB neurons[39], and *kyIs140[str-2::GFP + lin-15(+)]* for examining AWC neurons[39]. The AWA, AWB, and AWC neurons expressing the above stably integrated GFP markers were also examined in *unc-119(ed3)* mutants. Double mutant strains were generated using standard methods.

Crystallization of UNC119. Expression and purification of truncated human UNC119 protein (residues 56-240) was carried out as a part of the established high throughput protein production pipeline[40] (Northeast Structural Genomics Consortium (NESG) target HR3066a). The protein was cloned into the pET 14-15C expression vector (Novagen). Selenomethionyl protein was expressed in *Escherichia coli* BL21(DE3) +

Magic, purified using Ni-NTA affinity chromatography (Qiagen) and gel filtration (Superdex 75, Amersham/GE Healthcare) in buffer containing 10 mM TrisHCl , 100 mM NaCl, 5 mM DTT, pH 7.5. Protein homogeneity was verified by SDS-PAGE and MALDI-TOF mass spectrometry.

Preliminary crystallization trials were performed using the microbatch crystallization under paraffin oil at 4°C[41]. UNC119 crystals useful for structure determination were grown in a 1:1 ratio with solution containing 40% PEG 4000, 0.1M K acetate, 0.1M Na acetate, pH 5.0 at 4°C. The crystals grew to 0.025 – 0.05 – 0.1 mm after three - four weeks and were transferred to paratone oil and frozen in liquid propane. Single crystals were maintained at 100K and used to collect a SAD data set at beamline X4A at the National Synchrotron Light Source (NSLS) using an ADSC Quantum-4 CCD detector. Data were integrated and scaled using the HKL2000 package[42]. SHELXE/D [43] was used to locate selenium sites and calculate initial phases. Solvent flattening and partial model building were performed using RESOLVE [44]. The remainder of the model was built manually using COOT[45] and was refined with PHENIX [46]. Data collection and refinement statistics are presented in **Table 2.1**. The quality of the model was checked using MolProbity[47]. The atomic coordinates and structure factors for UNC119 (PDB ID 3GQQ) have been deposited in the Protein Data Bank.

UNC119/ lauroyl-GAGASAEEKH crystal growth and data collection.

UNC119 (**Table 2.1**) was co-crystallized with a Tα peptide (lauroyl-GAGASAEEKH). Purified UNC119 and the Tα peptide were dissolved in 10 mM Tris pH 7.4, 100 mM NaCl, and 5 mM DTT. The protein solution was prepared by mixing purified UNC119 and the Tα peptide (1:1.1 molar ratio) for at least 1 hour at 4 °C. Crystals were grown in

drops containing 3 μL UNC119 Tα peptide mixture and 3 μL 40% PEG 5000, 0.1 M sodium acetate, 0.1 M potassium acetate, pH 5.0, and 1.8 μL 30% isopropanol at 4 °C, under 40 μL paraffin oil. Crystals were harvested for data collection after 10 to 14 days. Crystals were mounted in a nylon loop, briefly immersed in cryoprotection buffer (40% PEG 5000, 0.1 M sodium acetate, 0.1 M potassium acetate, 12% glycerol, pH 5.0) and cooled by plunging into liquid nitrogen. Crystals were maintained at 100 K during data collection. Data were collected at beam line BL9-2 of the Stanford Synchrotron Radiation Lightsource. Data were integrated and scaled using DENZO and SCALEPACK, respectively[42]. Data were phased by molecular replacement using PHASER[48] using PDB code 3GQQ as the search model. The models were rebuilt using O[49] and refined against a maximum likelihood target function using REFMAC[50]. Structures were checked using MolProbity[47].

Expression and purification of recombinant bovine UNC119 protein. The *UNC119* cDNA was amplified by PCR from a bovine retina cDNA library and cloned into the BamHI/EcoRI sites of a pGEX-2T vector (Amersham/GE Healthcare). A His-tag (6 histidines) was placed immediately following the ATG of the *UNC119* cDNA. The construct was transformed into an expression *E. coli* strain ER2556 (New England Biolab). Expression of the recombinant protein was induced by 0.1 mM IPTG for 5 hours at 37 °C. The protein was purified by a Histrap (Amersham/GE Healthcare) column followed by a GSTrap column (Amersham/GE Healthcare) according to the manufacturer's protocol and reduced GSH was removed by a Microcon centrifuge filter with an exclusion size of 30 kD (Millipore).

Expression and purification of recombinant human UNC119. *Unc119* cDNA was amplified by PCR from a human retina cDNA library and directionally cloned into a pET151/D-TOPO vector (Invitrogen). The 6x His-tag in the vector was converted to a 12x His-tag using a QuickChange site-directed mutagenesis kit (Stratagene) and verified by DNA sequencing. The construct was expressed in BL21 Codon+ *E. coli* cells (Stratagene) in ZY autoinduction media for 6 hours at 37^{o} C and then overnight at 19^{o} C. Cells were harvested by centrifugation, resuspended, and lysed in 10 mg/mL lysozyme in lysis buffer (20 mM imidazole, 700 mM NaCl, 50 mM Tris pH 7.4, 1 mM DTT) and protease inhibitors (PMSF, aprotinin, leupeptin, pepstatin) for 1 hour at 4^{o} C, followed by sonication. The lysate was clarified by centrifugation (45 min, 15000 rpm) and soluble hUNC119 protein was bound to a Ni^{2+} sepharose column (Amersham/GE Healthcare), washed with 10 column volumes of lysis buffer and eluted with 300 mM imidazole in 700 mM NaCl, 50 mM Tris pH 7.4, and 1 mM DTT. Fractions were assayed by SDS-PAGE, pooled, and the 12x His-tag was removed by incubation with TEV protease (~1 mg/100mg protein, 20 h at 25^{o} C.) in 2 L of 500 mM NaCl, 50 mM Tris pH 7.4, and 1 mM DTT. Unprocessed protein and TEV were removed by Ni^{2+} sepharose chromatography, cleaved protein was collected in the flow through, concentrated, and purified to homogeneity by anion exchange (HiTrap Q FF, GE Life Sciences, 20-1000 mM NaCl gradient in 25 mM Tris pH 7.4, 1 mM DTT) and gel filtration (SD200, Amersham/GE Healthcare), 100mM NaCl, 25 mM Tris pH 7.4, 1 mM DTT) chromatography.

Pulldown assays. For protein sequencing, a bovine retina was homogenized by brief sonication in 1 ml PBS buffer (137 mM NaCl, 2.7 mM KCl, 10 mM Na_2HPO_4. 1.76

mM KH_2PO_4 pH 7.4) with 1mM DTT and protease inhibitor cocktail (Roche). The insoluble debris was removed by centrifugation. The retina lysate was mixed with 10-80 μg of purified GST-UNC119 or 40 μg of GST followed by overnight incubation at 4°C. GST-UNC119 and its interacting proteins were pulled down by glutathione beads and the bound proteins were eluted with SDS gel loading buffer. The proteins were resolved by 12.5% SDS-PAGE. The protein sequencing by LC-MS/MS was carried out in the Mass Spectrometry Core Facility at the University of Utah.

For the competitive binding assay (**Fig. 2.5A**), 400 μl of retina lysate was incubated with 10 μg GST-UNC119 in the presence of 150 μg lauroyl-GAGASAEEKH and GAGASAEEKH peptides, respectively. All peptides were synthesized by the Utah Peptide Core facility.

For pull downs with light- and dark-adapted retinas, mouse retinas were homogenized in 1xPBS buffer containing 40 μM GTP (light) or hypotonic buffer (dark) (10 mM TrisHCl pH 7.4, 1 mM EDTA, 0.1 mM DTT). The insoluble fraction was removed by centrifugation. The supernatant was used for pulldown assays using GST and GST-UNC119. Solubilized transducin was reconstituted in 1xPBS buffer, pulled down with GST-UNC119 and identified by western blot using anti-Tα antibody (UUTA).

Immunoblot. Proteins were separated by 12.5% (for detection of Tα and GCAP1) or 15% (for detection of Tα and Tγ) SDS-PAGE and transferred to a nitrocellulose membrane. Membranes were processed as described [24]. The dilutions of the primary antibodies were 1:10,000 for SC389 (anti-rod Tα, Santa Cruz Biotechnology), 1:6,000 UW101 (anti-GCAP1), 1:10,000 for UUTA (anti-rod Tα) and 1:5000 for GN2 (anti-rod Tγ). UUTA and GN2 were obtained from Dr. CK Chen (VCU).

Extraction of transducin from mouse retinal membrane by UNC119. Mouse retinas were prepared from wild-type mice undergoing 20 min light-adaptation followed by 30 min dark-adaptation. The retinas were homogenized in 200 µl PBS with 1 mM DTT and protease inhibitors. The soluble components were removed by centrifugation at 4 °C for 10 min. The pellet was washed once with PBS, resuspended in 400 µl PBS, and aliquoted in four microcentrifuge tubes. In these four tubes, 9 µg GST, 9 µg GST and 40 µM GTP (final concentration), 18 µg GST-UNC119, and 18 µg GST-UNC119 and 40 µM GTP (final concentration) were added, respectively. After overnight incubation at 4°C, the membrane was pelleted and the supernatant was removed. The pellet was resuspended in 100 µl PBS. 10 µl of the supernatant from each tubes and their corresponding pellets were subjected to western blot using anti-Tα antibody (UUTA).

***In vitro* expression of Tα and Tα(G2A).** *Gnat1* cDNA was amplified from a bovine cDNA library and cloned into the XhoI and NotI sites of pEGFP-N2 vector to replace the eGFP gene. The G2A mutant construct was generated by site-directed mutagenesis kit (Stratagene). Hek293 cells were transfected using Lipofectamine 2000 (Invitrogen) following the manufacturer's instructions. The cells were harvested 48 hours after transfection.

Immunocytochemistry of retina sections. Immunocytochemistry was peformed as described [5]. Dilutions for the primary antibodies were 1:1000 for UUTA (anti-rod Tα), 1:1000 for G8 (anti-GRK1). FITC-conjugated secondary antibodies were diluted 1:300.

Isothermal titration calorimetry. The transducin N-terminal peptides lauroyl-, myristoyl-GAGASAEEKH or GAGASAEEKH, and recombinant human UNC119 protein samples were suspended in 25 mM Tris (pH 7.4), 100 mM NaCl, and 1 mM DTT.

Peptide and hUNC119 concentrations were varied as a result of the varying solubility of the peptides in the above-described buffer. ITC measurements were done on a MicroCal ITC-200 MicroCalorimeter at 25 ^{o}C. The peptide was injected into the hUNC119 samples at 180 sec intervals. Data obtained from the peptide injections into the buffer blanks were subtracted from the experimental data for analysis using the MicroCal Origin Software.

GTPase assay. Transducin and depleted ROS membranes were purified from bovine retinas as previously described [27].The GTPase assay mix (20 µl) contained 4 pmoles (0.17 µg) rhodopsin (in depleted ROS membranes), 54 pmoles transducin (4.5 µg), 61 µM GTP spiked with γ-P^{32}-GTP, 20 mM Tris HCl pH 7.5, 5 mM $MgCl_2$, 1 mM DTT, and 0.1 mM EDTA. Some assays included 133 pmoles UNC119 (2.27 µg) or 130 pmoles of bovine serum albumin (BSA). Assays were incubated at 35^{o}C, 2 ul aliquots were withdrawn at 0, 5,10,15,20 minutes and spotted on PEI cellulose (Brinkmann). The PEI plates were washed in 0.12 M LiCl (30 min) and quantitated using a Typhoon Trio (GE Health Sciences) and Image Quant software.

Immunocytochemistry of *C. elegans.* Animals were permeabilized, fixed, and stained following standard methods. The images were acquired using an FV1000 Olympus confocal microscope. Polyclonal ODR-3 and GPA-13 antibodies were gifts from Dr. Gert Jansen (Center for Biomedical Genetics, Rotterdam, The Netherlands).

Cell-specific rescue of *C. elegans unc-119* mutant. The DNA used for microinjection was generated by fusion PCR. Briefly, the GFP gene was amplified by PCR from pPD104.53 (provided by Andrew Fire, Stanford) and cloned into P#MM016, in which the GFP cDNA was fused in frame to the 5' of *unc-119* genomic DNA. The gfp-*unc119* fusion gene including the flanking transcription termination sequence was

amplified by PCR. A 2.7 kb promoter sequence of *gpa-13* was amplified from *C. elegans* genomic DNA. The 3' end of the *gpa-13* promoter was fused to the 5' end of the *gfp-unc119* fusion gene by nested-PCR. The PCR product from the fusion PCR was microinjected into the germline.

References

1. Rosenbaum,J.L. & Witman,G.B. Intraflagellar transport. *Nat. Rev. Mol. Cell Biol.* 3, 813-825 (2002).

2. Jin,H. *et al.* The conserved Bardet-Biedl syndrome proteins assemble a coat that traffics membrane proteins to cilia. *Cell* 141, 1208-1219 (2010).

3. Kim,J., Krishnaswami,S.R., & Gleeson,J.G. CEP290 interacts with the centriolar satellite component PCM-1 and is required for Rab8 localization to the primary cilium. *Hum. Mol. Genet.* 17, 3796-3805 (2008).

4. Gillingham,A.K. & Munro,S. The small G proteins of the Arf family and their regulators. *Annu. Rev. Cell Dev. Biol.* 23, 579-611 (2007).

5. Zhang,H. *et al.* Deletion of PrBP/{delta} impedes transport of GRK1 and PDE6 catalytic subunits to photoreceptor outer segments. *Proc. Natl. Acad. Sci U. S. A* 104, 8857-8862 (2007).

6. Keller,L.C. *et al.* Molecular architecture of the centriole proteome: the conserved WD40 domain protein POC1 is required for centriole duplication and length control. *Mol. Biol. Cell* 20, 1150-1166 (2009).

7. Chung,S., Kang,S., Paik,S., & Lee,J. NgUNC-119, Naegleria homologue of UNC-119, localizes to the flagellar rootlet. *Gene* 389, 45-51 (2007).

8. Maduro,M. & Pilgrim,D. Identification and cloning of unc-119, a gene expressed in the Caenorhabditis elegans nervous system. *Genetics* 141, 977-988 (1995).

9. Liu,Q. *et al.* The proteome of the mouse photoreceptor sensory cilium complex. *Mol. Cell Proteomics.* 6, 1299-1317 (2007).

10. Higashide,T., Murakami,A., McLaren,M.J., & Inana,G. Cloning of the cDNA for a novel photoreceptor protein. *J. Biol. Chem.* 271, 1797-1804 (1996).

11. Swanson,D.A., Chang,J.T., Campochiaro,P.A., Zack,D.J., & Valle,D. Mammalian orthologs of C. elegans unc-119 highly expressed in photoreceptors. *Invest. Ophthalmol. Vis. Sci.* 39, 2085-2094 (1998).

12. Ishiba,Y. *et al.* Targeted inactivation of synaptic HRG4 (UNC119) causes dysfunction in the distal photoreceptor and slow retinal degeneration, revealing a new function. *Exp Eye Research* 84, 473-485 (2007).

13. Higashide,T., McLaren,M.J., & Inana,G. Localization of HRG4, a photoreceptor protein homologous to Unc-119, in ribbon synapse. *Invest Ophthalmol. Vis. Sci* 39, 690-698 (1998).

14. Kobayashi,A., Kubota,S., Mori,N., McLaren,M.J., & Inana,G. Photoreceptor synaptic protein HRG4 (UNC119) interacts with ARL2 via a putative conserved domain. *FEBS Lett.* 534, 26-32 (2003).

15. Veltel,S., Kravchenko,A., Ismail,S., & Wittinghofer,A. Specificity of Arl2/Arl3 signaling is mediated by a ternary Arl3-effector-GAP complex. *FEBS Lett.* 582, 2501-2507 (2008).

16. Haeseleer,F. Interaction and colocalization of CaBP4 and Unc119 (MRG4) in Photoreceptors. *Invest Ophthalmol. Vis. Sci* 49, 2366-2375 (2008).

17. Alpadi,K. *et al.* RIBEYE recruits Munc119, a mammalian ortholog of the Caenorhabditis elegans protein unc119, to synaptic ribbons of photoreceptor synapses. *J Biol. Chem.* 283, 26461-26467 (2008).

18. Kobayashi,A. *et al.* HRG4 (UNC119) mutation found in cone-rod dystrophy causes retinal degeneration in a transgenic model. *Invest Ophthalmol. Vis. Sci* 41, 3268-3277 (2000).

19. Vepachedu,R., Karim,Z., Patel,O., Goplen,N., & Alam,R. Unc119 protects from Shigella infection by inhibiting the Abl family kinases. *PLoS. ONE.* 4, e5211 (2009).

20. Gorska,M.M., Cen,O., Liang,Q., Stafford,S.J., & Alam,R. Differential regulation of interleukin 5-stimulated signaling pathways by dynamin. *J Biol. Chem.* 281, 14429-14439 (2006).

21. Bork,P., Holm,L., & Sander,C. The immunoglobulin fold. Structural classification, sequence patterns and common core. *J. Mol. Biol.* 242, 309-320 (1994).

22. Hoffman,G.R., Nassar,N., & Cerione,R.A. Structure of the Rho family GTP-binding protein Cdc42 in complex with the multifunctional regulator RhoGDI. *Cell* 100, 345-356 (2000).

23. Hanzal-Bayer,M., Renault,L., Roversi,P., Wittinghofer,A., & Hillig,R.C. The complex of Arl2-GTP and PDE delta: from structure to function. *EMBO J.* 21, 2095-2106 (2002).

24. Zhang,H. *et al.* Photoreceptor cGMP phosphodiesterase delta subunit (PDEdelta) functions as a prenyl-binding protein. *J. Biol. Chem.* 279, 407-413 (2004).

25. Goc,A. *et al.* Different properties of the native and reconstituted heterotrimeric G protein transducin. *Biochemistry* 47, 12409-12419 (2008).

26. Kerov,V. *et al.* N-terminal fatty acylation of transducin profoundly influences its localization and the kinetics of photoresponse in rods. *J Neurosci.* 27, 10270-10277 (2007).

27. Baehr,W., Morita,E., Swanson,R., & Applebury,M.L. Characterization of bovine rod outer segment G protein. *J. Biol. Chem.* 257, 6452-6460 (1982).

28. Marrari,Y., Crouthamel,M., Irannejad,R., & Wedegaertner,P.B. Assembly and trafficking of heterotrimeric G proteins. *Biochemistry* 46, 7665-7677 (2007).

29. Slepak,V.Z. & Hurley,J.B. Mechanism of light-induced translocation of arrestin and transducin in photoreceptors: interaction-restricted diffusion. *IUBMB. Life* 60, 2-9 (2008).

30. Sokolov,M. *et al.* Massive light-driven translocation of transducin between the two major compartments of rod cells: a novel mechanism of light adaptation. *Neuron* 34, 95-106 (2002).

31. Elias,R.V., Sezate,S.S., Cao,W., & McGinnis,J.F. Temporal kinetics of the light/dark translocation and compartmentation of arrestin and alpha-transducin in mouse photoreceptor cells. *Mol. Vis.* 10, 672-681 (2004).

32. Calvert,P.D., Strissel,K.J., Schiesser,W.E., Pugh,E.N., Jr., & Arshavsky,V.Y. Light-driven translocation of signaling proteins in vertebrate photoreceptors. *Trends Cell Biol.* 16, 560-568 (2006).

33. Knobel,K.M., Davis,W.S., Jorgensen,E.M., & Bastiani,M.J. UNC-119 suppresses axon branching in C. elegans. *Development* 128, 4079-4092 (2001).

34. Roayaie,K., Crump,J.G., Sagasti,A., & Bargmann,C.I. The G alpha protein ODR-3 mediates olfactory and nociceptive function and controls cilium morphogenesis in C. elegans olfactory neurons. *Neuron* 20, 55-67 (1998).

35. Lans,H., Rademakers,S., & Jansen,G. A network of stimulatory and inhibitory Galpha-subunits regulates olfaction in Caenorhabditis elegans. *Genetics* 167, 1677-1687 (2004).

36. Perkins,L.A., Hedgecock,E.M., Thomson,J.N., & Culotti,J.G. Mutant sensory cilia in the nematode Caenorhabditis elegans. *Dev. Biol.* 117, 456-487 (1986).

37. Sokolov,M. *et al.* Phosducin facilitates light-driven transducin translocation in rod photoreceptors. Evidence from the phosducin knockout mouse. *J Biol. Chem.* 279, 19149-19156 (2004).

38. Cowan,C.W., Wensel,T.G., & Arshavsky,V.Y. Enzymology of GTPase acceleration in phototransduction. *Methods Enzymol.* 315, 524-538 (2000).

39. Troemel,E.R., Kimmel,B.E., & Bargmann,C.I. Reprogramming chemotaxis responses: sensory neurons define olfactory preferences in C. elegans. *Cell* 91, 161-169 (1997).

40. Acton,T.B. *et al.* Robotic cloning and Protein Production Platform of the Northeast Structural Genomics Consortium. *Methods Enzymol.* 394, 210-243 (2005).

41. Chayen,N.E., Stewart,P.D., Maeder,D.L., & Blow,D.M. An automated system for micro-batch protein crystallization and screening. *J. Appl. Cryst.* 23, 297-302 (1990).

42. Otwinowski,Z. & Minor,D. Processing of X-ray diffraction data collected in oscillation mode. *Meth. Enzymol.* 276, 307-326 (1997).

43. Schneider,T.R. & Sheldrick,G.M. Substructure solution with SHELXD. *Acta Crystallogr. D. Biol. Crystallogr.* 58, 1772-1779 (2002).

44. Terwilliger,T.C. SOLVE and RESOLVE: automated structure solution and density modification. *Methods Enzymol.* 374, 22-37 (2003).

45. Emsley,P. & Cowtan,K. Coot: model-building tools for molecular graphics. *Acta Crystallogr. D. Biol. Crystallogr.* 60, 2126-2132 (2004).

46. Adams,P.D. *et al.* PHENIX: building new software for automated crystallographic structure determination. *Acta Crystallogr. D. Biol. Crystallogr.* 58, 1948-1954 (2002).

47. Davis,I.W. *et al.* MolProbity: all-atom contacts and structure validation for proteins and nucleic acids. *Nucleic Acids Res.* 35, W375-W383 (2007).

48. McCoy,A.J. *et al.* Phaser crystallographic software. *J. Appl. Crystallogr.* 40, 658-674 (2007).

49. Jones,T.A., Zou,J.Y., Cowan,S.W., & Kjeldgaard,M. Improved methods for building protein models in electron density maps and the location of errors in these models. *Acta Crystallogr. A* 47 (Pt 2), 110-119 (1991).

50. Murshudov,G.N., Vagin,A.A., & Dodson,E.J. Refinement of macromolecular structures by the maximum-likelihood method. *Acta Crystallogr. D. Biol. Crystallogr.* 53, 240-255 (1997).

CHAPTER 3

THE STRUCTURAL DETERMINATION OFA PDE6-PrBP/δ COMPLEX AND AN UNC119-Tα-GMP•PNP COMPLEX

Introduction

The mouse *Pde6d* gene encodes PDE6δ, a 17 kDa protein that was renamed to PrBP/δ after determining that it functions as a prenyl binding protein (PrBP) (Ismail *et al*., 2011; Gillespie *et al*., 1989; Cook *et al*., 2000a; Zhang *et al*., 2005). By gene blasting, PrBP/δ orthologs have been identified in essentially all animals (**Fig. 3.1**), including fruitfly, the eyeless *C. elegans* (Li and Baehr, 1998), and the unicellular protozoan *Paramecium* (Zhang *et al*., 2007). The PrBP/δ protein sequence is highly conserved throughout the animal kingdom, maintaining at least 70% sequence identity within vertebrates, and ~50% sequence identity among invertebrates. The closest relatives of PrBP/δ are the two UNC119 paralogs UNC119A and UNC119B. Both UNC119 paralogs and PrBP/δ constitute a new class of neural genes whose common function as lipid-binding proteins has been maintained through metazoan evolution.

The Prenyl Binding Protein PrBP/δ

Rod-specific cGMP phosphodiesterase 6 (PDE6) belongs to a large PDE superfamily (PDE1–11), whose members regulate cellular concentrations of cAMP and cGMP (Conti and Beavo, 2007). PDE6 is expressed in rods and cones and consists of two catalytic subunits (rod Pde6αβ and cone Pde6α', respectively), and two inhibitory PDE6γ subunits (Miki *et al*., 1975; Baehr *et al*., 1979). PDE6α (~99 kDa), PDE6β (~99 kDa) and PDE6γ (~10 kDa) form a heterotetramer in a molar ratio of 1:1:2 (Fung *et al*., 1990). Both catalytic subunits harbor a CAAX motif at their C-terminus for post-translational isoprenylation (Anant *et al*., 1992). Mammalian PDE6α is farnesylated while PDE6β is

Figure 3.1. Dendrogram of 21 PrBP/δ orthologs. Amino acid sequences were retrieved using the accession numbers shown, and aligned using ClustalW. The dendrgram was generated from the alignment. Sequences in vertebrates are highly conserved. PrBP/δ sequences of C. elegans and human are 65% similar suggesting conserved function through evolution.

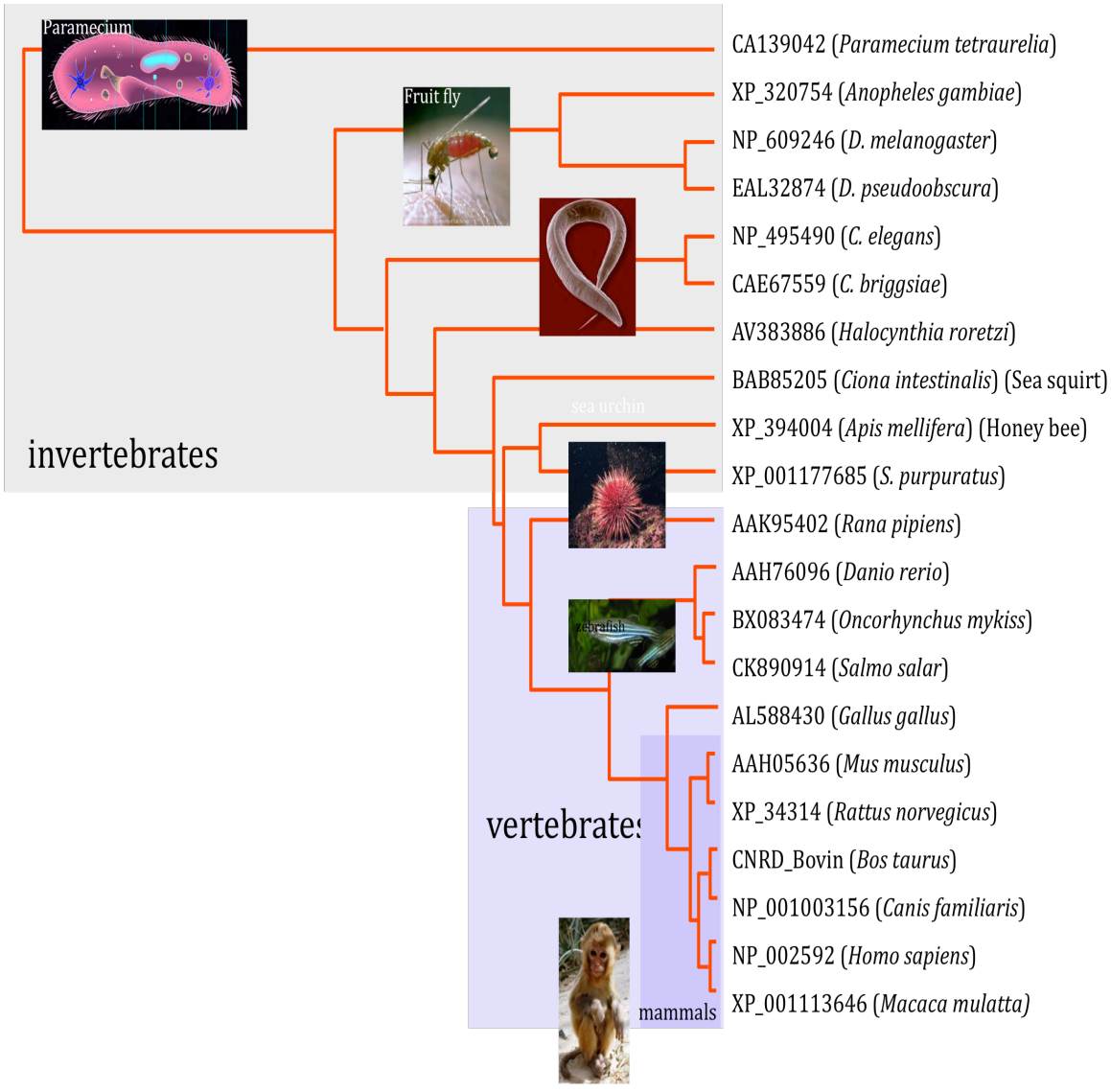
Paramecium
Fruit fly
sea urchin
zebrafish
invertebrates
vertebrates
mammals
CA139042 (Paramecium tetraurelia)
XP_320754 (Anopheles gambiae)
NP_609246 (D. melanogaster)
EAL32874 (D. pseudoobscura)
NP_495490 (C. elegans)
CAE67559 (C. briggsiae)
AV383886 (Halocynthia roretzi)
BAB85205 (Ciona intestinalis) (Sea squirt)
XP_394004 (Apis mellifera) (Honey bee)
XP_001177685 (S. purpuratus)
AAK95402 (Rana pipiens)
AAH76096 (Danio rerio)
BX083474 (Oncorhynchus mykiss)
CK890914 (Salmo salar)
AL588430 (Gallus gallus)
AAH05636 (Mus musculus)
XP_34314 (Rattus norvegicus)
CNRD_Bovin (Bos taurus)
NP_001003156 (Canis familiaris)
NP_002592 (Homo sapiens)
XP_001113646 (Macaca mulatta)

geranylgeranylated, resulting in modifications that facilitate membrane attachment. PrBP/δ was originally identified as a protein co-purifying with PDE6$\alpha\beta\gamma_2$ and named PDE6δ (Gillespie *et al*., 1989). Under isotonic conditions the majority (70-80%) of PDE6 is peripherally membrane associated (Baehr e*t al*., 1979), while a fraction (20-30%) of PDE6 remains soluble (Gillespie *et al*., 1989). Affinity purification of soluble PDE6 using a monoclonal antibody column yielded a novel 15 kDa polypeptide. Cloning this polypeptide's cDNA and northern blotting revealed that PrBP/δ was present in several different bovine tissue mRNA preparations, the strongest of which was present in the retina (Florio *et al*., 1996).

The addition of a GST-PrBP/δ fusion protein to permeabilized rod outer segment preparations resulted in a reduction of the maximal rate of cGMP hydrolysis in response to light (Cook *et al*., 2001) suggesting that GST-PrBP/δ may modify the activity of the phototransduction cascade by uncoupling transducin's normal activation of PDE6. However, it was later demonstrated that very little PrBP/δ is present in the rod outer segment (ROS) rendering this *in vitro* uncoupling mechanism physiologically insignificant (Norton *et al*., 2004).

Micromolar concentrations of prenylated and carboxymethylated PrBP/δ C-terminal peptides inhibit the PDE6-PrBP/δ interaction. Soluble PDE6 from ROS was 5-fold more highly methylated than membrane-bound PDE6 suggesting that PrBP/δ preferentially binds to carboxymethylated PDE6 (Cook *et al*., 2000b). The PDE6-PrBP/δ complex is relatively stable with a half-life of about 3.5 h. By exploiting the intrinsic tryptophan fluorescence of PrBP/δ and using dansylated prenyl cysteines as fluorescent ligands in a fluorescence resonance energy transfer (FRET) experiment, recombinant

PrBP/δ was shown to specifically bind geranylgeranyl and farnesyl moieties lacking bound amino acids with K_ds of ~20 uM and ~1 uM, respectively, establishing unambiguously that PrBP/δ functions as a prenyl-binding protein (Zhang *et al*., 2004). In photoreceptors, PrBP/δ was shown to interact with PDE6 subunits, farnesylated rhodopsin kinase (GRK1) and geranylgeranylated GRK7 (Zhang *et al*., 2004). A cryo-EM reconstruction of the PDE6/PrBP/δ complex at 18 Å resolution shows a structure that roughly resembles a skull with two pronounced cavities, the larger of which is formed by the catalytic domains at its top (behind the γ binding sites) and the GAF-A domains at its bottom (**Fig. 3.2**) (Goc *et al*., 2010) . GAF domains are important as they function as noncatalytic cGMP binding sites, sequestering most of the cGMP present in photoreceptors (Martinez *et al*., 2008; Ho *et al*., 2000).

PrBP/δ Interactions with Prenylated Ras and Rho GTPases

Doubts concerning the identity of PrBP/δ as a PDE6 subunit arose when it was shown that the eyeless nematode *C. elegans* expressed a PrBP/δ ortholog (C27H5) whose functional properties were identical to human PrBP/δ. Both proteins eluted native PDE6 from ROS membranes with nearly identical efficiencies (Li and Baehr, 1998). It has also been shown that human PrBP/δ interacts with a large number of small prenylated GTPases of the Ras and Rho subfamilies present in essentially all cells (**Table 3.1**). Almost all members of the Ras family carry the CAAX motif and are prenylated, which is essential for their function.

Recombinant PrBP/δ extracts Rab13 from cellular membranes much like how it dissociates PDE6 from photoreceptor disk membranes (Marzesco *et al*., 1998). This PrBP/δ function is specific as RhoGDI, another known prenyl binding protein specific for

Figure 3.2. PDE6 may be membrane bound or soluble. **A**, Schematic of PDE6αβγγ bound to ROS disc membranes vis prenyl side chains. **B**, association of PDE6αβγγ with PrBP/δ (delta) forms a soluble and diffusable complex. **C**, Structure of soluble PDE6αβγγδδ by Cryo-EM at 18 Å resolution in two orientations (Goc *et al*., 2010).

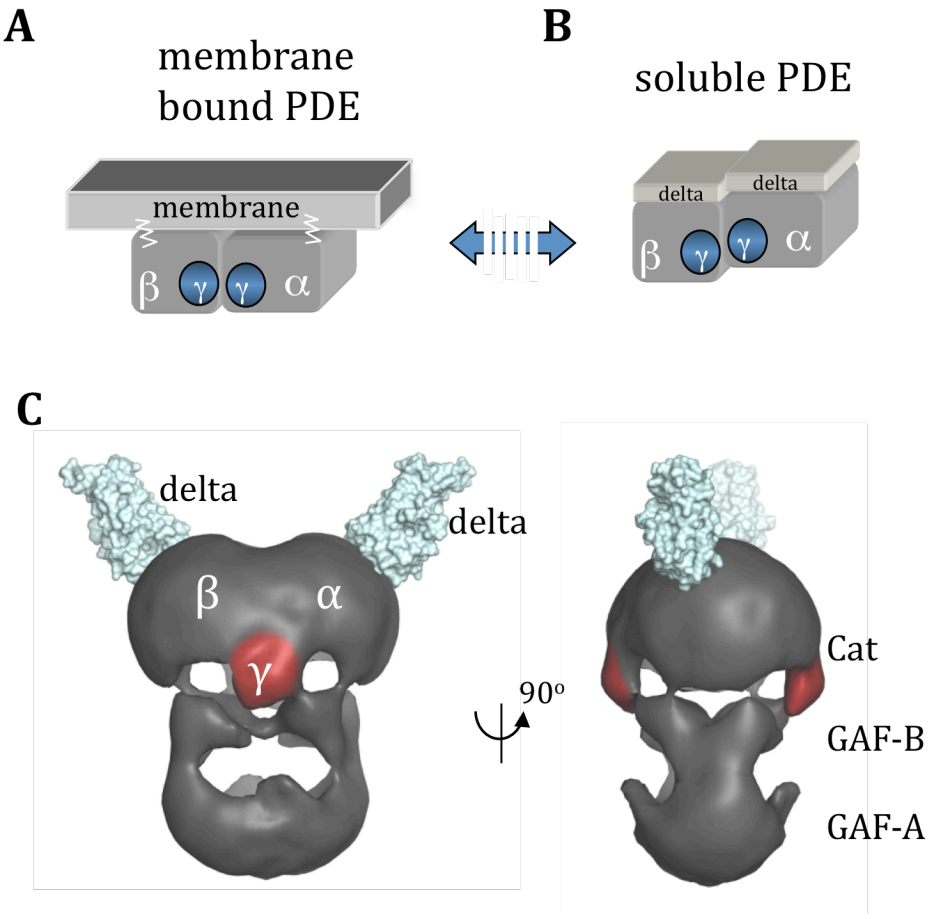
A
membrane
bound PDE
membrane
β
γ
γ
α
B
soluble PDE
delta
delta
β
γ
γ
α
C
delta
delta
β
α
γ
90°
Cat
GAF-B
GAF-A

Table 3.1. Polypeptides interacting with PrBP/δ. Column 1, proteins involved in phototransduction (red); small G proteins (green); other interacting proteins (black). Column 2, CAAX box sequences. Column 3, prenyl side chains at the C-terminal Cys. Column 4, acyl side chains at G2. Columns 5,6, methods used to determine interaction. Column 7, references. F = farnesyl; GG = geranylgeranyl.

PrBP/δ Interacting Partners

Target	CAAX	Prenyl	Acyl	Y2H	Pulldown	References
PDEα	CCIQ	F	-			(Cook *et al*., 2001)
PDEβ	CCIL	GG	-			(Cook *et al*., 2001)
GRK1	CLIS	F	-	+	+	(Zhang *et al*., 2004)
GRK7	CLLL	GG	-	+	+	(Zhang *et al*., 2004)
cTγ	CVLS	F	-			(Zhang *et al*., 2007)
Tγ	CVIS	F	-			(Zhang *et al*., 2007)
Gγ13	CTIL	GG	-		+	(Stamm *et al*., 2011)
DmPDE5/6	CALL	GG	-			(Day *et al*., 2008)
Rab13	CLLG	F	-	+		(Marzesco *et al*., 1998)
Rheb	CSVM	F				(Hanzal-Bayer *et al*., 2002; Ismail *et al*., 2011; Gelb *et al*., 2006)
Rho6 (Rnd1)	CSIM	F	16:0?	+		(Nancy *et al*., 2002)
Rap1a	CLLL	GG	-	+		(Nancy *et al*., 2002)
Rap1b	CQLL	GG	-	+		(Nancy *et al*., 2002)
Rap2a	CNIQ	F				(Nancy *et al*., 2002)
Rap2b	CVIL	GG	16:0?			(Nancy *et al*., 2002)
H-Ras	CVLS	F				(Nancy *et al*., 2002)
N-Ras	CVVM	F	16:0	+		(Nancy *et al*., 2002)
K-Ras	CVIM	F				(Nancy *et al*., 2002)
RhoA	CLVL	GG	-	+		(Nancy *et al*., 2002)
RhoB	CKVL	GG	16:0?	+		(Nancy *et al*., 2002; Hanzal-Bayer *et al*., 2002)
Prostacyclin-R	CSLC	F				(Wilson and Smyth, 2006)
RPGR-ORF15	-	-	-			(Li *et al*., 1998; Linari *et al*., 1999b)
ARL2-GTP	-	-		+		(Renault *et al*., 2001)
ARL3-GTP	-	-		+		(Linari *et al*., 1999a)

Rho GTPases, was unable to recapitulate this PrBP/δ function. PrBP/δ also interacts with many other small GTPases including Ras, Rac, Rap, Rho, Rheb, RhoA, RhoB and Rho6 (**Table 3.1**), each of which are prenylated (Nancy *et al*., 2002; Hanzal-Bayer *et al*., 2002), establishing PrBP/δ as a promiscuous prenyl-binding. For most of these GTPases the physiological significance of their interaction with PrBP/δ remains unknown. Yeast two-hybrid screens indicate that many prenylated proteins do not interact with PrBP/δ, suggesting that specificity is mediated in part by protein-protein interactions. Examples of non-interacting prenylated GTPases include Rala, Ralb, and Rab6 (Nancy *et al*., 2002), as well as Arf1, Arf6, Arl6, Rac1, Rab1, Rab2, Rab7, and Ran (Hanzal-Bayer *et al*., 2002).

PrBP/δ-interacting Ras GTPases function as oncogenes, which, in normal cells, act as a switch to signal cell growth when hormones or other agents stimulate cell surface receptors. For example, if HRAS is "switched on," it signals the cell to grow, but when "switched off," the cell lies dormant. HRAS is an important oncogene as it is mutated in approximately one third of human cancers. Rho-related GTP-binding protein 6 (Rho6) lacks intrinsic GTPase activity, constitutively binding GTP, and also functions to control actin cytoskeleton rearrangements. In general, the Rho family of small GTPases helps to regulate the actin cytoskeleton in various cell types (Etienne-Manneville and Hall, 2002). Like other GTPases of the Ras superfamily, RhoGTPases serve as molecular switches by cycling between GDP- and GTP-bound states. In the GTP bound state, interaction with effectors leads to a variety of biological functions. The physiological role for PrBP/δ interactions with Rho and Ras GTPases remains unknown, but it seems likely that PrBP/δ

acts as a GDI-like solubilizing factor contributing to Ras and Rho signaling in cells (Chandra *et al*., 2012).

PrBP/δ Interactions with Nonprenylated Proteins

Yeast two-hybrid screens have shown that PrBP/δ interacts with the RCC1-like domain of retinitis pigmentosa GTPase regulator (RPGR) (Becker *et al*., 1998; Linari *et al*., 1999b). RCC1 is a GEF for the small GTP-binding protein Ran, which helps to control transport between the nucleus and cytoplasm (Clarke and Zhang, 2008). The interaction between RPGR and PrBP/δ was confirmed by both pull-down assays (Li and Baehr, 1998) and surface plasmon resonance experiments (Linari *et al*., 1999b). Interestingly, the C-terminal region of RPGR, which carries a CAAX box motif did not interact with PrBP/δ suggesting that it may lack posttranslational prenylation (Linari *et al*., 1999b). Missense mutations in RPGR showed reduced interaction with PrBP/δ, suggesting that RPGR mutations may give rise to retinal degeneration via the dysregulation of intracellular protein localization and transport. PrBP/δ also interacts with the Arf-like proteins Arl2 and Arl3 in a GTP-specific manner (Linari *et al*., 1999a; Renault et al., 2001). Although closely-related, Arl2 and Arl3 are neither myristoylated nor prenylated (Hanzal-Bayer et al., 2002), but the interaction between PrBP/δ and Arl2 or Arl3 was verified by co-crystallization (Hanzal-Bayer *et al*., 2002; Renault *et al*., 2001), fluorescence spectroscopy, and co-immunoprecipitation (Hanzal-Bayer *et al*., 2005).

The Structure of the PrBP/δ-Arl2•GTP Complex

The 2.3 Å co-crystal structure of PrBP/δ and Arl2-GTP was a significant breakthrough in helping to understand how PrBP/δ interacts with nonprenylated proteins (**Fig. 3.3**) (Renault *et al*., 2001; Hanzal-Bayer *et al*., 2002). The complex crystallized in two crystal forms (Renault *et al*., 2001) (Protein Data Bank codes 1KSG, 1KSH and 1KSJ) with form-1 growing within days and form-2 crystallizing over the course of several months to 1 year (Renault *et al*., 2001; Hanzal-Bayer *et al*., 2002). Form-1 contained Arl2-GTP, whereas form-2 contained partially hydrolyzed GTP (GDP and phosphate). The Arl2 structure in both forms is very similar exhibiting no significant structural differences. The PrBP/δ structure (**Figs. 3.3, 3.4**) contains an immunoglobulin-like β-sandwich fold comprised of two β-sheets forming a hydrophobic pocket. The interface between Arl2-GTP and PrBP/δ is formed by β-sheet interactions involving β2 from Arl2 and β7 from PrBP/δ. The immunoglobulin-like β-sandwich fold of PrBP/δ is closely related to RhoGDI (Hoffman *et al*., 2000) and UNC119A (Zhang *et al*., 2011) despite the relatively low sequence similarity between these proteins (**Fig. 3.5**). The major structural differences between these three proteins include the length and structure of the loops connecting the β-sheets and the N-terminal regions (Hanzal-Bayer *et al*., 2002). In contrast to the prenyl-binding proteins RhoGDI and PrBP/δ, UNC119A is an acyl binding protein that specifically interacts with lauroylated and myristoylated N-termini of G-protein α-subunits (**Fig. 3.5**) (Zhang *et al*., 2011).

Figure 3.3. Ribbon representation of the PrBP/δ-Arl2/GTP complex (PDB 1KSH). Arl2 blocks the entrance (arrow) through which the lipid side chain of prenylated proteins is inserted. GTP is shown as sticks in dark blue. Figure was created with PyMOL (www.pymol.org).

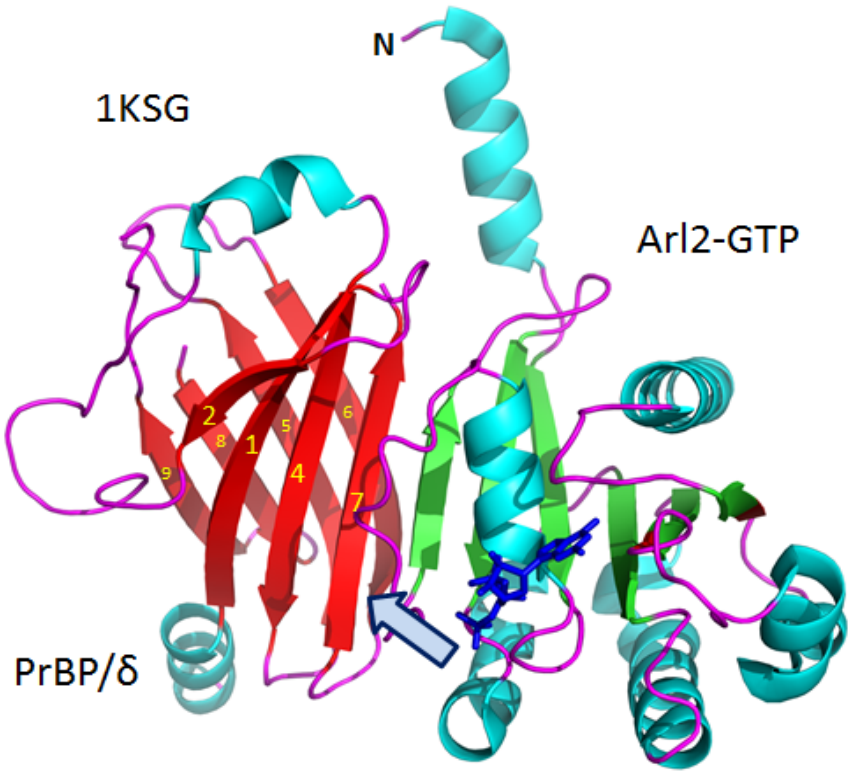
N
1KSG
Arl2-GTP
2
8
1
5
6
9
4
7
PrBP/δ

Figure 3.4. Structure of the Rheb(GDP)-PrBP/δ complex. **A**. Structure modified from Ismail, et al. (PDB 3T5I). The C-terminal farnesyl chain of Rheb (green) is inserted into the β-sandwich structure of PrBP/δ. GDP of Rheb is shown in dark gray. **B**. The structure of PrBP/δ with inserted farnsyl (green). Cys of Rheb is shown in yellow. The middle and right structures were generated by 90^{o} counterclockwise rotation.

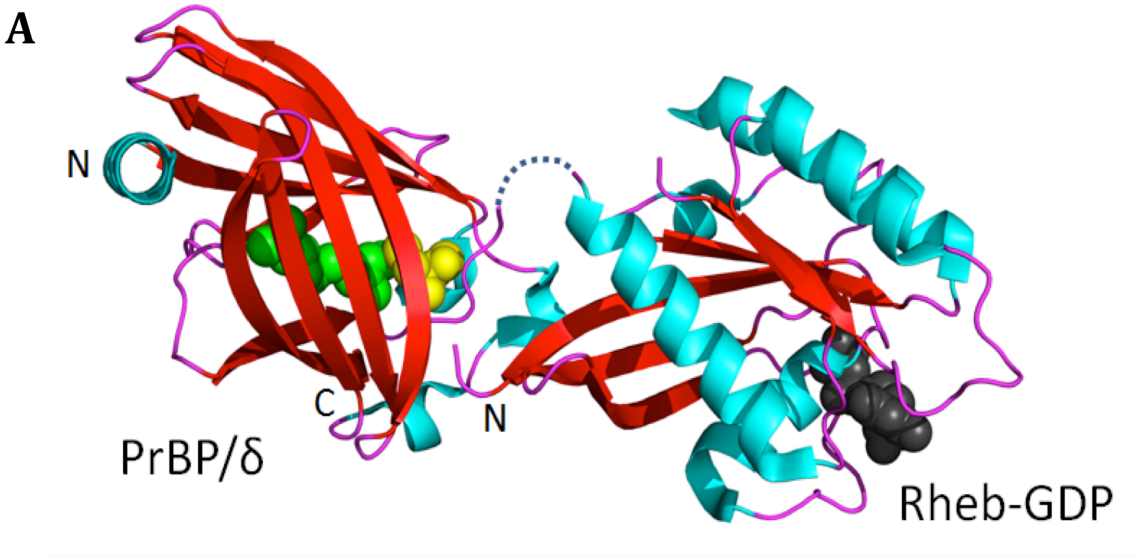
A
N
C
N
PrBP/δ
Rheb-GDP

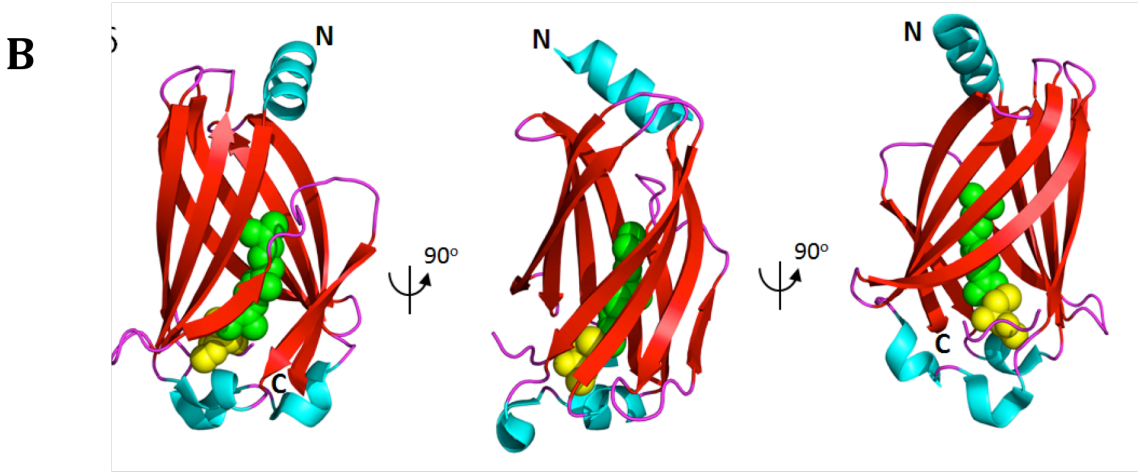
B
N
90°
C
N
90°
N
C

Figure 3.5. Comparison of RhoGDI, PrBP/δ, and UNC119 strctures and sequences. **A**, structures of RhoGDI, PrBP/δ, and UNC119A with lipid ligands inserted into the hydrophobic binding groove. Note the distinct entrance in UNC119. **B**, Sequence Alignment of Human UNC119A, PrBP/δ, and RhoGDI. Only C-terminal residues of UNC119A (60-240) and RhoGDI (41-204) are shown. β-strands are depicted as large dark arrows for UNC119A. Identical residues are shaded blue and similar residues shaded gray.

A

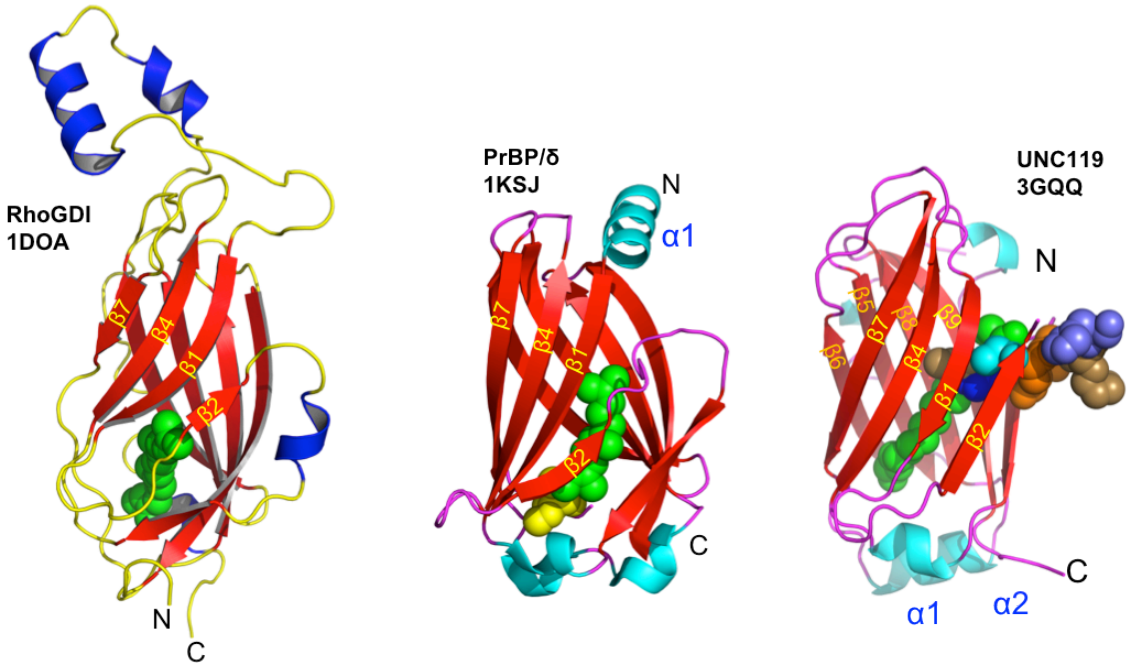
RhoGDI
1DOA
β7
β4
β1
β2
N
C
PrBP/δ
1KSJ
N
α1
β7
β4
β1
β2
C
UNC119
3GQQ
N
β5
β7
β3
β6
β4
β1
β2
C
α1
α2

B

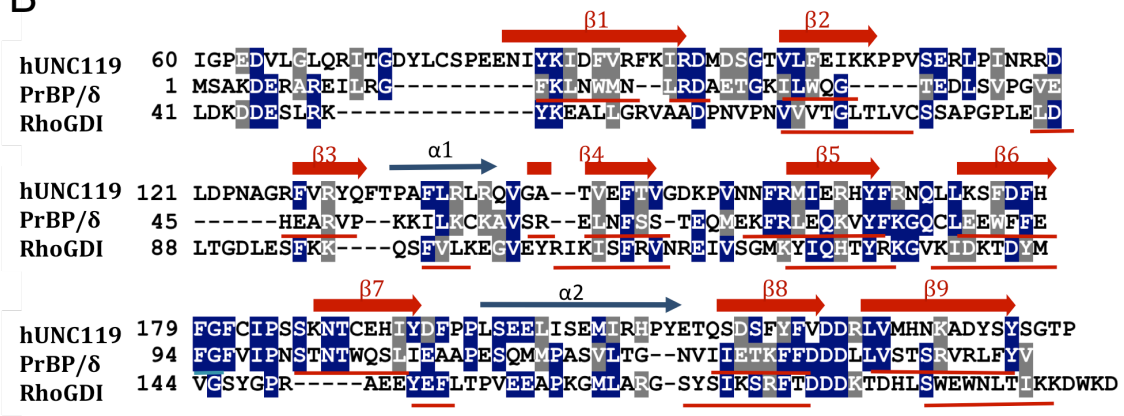
β1
β2
hUNC119 60 IGPEDVLGLQRITGDYLCSPEENIYKIDFVRFKIRDMDSGTVLEEIKKPPVSERLPINRRD
PrBP/δ 1 MSAKDERAREILRG----------FKLNWMN--LRDAETGKILWQG-----TEDLSVPGVE
RhoGDI 41 LDKDDDESLRK----------YKEALLGRVAADPNVPNVVVTGLTLVCSSAPGPLELD
β3
α1
β4
β5
β6
hUNC119 121 LDPNAGRFVRYQFTPAFLRLRQVGA--TVEFTVGDKPVNNFRMIEFHYFFNQLLKSFDFH
PrBP/δ 45 ------HEARVP--KKILKCKAVSR--ELNFSS-TEQMEKFRIEQKVYFKGQCLEEWFFE
RhoGDI 88 LTGDLESFKK----QSFVLKEGVEYRIKISFRVNREIVSGMKYIQHTYRKGVKIDKTDYM
β7
α2
β8
β9
hUNC119 179 FGFCIPSSKNTCEHIYDFPPLSEELISEMIRHPYETQSDSFYFVDDRLVMHNKADYSYSGTP
PrBP/δ 94 FGFVIPNSTNTWQSLIEAAPESQMMPASVLTG--NVIIETKFFDDDLLVSTSRVRLFYV
RhoGDI 144 VGSYGPR-----AEEYEFLTPVEEAPKGMLARG-SYSIKSRFTDDDKTDHLSWEWNLTIKKDWKD

The Structure of the Rheb•GDP-PrBP/δ Complex

Rheb (Ras homolog enriched in brain), a novel, highly conserved member of the Ras superfamily of G-proteins, regulates the mammalian Target of Rapamycin complex 1(mTORC1), which in turn regulates cell growth and proliferation (Avruch *et al*., 2006; Aspuria and Tamanoi, 2004; Ismail *et al*., 2011). The 1.7-Å structure of PrBP/δ in complex with farnesylated Rheb was solved using a combination of model building with a non-prenylated truncated Rheb and the crystal structure of PrBP/δ with a C-terminal prenylated octopeptide (Ismail *et al*., 2011). The complex shows the farnesyl group of Rheb deeply buried in the hydrophobic pocket of PrBP/δ, an interaction that is independent of the nucleotide status of Rheb (**Fig. 3.4**) (Ismail *et al*., 2011). Arl2 and Arl3 regulate the interaction of Rheb with PrBP/δ allosterically in a GTP-dependent manner, establishing that GTP bound Arl proteins act as GDI displacement factors (GDFs). In general, GDFs function by helping to displace small prenylated G proteins (in photoreceptors GRK1 or PDEα') from their lipid-binding proteins, preventing further interaction by stabilizing the "closed" form of the GDI (in photoreceptors PrBP/δ or UNC119A) (**Fig. 3.6**).

PrBP/δ Deletion in Mouse

At least six prenylated proteins are involved in mammalian phototransduction (**Table 3.1**): the three catalytic subunits of PDE6 (α, β and α'), the two G protein-coupled receptor kinases (GRK1 and GRK7), and the rod and cone transducin γ subunits. PDE6α, GRK1, and both Tγ subunits are farnesylated, while PDE6β and GRK7 are geranylgeranylated. These proteins are synthesized in the cytosol and posttranslationally modified by soluble prenyl transferases. Prenylated proteins then dock to the ER surface

Figure 3.6. ARL3-GTP functions as a GDF (GDI-displacement factor). Step1; Rheb is extracted from membrane 1 by PrBP/δ, Step 2; an intermediate ternary complex is formed with ARL3-GDP, Step 3; Rheb is diplaced to membrane 2 after GTP/GDP exchange. The cycle is completed by the ARL3 GAP, RP2.

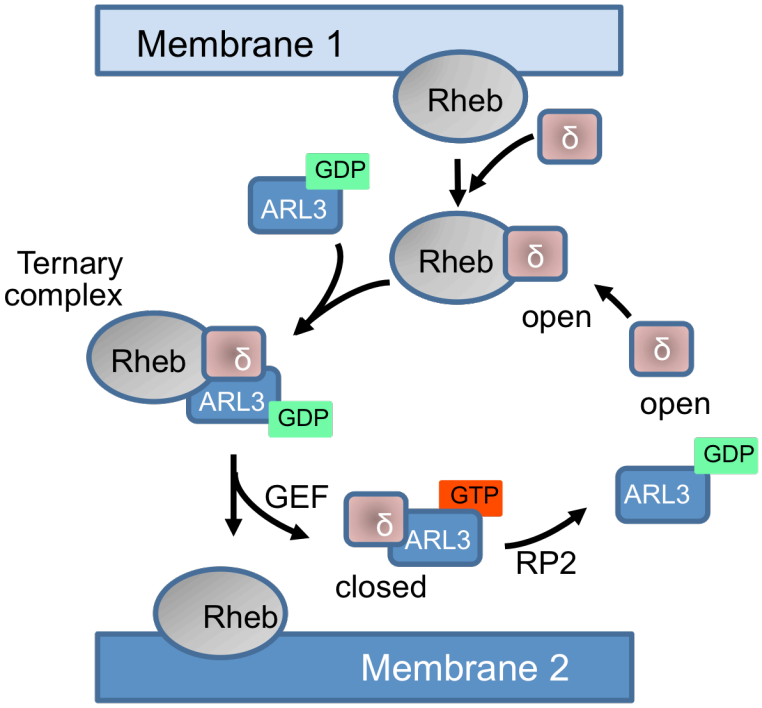
Membrane 1
Rheb
δ
GDP
ARL3
Rheb
δ
Ternary
complex
open
δ
Rheb
δ
ARL3
GDP
open
GDP
ARL3
GEF
GTP
δ
ARL3
RP2
closed
Rheb
Membrane 2

where further processing occurs including proteolytic cleavage of -AAX and carboxymethylation of cysteine (**Fig. 1.2**). Following ER processing GRK1 and PDE6 are targeted to outer segment disk membranes in order to participate in phototransduction.

Deletion of the *Pde6d* gene results in a fertile viable adult mouse that develops normally, but exhibits a significantly reduced body size (Zhang *et al*., 2007). Electro-olfactograms (EOGs) and behavioral tests established that the knockout mouse is dysosmic, providing an explanation for the reduced body weight (Stamm *et al*., under revision). Phenotypically the *Pde6d*$^{-/-}$ mouse primarily exhibits transport deficiencies of membrane-associated proteins (**Figs. 3.7, 3.8**). Specifically, defects are seen in the transport of GRK1 to photoreceptor outer segments and of cone PDE6 to cone outer segments (COS), which resulted in anomalous photoreceptor physiology. In *Pde6d* $^{-/-}$ rod single-cell recordings, sensitivity to single photons was increased (Zhang *et al*., 2007) and double-flash electroretinograms indicated a delay of more than 20 minutes in recovery to the dark state in *Pde6d* $^{-/-}$rods, which is likely due to severely reduced levels of GRK1 in rod outer segments (Zhang *et al*., 2007).

These data suggest that PrBP/δ is involved in extracting prenylated proteins from the ER surface (**Figs. 3.7, 3.8**) and delivering them to a post-TGN vesicular transport carrier in rods and cones (Zhang *et al*., 2007; Karan *et al*., 2008) or directly to ROS discs (Zhang *et al*., 2011), a process that is likely regulated by GTP-bound Arl proteins, which act in a GDF-like fashion. Curiously in *Pde6d*$^{-/-}$ mice, rod PDE6 subunits were only weakly affected and partially mislocalized to the inner segments (Zhang *et al*., 2007) despite PrBP/δ being known to interact strongly with PDE6.

Figure 3.7. PrBP/δ-dependent export of PDE6 and GRK1 from the ER in rods. **A**. GRK1 and PDE6 dock to the ER after prenylation and processing. Prenylated proteins may be extracted from the ER by PrBP/δ (δ, purple) forming a diffusible complex. Additional prenyl binding proteins may exist (x, in black). **B**. Deletion of PrBP/δ prevents GRK1 exit from the ER. With the help of X, PDE6 still travels to the OS although some PDE6 is retained and mislocalized in the inner segment (see Zhang *et al*., 2007).

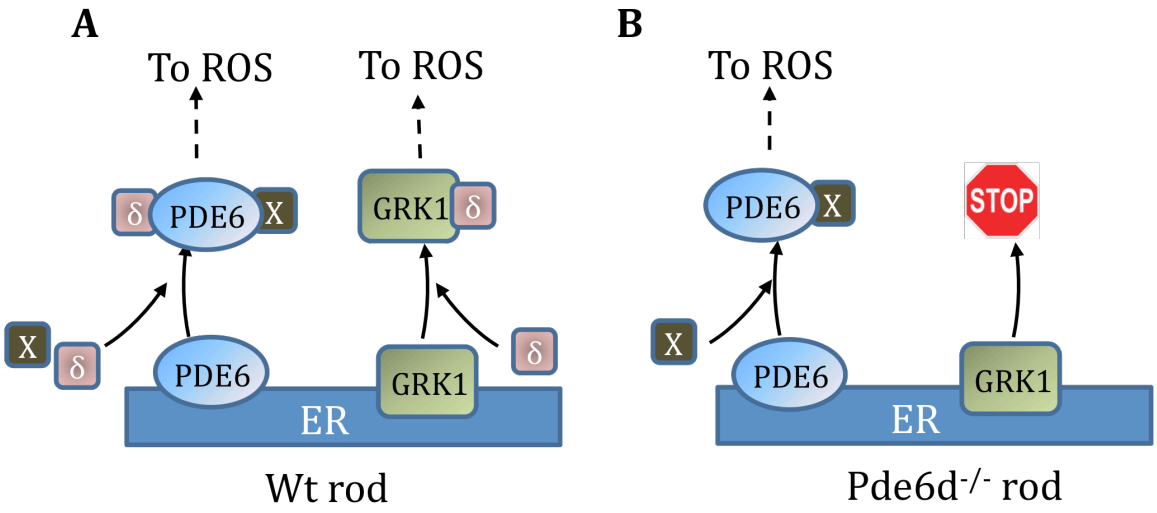
A
To ROS
To ROS
δ
PDE6
X
GRK1
δ
X
δ
PDE6
GRK1
δ
ER
Wt rod
B
To ROS
PDE6
X
STOP
X
PDE6
GRK1
ER
Pde6d-/- rod

Figure 3.8. PrBP/δ-dependent transport in cones. **A**. Processing of cone PDE6 and GRK1 in WT cones. Cone PDE consists of two identical geranylgeranylated subunits (PDEα'). Both are thought to interact with PrBP/δ. **B**. Deletion of PrBP/δ prevents trafficking of cone PDE6 subunits and GRK1 to the outer segments. Presumably, the prenylated subunits are unable to exit the ER and are degraded.

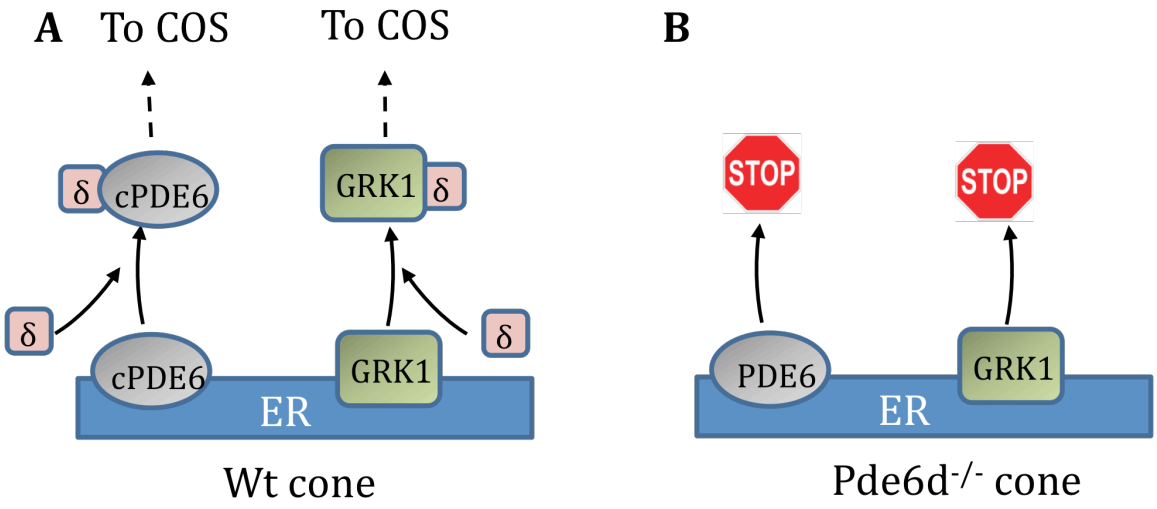
A
To COS
To COS
δ
cPDE6
GRK1
δ
δ
cPDE6
GRK1
δ
ER
Wt cone
B
STOP
STOP
PDE6
GRK1
ER
Pde6d-/- cone

In contrast to *Pde6d*$^{-/-}$ rod outer segments, Pde6α' was undetectable by immunofluorescence in *Pde6d*$^{-/-}$ COS (Zhang *et al*., 2007). Under photopic (bright light) ERG conditions, the *Pde6d*$^{-/-}$ cone response was diminished, which is consistent with reduced PDE6α' levels in COS. Mouse *Pde6d*$^{-/-}$ photoreceptors exhibit a variety of defects, transporting only a subset of prenylated proteins (PDE6 subunits and GRK1) to outer segments, suggesting that additional unidentified prenyl binding proteins may substitute for PrBP/δ loss in photoreceptors. In *Pde6d*$^{-/-}$ rods and cones, both of the visual pigments and transducin trafficked appropriately, but rod Tγ was partially mislocalized as some remained in the inner segment (Zhang *et al*., 2007).

Goals

This chapter focuses on the purification and isolation of two protein complexes, UNC119-Tα-GMP•PNP and PDE6-PrBP/δ. Initially, the crux of this work was focused on attempting to determine the molecular mechanism of how UNC119 inhibits the GTPase activity of Tα, data initially presented in Chapter 2 of this dissertation. My approach was to generate a protein complex of recombinant UNC119 with native bovine Tα bound to a nonhydrolyzable GTP analong (UNC119-Tα-GMP•PNP) to be used to grow protein crystals, solve the crystal structure, and ultimately understand how UNC119 inhibits GTPase activity.

Isolation of native Tα from bovine retina resulted in the ability to recover other native phototransduction components, particularly PDE6, a protein that remains to be crystallized. In an attempt to better understand the role PrBP/δ plays in trafficking post-biosynthesis prenylated PDE6 to the outer segments, I aimed to generate a PDE6-PrBP/δ complex to be used to grow protein crystals in hopes of gaining a more complete

understanding of how the complex assembles. Furthermore, gaining insight into whether PrBP/δ can extract prenyl moieties from membranes and if possible, exactly how this is accomplished would be valuable. Generating and obtaining structural data about the PDE6-PrBP/δ complex proved to be more fruitful and as a result became the main focus of this chapter.

Methods

Expression and purification of recombinant human PrBP/δ. *PrBP/δ* cDNA was amplified by PCR from a human retina cDNA library and directionally cloned into a pET151/D-TOPO vector (Invitrogen) and verified by DNA sequencing. The construct was expressed in BL21 Codon+ *E. coli* cells (Stratagene) in ZY autoinduction media for 6 hours at 37^{o} C and then overnight at 19^{o} C. Cells were harvested by centrifugation, resuspended, and lysed in 10 mg/mL lysozyme in lysis buffer (20 mM imidazole, 700 mM NaCl, 50 mM Tris pH 7.4, 1 mM DTT) and protease inhibitors (PMSF, aprotinin, leupeptin, pepstatin) for 1 hour at 4^{o} C, followed by sonication. The lysate was clarified by centrifugation (45 min, 15000 rpm) and soluble PrBP/δ protein was bound to a Ni^{2+} sepharose column (Amersham/GE Healthcare), washed with 10 column volumes of lysis buffer and eluted with 300 mM imidazole in 700 mM NaCl, 50 mM Tris pH 7.4, and 1 mM DTT. Fractions were assayed by SDS-PAGE, pooled, and dialyzed against 2 L of 20 mM NaCl, 25 mM Tris pH 7.4, and 1 mM DTT. PrBP/δ was purified to homogeneity by anion exchange (HiTrap Q FF, GE Life Sciences, 20-1000 mM NaCl gradient in 25 mM Tris pH 7.4, 1 mM DTT) and gel filtration (SD200, Amersham/GE Healthcare), 100mM NaCl, 10 mM Tris pH 7.4, 1 mM DTT) chromatography.

Expression and purification of recombinant human UNC119. Expression and purification of truncated human UNC119 protein (residues 56-240) was carried out as a part of the established high throughput protein production pipeline (Acton *et al*., 2005) (Northeast Structural Genomics Consortium (NESG) target HR3066a). The protein was cloned into the pET 14-15C expression vector (Novagen). Selenomethionyl protein was expressed in *Escherichia coli* BL21(DE3) + Magic, purified using Ni-NTA affinity chromatography (Qiagen) and gel filtration (Superdex 75, Amersham/GE Healthcare) in buffer containing 10 mM TrisHCl , 100 mM NaCl, 5 mM DTT, pH 7.5. Protein homogeneity was verified by SDS-PAGE and MALDI-TOF mass spectrometry.

Isolation and purification of native bovine PDE6 and Tα. PDE6 and Tα were purified from 800 bovine retinas as previously described (Baehr *et al*., 1982). Briefly, ROS membranes were purified by sucrose gradient centrifugation, and washed (5X each) extensively with 20 ml isotonic (0.1 M NaCl, 10 mM TrisHCl pH 7.4, 1 mM EDTA, 0.1 mM DTT) and hypotonic (10 mM TrisHCl pH 7.4, 1 mM EDTA, 0.1 mM DTT) buffers. A 10-fold molar excess of GMP•PNP was added to supernatants, they were combined, and concentrated using Vivaspin 15 concentrators (Sartorius Stedim, Goettingen Germany). PDE6 was separated from Tα and Tβγ by gel filtration chromatography (SD200, Amersham/GE Healthcare) in 100mM NaCl, 10 mM Tris pH 7.4, 1 mM DTT. Typical yields were approximately ~1.5 mg of 99% pure PDE6 and ~44 mg of a 99% pure mixture of Tα-GMP•PNP and Tβγ.

PDE6-PrBP/δ complex formation and purification. A 3-fold molar excess of pure recombinant PrBP/δ was added to purified PDE6 and incubated at 4 ^{o}C for a minimum of 4 hours. The complex was purified by gel filtration chromatography

(SD200, Amersham/GE Healthcare) in 100mM NaCl, 10 mM Tris pH 7.4, 1 mM DTT, fractions were analyzed by SDS-PAGE, and pure fractions were combined and concentrated yielding ~850 uL of pure PDE6-PrBP/δ complex at ~10.4 mg/mL. The protein complex was used to setup 96-well Intelliplate crystal trays at 21 ^{o}C using the following commercially available crystal screens; Salt Rx, PACT, Emerald Cryo I and II, Hampton I and II, Index I and II, JCSG and Suite, Natrix, Hampton Lite, and JBScreen Classic 1 HTS. Crystallization trials proved to be unsuccessful.

UNC119-Tα-GMP•PNP complex formation and purification. A 2-fold molar excess of UNC119 was added to the Tα-GMP•PNP and Tβγ mixture and incubated at 4 ^{o}C for a minimum of 4 hours. The UNC119-Tα-GMP•PNP complex was then separated from Tβγ by taking advantage of the 6X-His tag on the UNC119 construct and using a HisTrap FF column (GE Life Sciences, 20mM-300mM imidazole gradient in 10 mM Tris, pH 7.4, 1 mM DTT). Fractions were analyzed by SDS-PAGE, and pure fractions were combined and dialyzed against 2L of 100 mM NaCl, 10 mM Tris, pH 7.4, 1 mM DTT overnight at 4 ^{o}C. The complex was concentrated and finally purified by gel filtration chromatography (SD200, Amersham/GE Healthcare) in 100mM NaCl, 10 mM Tris pH 7.4, 1 mM DTT, fractions were analyzed by SDS-PAGE, and pure fractions were combined and concentrated yielding ~2 mL of pure UNC119-Tα-GMP•PNP complex at ~13.5 mg/mL. The protein complex was used to setup 96-well Intelliplate crystal trays at 21 ^{o}C and 4 ^{o}C using the following commercially available crystal screens; Salt Rx, PACT, Emerald Cryo I and II, Hampton I and II, Index I and II, JCSG and Suite, Natrix, Hampton Lite, and JBScreen Classic 1 HTS. Crystallization trials proved to be unsuccessful.

Electron cryo-microscopy. In preparation for cryo-EM experiments, the PDE6-PrBP/δ complex was dialyzed against 20 mM Tris, pH 7.5, 150 mM NaCl and 2 mM $MgCl_2$ at 4 ^oC overnight to remove all traces of glycerol. The complex was concentrated using Centricon-50 spin concentrators and 0.5 mL of the protein complex was injected into a BioRad, Bio-Sil^Ò SEC 250-5 gel filtration column that had previously been equilibrated with 20 mM Tris, pH 7.5, 150mM NaCl and 2 mM $MgCl_2$, and purified. Fractions were collected and analyzed by SDS-PAGE. Peak fractions were pooled and diluted to 0.2-0.3 mg/ml using gel filtration buffer. An aliquot of 2.5 uL of the PDE6-PrBP/δ protein complex at 0.1-0.2 mg/mL was applied to a 400 mesh Quantifoil R 2/1 copper grid (hole size 2.0 um) and was rapidly plunged into liquid ethane to freeze the sample by a FEI Vitrobot. Cryo-EM images were collected in a JEM2100 electron cryo-microscope operated at 200 keV with a Gatan 4K x 4K CCD camera with the specimen held at the temperature of liquid nitrogen. CCD images were recorded at a detector magnification of 60,000X (1.81 Å/pixel) with a dose of 15-18 e/$Å^2$.

Cryo-EM image processing. A total of 3,000 particles were boxed out using *Boxer in EMAN1*. The images were then subjected to low-pass filtering to 20Å prior to beginning refinement by *EMAN1* using the standard projection matching method under enforcing C2 symmetry. The initial EM model used included only PDE6 at a resolution of ~30Å. The final refined model was obtained at 30Å resolution as assessed by Fourier Shell Correlation (FSC) after several iterations.

Results

Isolation of native PDE6 and Tα. Native bovine PDE6 and Tα-GMP•PNP, carrying their lipid modifications (farnesylated-PDEα, geranylgeranylated-PDEβ, myristoylated-Tα) were isolated as a heterogeneous mixture containing Tβγ from ~800 bovine retinas. ROS membranes were washed in hypotonic buffer in the presence of ~10 molar equivalents of GMP•PNP relative to Tα. The addition of the nonhydrolyzable GTP analog, GMP•PNP, in the presence of light, promoted the dissociation of Tα from Tβγ yielding a heterogeneous mixture of PDE6, Tα-GMP•PNP, and Tβγ (**Fig. 3.9**). Gel filtration chromatography using a Superdex 200 column isolated PDE6 from the Tα-GMP•PNP Tβγ mixture (**Fig. 3.10A,B**). PDE6 fractions were collected, pooled and saved to be used in conjunction with recombinant PrBP/δ to generate a PDE6-PrBP/δ protein complex. The Tα-GMP•PNP, Tβγ mixture fractions were also collected, pooled, and saved to be used to generate an UNC119-Tα-GMP•PNP protein complex.

PDE6-PrBP/δ complex formation. Native PDE6 exists as a multi-subunit complex consisting of α, β, and γ subunits in the ratio of 1:1:2, respectively (Goc *et al*., 2010). The α and β subunits are farnesylated and geranylated, respectively, suggesting that two PrBP/δ subunits are capable of binding to PDE6, resulting in a multi-subunit complex with the following stoichiometry, PDE6αβγγδδ. Purified, native bovine PDE6 (**Fig. 3.10A,B**) was isolated from ~800 bovine retinas and combined with a 3X molar excess of pure recombinant PrBP/δ and the complex was purified on a Superdex 200 column by gel filtration chromatography (**Fig. 3.11A,B**). Fractions were collected, pooled, and purified complex was used in crystallization trials, which proved to be unsuccessful.

Figure 3.9. SDS-PAGE gel following ROS isolation. Washes 1-6 in hypotonic buffer show the gradual elution of both PDE6 and Tαβγ. Lane 8 shows all pooled washes following ultra-centrifugation to remove excess ROS membranes and rhodopsin that can be seen in washes 1-6.

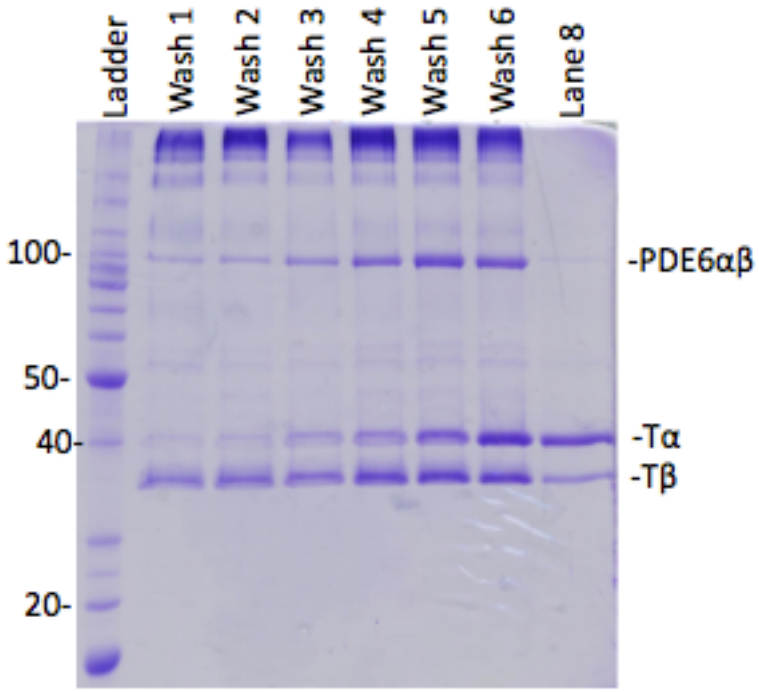
Ladder
Wash 1
Wash 2
Wash 3
Wash 4
Wash 5
Wash 6
Lane 8
100-
50-
40-
20-
-PDE6αβ
-Tα
-Tβ

Figure 3.10. Separation of PDE6 from Tα-GMP•PNP and Tβγ. **A**. Chromatogram showing the separation of PDE6, Tα-GMP•PNP and Tβγ. X_1 corresponds to the peak containing PDE6 and X_2 corresponds to the peak containing a mixture of Tα-GMP•PNP and Tβγ. **B**. SDS-PAGE gel showing the protein components of peaks X_1 and X_2 as seen in A. All subunits of PDE6 (PDE6αβγγ) and transducin (Tαβγ) are labeled and visible. M represents the molecular weight marker.

A.

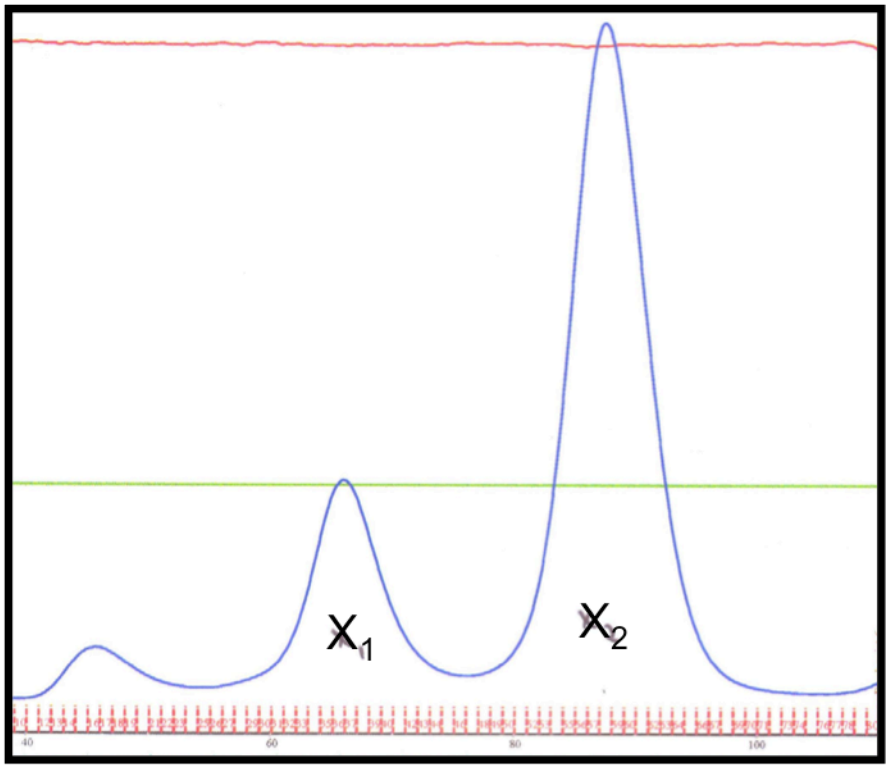

B.

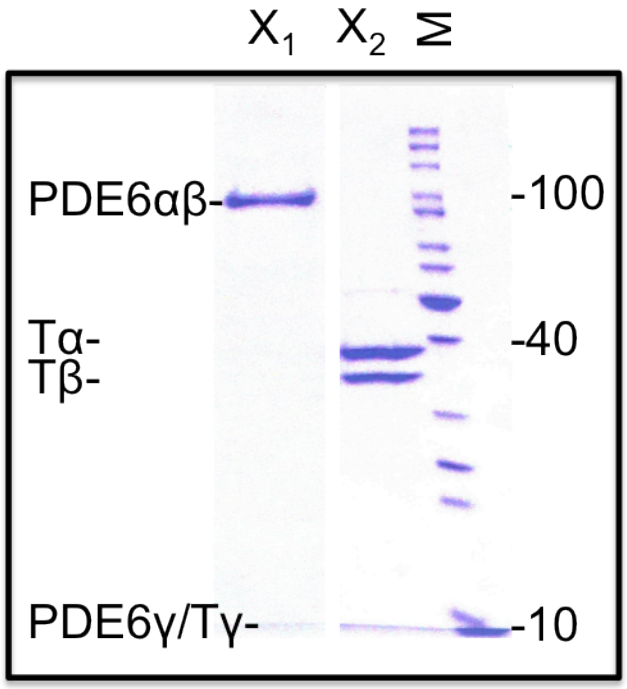

Figure 3.11. PDE6-PrBP/δ Complex formation. **A.** Chromatogram showing the separation of a peak containing PDE6-PrBP/δ complex (X_1) from excess PrBP/δ (X_2). **B**. SDS-PAGE gel showing the protein components of peaks X_1 and X_2 as seen in A. Fractions from X_1 are found in lanes 1-8, lane 9 is an example fraction from X_2, and M represents the molecular weight marker.

A.

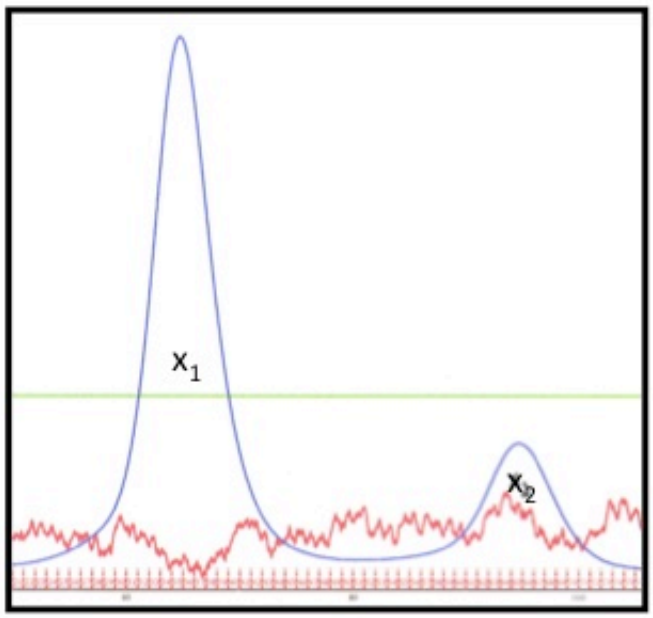

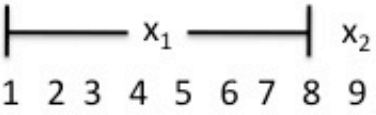

B.

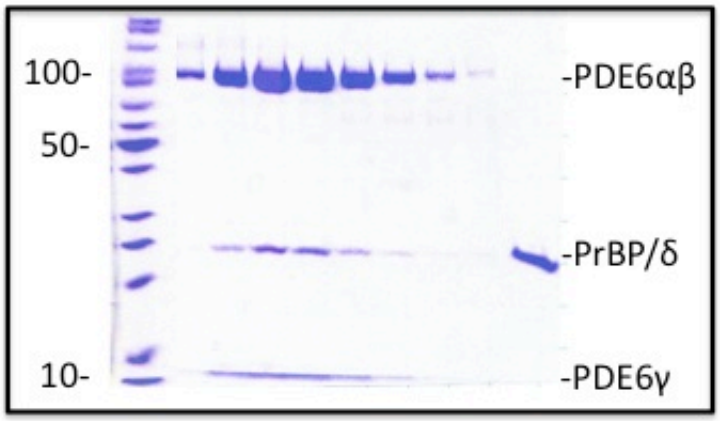

UNC119-Tα-GMP•PNP complex formation. Gaining a molecular understanding of the mechanism by which UNC119 inhibits Tα GTPase activity is a lingering question raised by the data presented in Chapter 2 of this dissertation (**Fig. 2.8C**). To address this question, we set out to generate a co-crystal complex of UNC119 and native full length Tα. Purified, recombinant UNC119 was combined with a solution of native Tα and Tβγ and Tβγ was separated from the UNC119-Tα-GMP•PNP complex by taking advantage of the 6X-His tag on the UNC119 construct. The solution was separated using a HisTrap FF column (GE Life Sciences) and fractions containing UNC119-Tα-GMP•PNP were collected and pooled (**Fig. 3.12A,B**). Pooled fractions of the UNC119-Tα-GMP•PNP complex were further purified to homogeneity by gel filtration chromatography using a Superdex 200 column (**Fig. 3.13A,B**). Fractions were collected, pooled, and purified complex was used in crystallization trials, which proved to be unsuccessful.

Cryo-EM images of the PDE6-PrBP/δ complex. Liquid nitrogen frozen PDE6-PrBP/δ images show particles that are ~190 Å wide and ~150 Å long, which appear to have a wide flat end that transitions to a narrow end with what appears to be two empty cavities connecting the two ends (**Fig. 3.14**). Close inspection of these particle images shows additional density located immediately adjacent to the wide, flat base that likely corresponds to the PrBP/δ subunits (**Fig. 3.14, yellow arrows**). Previous work has shown that the wide flat end is the catalytic base that houses the α and β subunits and their associated prenyl moieties (Goc *et al*., 2010), so it is logical that the density likely corresponding to PrBP/δ is adjacent to the catalytic base of PDE6 (**Fig. 3.14**). The

Figure 3.12. Separation of UNC119-Tα-GMP•PNP from Tβγ. **A.** Chromatogram showing the separation of a peak containing Tβγ (X_1) from an UNC119-Tα-GMP•PNP protein complex (X_2). **B**. SDS-PAGE gel showing the protein components of peaks X_1 and X_2 as seen in A. Fractions from X_1 are found in lanes 1-3, lanes 4-13 correspond to fractions collected from X_2, and M represents the molecular weight marker.

A.

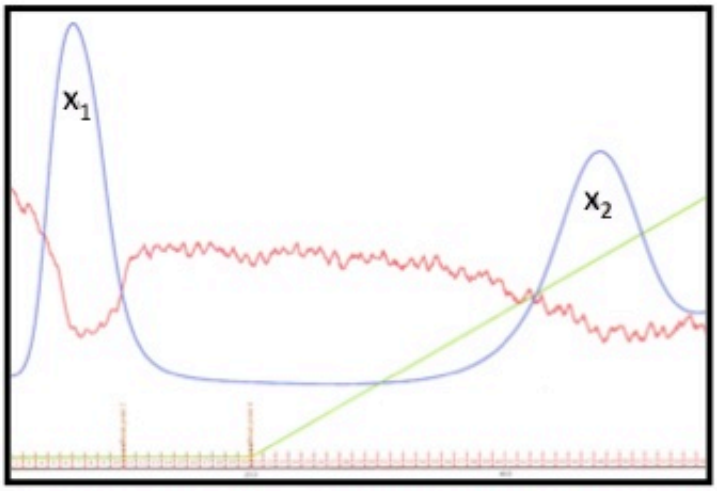

B.

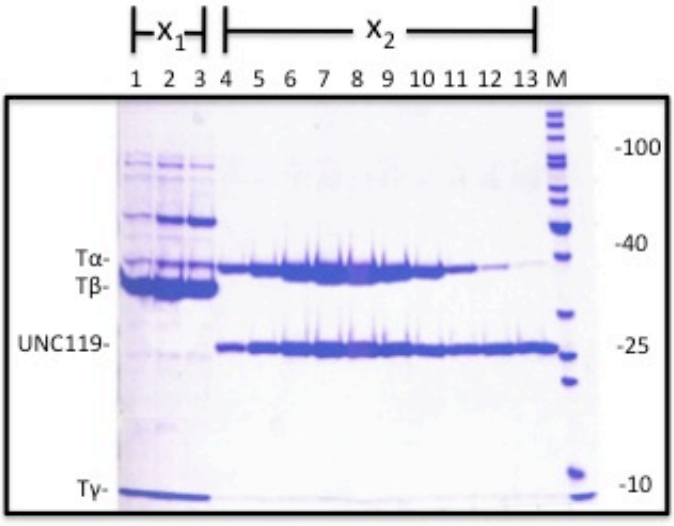

Figure 3.13. Isolation of an UNC119-Tα-GMP•PNP complex. **A**. Chromatogram showing the separation of a peak containing UNC119-Tα-GMP•PNP complex (X_1) from excess UNC119 (X_2). **B**. SDS-PAGE gel showing the protein components of peaks X_1 and X_2 as seen in A. Fractions from X_1 are found in lanes 1-11, lane 12 is an example fraction from X_2, and M represents the molecular weight marker.

A.

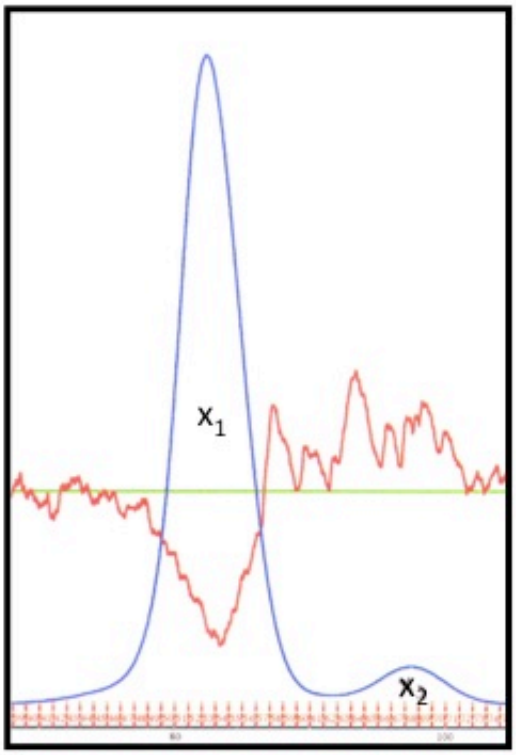

B.

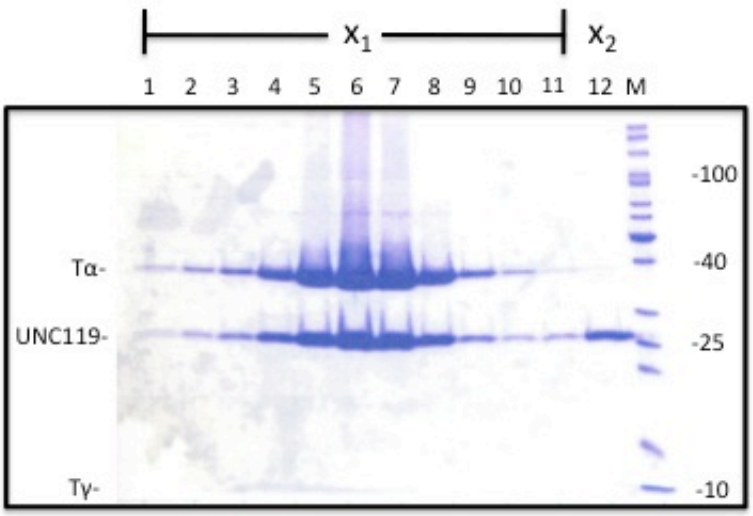

Figure 3.14. Cryo-EM images of a PDE6-PrBP/δ complex. EM images exhibit an elongated shape with a wide flat base and a narrow top end. The bottom panel displays individual protein complexes at higher magnification enabling visualization of the PrBP/δ subunits (yellow arrows) adjacent to the PDE6 base (Zhang, Z., He, F., Constantine, R. Baehr, W., Wensel, T., in preparation).

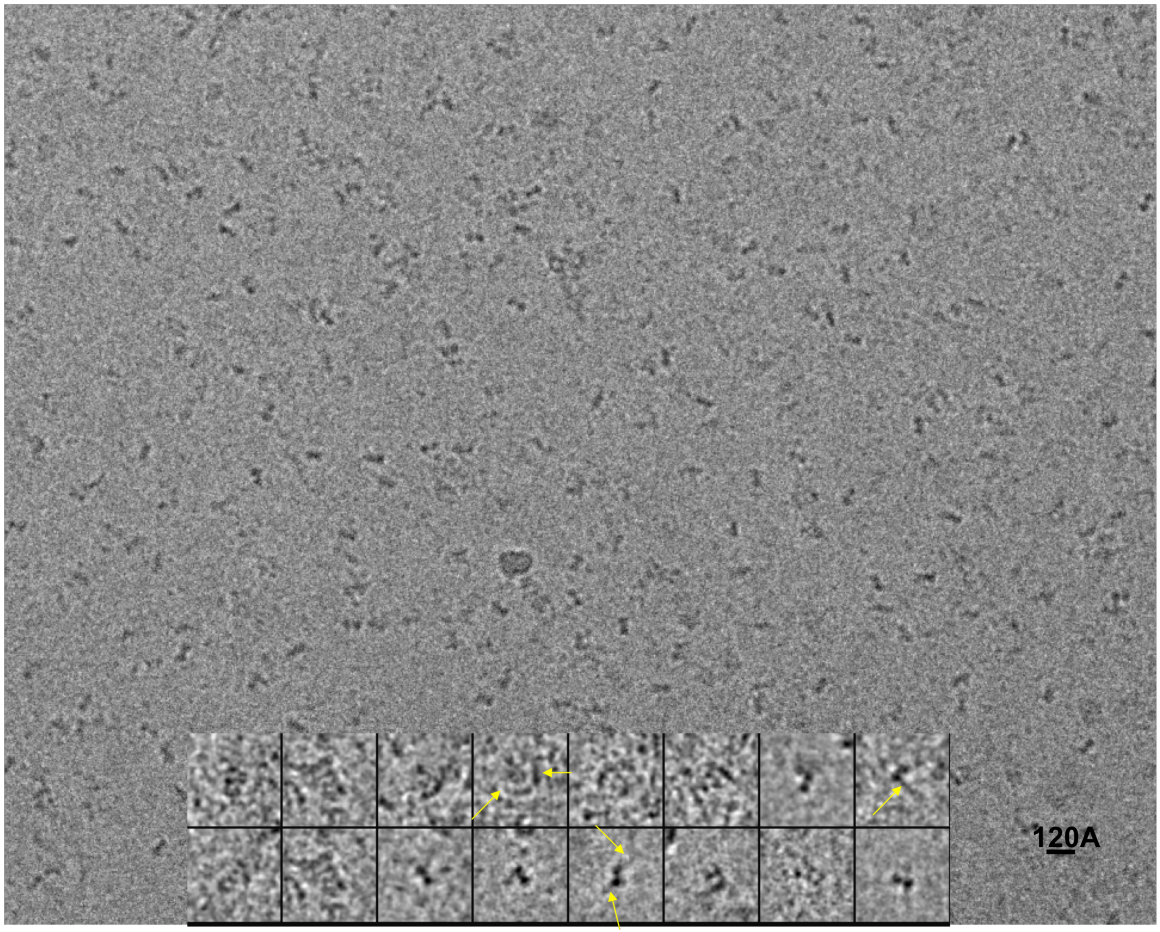
120A

resolution of these images make them challenging to interpret, but do provide evidence that Pr/BPδ interacts with the catalytic base of PDE6, which is where the prenyl moieties are located. The overall tube-like structure, which encloses two hollow cavities and narrows from one end towards the other, generally agrees with other higher resolution cryo-EM reconstructions of PDE6 (Goc *et al*., 2010).

Three-dimensional reconstruction of the PDE6-PrBP/δ complex. Despite the poor resolution and difficult interpretation of the projection maps, sufficient data was obtained to generate a 3D reconstruction of the PDE6-PrBP/δ complex. Visualizing the PrBP/δ density on the projection maps proved to be challenging due to the fact that a large percentage of the complex had dissociated. However, a sufficient number of images (3,000) were merged in order to generate a 3D structure of the PDE6-PBP/δ complex. Each of the images was subjected to low pass filtering while enforcing C2 symmetry with PDE6 being the only model used. The Fourier shell correlation (FSC) indicates the resolution of the structure to be 30 Å (**Fig. 3.15**). The overall structure looks like a like a diamond with rounded corners (face) that connects via two legs to a wide flat base (catalytic domain) with wings projecting from each side (**Fig. 3.16**). A central cavity is found interrupting the connection between the face and the catalytic domain. The wings attached to the catalytic domain appear to be tethered by thin stalks, which are likely the prenyl moieties found on the α and β subunits of PDE6. The mass adjacent to the catalytic base that appears as wings on the overall structure, is appropriately sized to accommodate the PrBP/δ-Arl2 co-crystal complex (Hanzal-Bayer *et al*., 2002), providing unambiguous localization and stoichiometric confirmation of

Figure 3.15. Fourier Shell Correlation (FSC) for a PDE6-PrBP/δ Complex. The FSC provides a measure of the normalised cross-correlation coefficient between two 3D volumes as a function of spatial frequency (van Heel and Schatz, 2005). A FSC cutoff of 0.5 is typically used to determine the resolution of a structure indicating that the resolution of the PDE6-PrBP/δ complex is 30 Å (Zhang, Z., He, F., Constantine, R. Baehr, W., Wensel, T., in preparation).

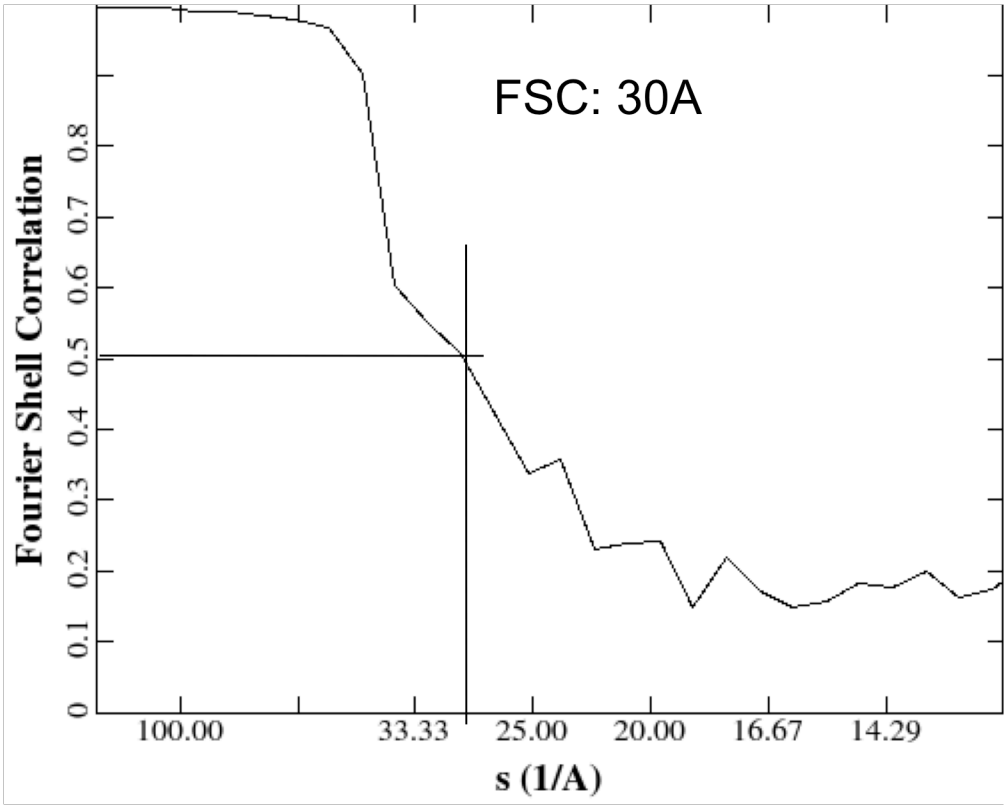
FSC: 30A
Fourier Shell Correlation
0
0.1
0.2
0.3
0.4
0.5
0.6
0.7
0.8
100.00
33.33
25.00
20.00
16.67
14.29
s (1/A)

Figure 3.16. Three-dimensional reconstruction of a PDE6-PrBP/δ complex at 30 Å resolution. The overall structure looks like a like a diamond with rounded corners (face) that connects via two legs to a wide flat base (catalytic domain) with wings projecting from each side (**Front View)**. A central cavity is found interrupting the connection between the face and the catalytic domain. The wings attached to the catalytic domain appear to be tethered by thin stalks, which are likely the prenyl moieties found on the α and β subunits of PDE6 (**Bottom View**). The mass adjacent to the catalytic base that appears as wings on the overall structure is appropriately sized and a PrBP/δ-Arl2 co-crystal complex (Hanzal-Bayer *et al*., 2002) has been modeled into this density, providing unambiguous localization and stoichiometric confirmation of PrBP/δ in the PDE6-PrBP/δ complex. When tipped on its side 90^{o} and viewed from the bottom the catalytic base appears to contain two cavities (Zhang, Z., He, F., Constantine, R. Baehr, W., Wensel, T., in preparation).

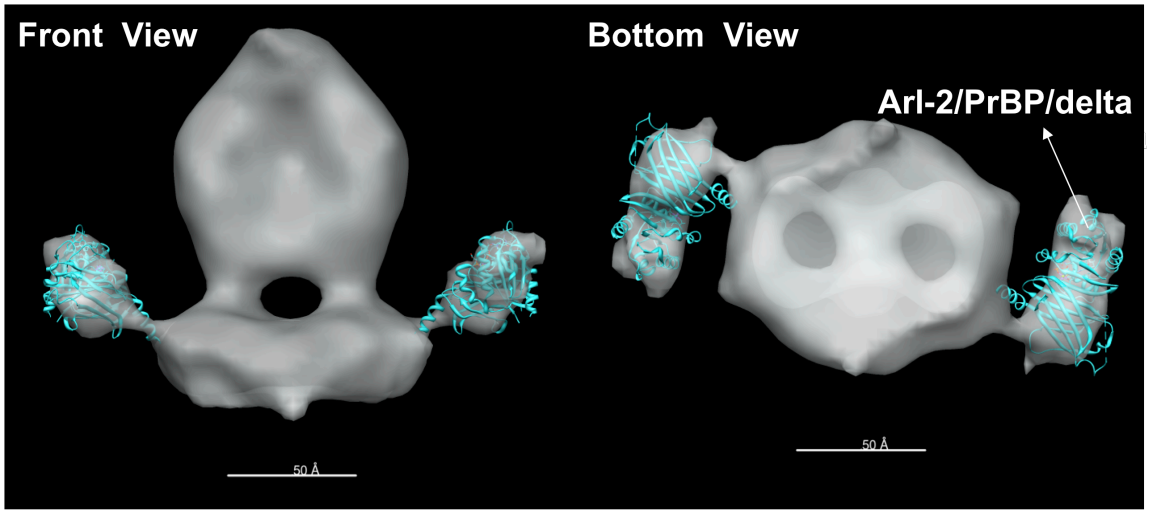
Front View
50 Å
Bottom View
Arl-2/PrBP/delta
50 Å

PrBP/δ in the PDE6-PrBP/δ complex (**Fig. 3.16, front view**). When tipped on its side 90^{o} and viewed from the bottom the catalytic base appears to contain two cavities (**Fig. 3.16, bottom view**).

Discussion

The purpose of these studies was to determine the molecular mechanism by which UNC119 inhibited Tα GTPase activity and to further clarify the role PrBP/δ plays in PDE6 trafficking and how the overall PDE6αβγγ-PrBP/δ complex assembles. This was done by isolating both native bovine Tα and PDE6 and generating protein complexes with recombinant UNC119 and PrBP/δ, respectively. These protein complexes were then used in an attempt to grow protein crystals for crystallographic elucidation. Unfortunately, we were unsuccessful in generating crystals and as an alternative, in collaboration with Ted Wensel's Lab at Baylor College of Medicine generated a preliminary cryo-EM reconstruction of the PDE6-PrBP/δ complex.

UNC119-Tα-GMP•PNP complex formation. None of the Tα crystal structures that have previously been solved include the N-terminal myristoyl group or five amino acids immediately C-terminal to this lipid modification (Noel, *et al*., 1993; Lambright *et al*., 1994). We have previously shown that the myristoyl group is necessary for UNC119 to bind Tα and that this interaction results in Tα GTPase inhibition (Zhang, *et al*., 2011). Therefore, we sought to isolate native bovine Tα in order to gain insight into how its interaction with UNC119 results in Tα GTPase inhibition at the molecular level. Tα was isolated from bovine retinas in bright light by sucrose gradient centrifugation followed by a series of isotonic washes and hypotonic washes in the presence of the nonhydrolyzable GTP analog, GMP•PNP (Baehr *et al*., 1982). Transducin exists in its heterotrimeric

form, Tαβγ, but in the presence of light and GTP the heterotrimer dissociates into Tα and Tβγ. We were able to adequately isolate Tα and generate an UNC119-Tα-GMP•PNP complex by adding recombinant UNC119 to native Tα (**Figs. 3.9, 3.13**). Gel filtration chromatograms exhibit a symmetric sharp peak and SDS-PAGE gels qualitatively show that the molar ratio of UNC119 to Tα is 1:1, indicating that the complex is free of unbound Tα or UNC119 (**Fig. 3.13**). Despite our ability to generate pure UNC119-Tα-GMP•PNP complex, continued efforts to fully understand how UNC119 inhibits Tα GTPase activity will be needed as we were unable to grow crystals of this protein complex and therefore, cannot offer an explanation of the underlying mechanism for this phenomenon.

PDE6-PrBP/δ complex formation. Previous isolation methods for PDE6-PrBP/δ protein complexes have generated complexes in which the stoichiometry between PDE6 and PrBP/δ has been either 1:1 or 1:2 (Gillespie *et al*., 1989; Goc *et al*., 2010). While it is assumed that the correct ratio of PrBP/δ to PDE6 is 2:1 due to the prenyl modifications on the α and β subunits, we modified previous experimental approaches in an attempt to quell this discrepancy and also take full advantage of the components in the bovine ROS for other experiments (see Tα isolation above). Following isolation from bovine retinas, a mixture of PDE6 and Tαβγ was easily separated by gel filtration chromatography (**Fig. 3.10A**). Excess addition of recombinant PrBP/δ generated a stable PDE6-PrBP/δ complex that could be separated from the excess PrBP/δ by gel filtration chromatography as can be seen by the symmetrical sharp peak in the chromatogram (**Fig. 3.11A**). Immediately following complex purification, the majority of the complex was used to setup crystallization trials, which proved to be unsuccessful. To maximize the quantity of

PDE6-PrBP/δ complex available for crystallization, we did not quantitatively analyze the stoichiometry of the PDE6-PrBP/δ complex. While challenging to discern, single particle projections show density corresponding to two PrBP/δ subunits adjacent to the catalytic base of PDE6 (**Fig. 3.14**). Excess complex that remained following crystallization trials was saved for cryo-EM experiments. The PDE6-PrBP/δ complex remained stable throughout purification, but it was noted that less than 50% of PDE6 molecules had PrBP/δ bound during cryo-EM experiments. As mentioned previously, the half-life of the complex is 3.5 hours and the low occupancy can possibly be attributed to shipping the PDE6-PrBP/δ complex to our collaborators for cryo-EM experiments.

Three-dimensional reconstruction of a PDE6-PrBP/δ complex. 3,000 single-particle images from liquid nitrogen frozen PDE6-PrBP/δ samples were used to generate a 3D reconstruction of the complex. Maps were calculated while enforcing C2 symmetry as the PDE6α and PDE6β subunits are ~91% homologous. A previously reported PDE6 EM model was used as the initial search model and we were able to obtain a data to 30Å after several rounds of refinement (**Fig. 3.16**). These data are preliminary as cryo-EM experiments are ongoing. Previous reports have generated reconstructions with data to 18Å (Goc *et al*., 2010), but our initial model is in agreement with their overall structure of the PDE6-PrBP/δ complex. Our reconstruction is made up of two major regions, one which looks like a diamond with rounded corners (face) that connects to a wide flat base (catalytic domain) via two short legs (**Fig. 3.16, front view**). A wing projects from each side of the catalytic base, both of which appear to be connected to the catalytic base via thin stalks (**Fig. 3.16**). The catalytic base of PDE6 houses the α and β subunits, which are farnesylated and geranylgeranylated, respectively. Therefore, it seems likely that these

thin stalks represent the prenyl moieties connecting PDE6α and PDE6β with two PrBP/δ subunits in the overall complex. We have modeled the PrBP/δ-Arl2 co-crystal structure (Hanzal-Bayer *et al*., 2002) into the mass corresponding to the wings adjacent to the catalytic base. The overall fit of the PrBP/δ-Arl2 structure into the two wing masses coupled with their locations provides strong evidence for the localization and stoichiometry of PrBP/δ in the overall PDE6-PrBP/δ complex. Our reconstruction also shows a cavity that lies between the face and the catalytic base (**Fig. 3.16, front view**) as well as what appear to be two cavities found within the catalytic base (**Fig. 3.16, bottom view**). Previous analysis of the cavity found in the catalytic base indicates that it may be secluded from bulk solvent as a means of regulating activity by limiting its availability to substrate (Goc *et al*., 2010).

Our PDE6-PrBP/δ reconstruction at 30 Å is in overall agreement with a previously published reconstruction of the same complex at 18 Å (Goc *et al*., 2010). With our present data and resolution, further analysis is purely speculation and is not readily supported by our model and certainly not in greater depth than has already been published. We hope that continued efforts on this project will yield better resolution and therefore an increased understanding of the assembly and function of the PDE6-PrBP/δ complex.

References

Acton, T. B., Gunsalus, K. C., Xiao, R., Ma, L. C., Aramini, J., Baran, M. C., Chiang, Y. W., Climent, T., Cooper, B., Denissova, N. G., Douglas, S. M., Everett, J. K., Ho, C. K., Macapagal, D., Rajan, P. K., Shastry, R., Shih, L. Y., Swapna, G. V., Wilson, M., Wu, M., Gerstein, M., Inouye, M., Hunt, J. F., Montelione, G. T. (2005). Robotic cloning and Protein Production Platform of the Northeast Structural Genomics Consortium. *Methods Enzymol.* 394:210-243.

Anant, J. S., Ong, O. C., Xie, H., Clarke, S., O'Brien, P. J., Fung, B. K. K. (1992) In vivo differential prenylation of retinal cyclic GMP phosphodiesterase catalytic subunits. *J Biol Chem* 267:687-690.

Aspuria, P. J., Tamanoi, F. (2004). The Rheb family of GTP-binding proteins. *Cell Signal* 16:1105-1112.

Avruch, J., Hara, K., Lin, Y., Liu, M., Long, X., Ortiz-Vega, S., Yonezawa, K. (2006). Insulin and amino-acid regulation of mTOR signaling and kinase activity through the Rheb GTPase. *Oncogene* 25:6361-6372.

Baehr, W., Devlin, M. J., Applebury, M. L. (1979). Isolation and characterization of cGMP phosphodiesterase from bovine rod outer segments. *J Biol Chem* 254:11669-11677.

Baehr, W., Morita, E., Swanson, R., Applebury, M. L. (1982) Characterization of bovine rod outer segment G protein. *J. Biol. Chem.* 257:6452-6460.

Becker, J., Linari, M., Manson, F., Wright, A., Meindl, A., Meitinger, T. (1998). The delta subunit of rod phosphodiesterase interacts with the RCC1 homologpus domain of RPGR. *Invest Ophthalmol & Vis Sci* 39:S953.

Chandra, A., Grecco, H. E., Pisupati, V., Perera, D., Cassidy, L., Skoulidis, F., Ismail, S. A., Hedberg, C., Hanzal-Bayer, M., Venkitaraman, A. R., Wittinghofer, A., Bastiaens, P. I. (2012). The GDI-like solubilizing factor PDEdelta sustains the spatial organization and signalling of Ras family proteins. *Nat Cell Biol* 14:148-158.

Clarke, P. R., Zhang, C. (2008). Spatial and temporal coordination of mitosis by Ran GTPase. *Nat Rev Mol Cell Biol* 9:464-477.

Conti, M., Beavo, J. (2007). Biochemistry and physiology of cyclic nucleotide phosphodiesterases: essential components in cyclic nucleotide signaling. *Annu Rev Biochem* 76:481-511.

Cook, T. A., Ghomashchi, F., Gelb, M. H., Florio, S. K., Beavo, J. A. (2000a). Binding of the delta subunit to rod phosphodiesterase catalytic subunits requires methylated, prenylated C-termini of the catalytic subunits. *Biochemistry* 39:13516-13523.

Cook, T. A., Ghomashchi, F., Gelb, M. H., Florio, S. K., Beavo, J. A. (2000b). Binding of the delta subunit to rod phosphodiesterase catalytic subunits requires methylated, prenylated C-termini of the catalytic subunits. *Biochemistry* 39:13516-13523.

Cook, T. A., Ghomashchi, F., Gelb, M. H., Florio, S. K., Beavo, J. A. (2001). The delta subunit of type 6 phosphodiesterase reduces light-induced cGMP hydrolysis in rod outer segments. *J Biol Chem* 276:5248-5255.

Day, J. P., Cleghon, V., Houslay, M. D., Davies, S. A. (2008). Regulation of a Drosophila melanogaster cGMP-specific phosphodiesterase by prenylation and interaction with a prenyl-binding protein. *Biochem J* 414:363-374.

Etienne-Manneville, S., Hall, A. (2002). Rho GTPases in cell biology. *Nature* 420:629-635.

Florio, S. K., Prusti, R. K., Beavo, J. A. (1996). Solubilization of membrane-bound rod phosphodiesterase by the rod phosphodiesterase delta subunit. *J Biol Chem* 271:24036-24047.

Fung, B. K. K., Young, J. H., Yamane, H. K., Griswold-Prenner, I. (1990). Subunit stoichiometry of retinal rod cGMP phosphodiesterase. *Biochemistry* 29:2657-2664.

Gelb, M. H., Brunsveld, L., Hrycyna, C. A., Michaelis, S., Tamanoi, F., Van Voorhis, W. C., Waldmann, H. (2006). Therapeutic intervention based on protein prenylation and associated modifications. *Nat Chem Biol* 2:518-528.

Gillespie, P. G., Prusti, R. K., Apel, E. D., Beavo, J. A. (1989). A soluble form of bovine rod photoreceptor phosphodiesterase has a novel 15-kDa subunit. *J Biol Chem* 264:12187-12193.

Goc, A., Chami, M., Lodowski, D. T., Bosshart, P., Moiseenkova-Bell, V., Baehr, W., Engel, A., Palczewski, K. (2010). Structural characterization of the rod cGMP phosphodiesterase 6. *J Mol Biol* 401:363-373.

Hanzal-Bayer, M., Renault, L., Roversi, P., Wittinghofer, A., Hillig, R. C. (2002). The complex of Arl2-GTP and PDE delta: from structure to function. *EMBO J* 21:2095-2106.

Hanzal-Bayer, M., Linari, M., Wittinghofer, A. (2005). Properties of the interaction of Arf-like protein 2 with PDEdelta. *J Mol Biol* 350:1074-1082.

Ho, Y. S., Burden, L. M., Hurley, J. H. (2000). Structure of the GAF domain, a ubiquitous signaling motif and a new class of cyclic GMP receptor. *EMBO J* 19:5288-5299.

Hoffman, G. R., Nassar, N., Cerione, R. A. (2000). Structure of the Rho family GTP-binding protein Cdc42 in complex with the multifunctional regulator RhoGDI. *Cell* 100:345-356.

Ismail, S. A., Chen, Y. X., Rusinova, A., Chandra, A., Bierbaum, M., Gremer, L., Triola, G., Waldmann, H., Bastiaens, P. I., Wittinghofer, A. (2011). Arl2-GTP and Arl3-GTP regulate a GDI-like transport system for farnesylated cargo. *Nat Chem Biol* 7:942-949.

Karan, S., Zhang, H., Li, S., Frederick, J. M., Baehr, W. (2008). A model for transport of membrane-associated phototransduction polypeptides in rod and cone photoreceptor inner segments. *Vision Res* 48:442-452.

Lambright, D. G., Noel, J. P., Hamm, H. E., Sigler, P. B. (1994). Structural determinants for activation of the alpha-subunit of a heterotrimeric G protein. *Nature* 369:621-8.

Li, N., Baehr, W. (1998). Expression and characterization of human PDEd and its Caenorhabditis elegans ortholog CEd. *FEBS Lett* 440:454-457.

Linari, M., Hanzal-Bayer, M., Becker, J. (1999a). The delta subunit of rod specific cyclic GMP phosphodiesterase, PDE delta, interacts with the Arf-like protein Arl3 in a GTP specific manner. *FEBS Lett* 458:55-59.

Linari, M., Ueffing, M., Manson, F., Wright, A., Meitinger, T., Becker, J. (1999b). The retinitis pigmentosa GTPase regulator, RPGR, interacts with the delta subunit of rod cyclic GMP phosphodiesterase. *Proc Natl Acad Sci USA* 96:1315-1320.

Martinez, S. E., Heikaus, C. C., Klevit, R. E., Beavo, J. A. (2008). The structure of the GAF A domain from phosphodiesterase 6C reveals determinants of cGMP binding, a conserved binding surface, and a large cGMP-dependent conformational change. *J Biol Chem* 283:25913-25919.

Marzesco, A. M., Galli, T., Louvard, D., Zahraoui, A. (1998). The rod cGMP phosphodiesterase delta subunit dissociates the small GTPase Rab13 from membranes. *J Biol Chem* 273:22340-22345.

Miki, N., Baraban, J. M., Keirns, J. J., Boyce, J. J., Bitensky, M. W. (1975). Purification and Properties of the Light-activated Cyclic Nucleotide Phosphodiesterase of Rod Outer Segments. *J Biol Chem* 250:6320-6327.

Nancy, V., Callebaut, I., El Marjou, A., de Gunzburg, J. (2002). The delta subunit of retinal rod cGMP phosphodiesterase regulates the membrane association of Ras and Rap GTPases. *J Biol Chem* 277:15076-15084.

Noel, J. P., Hamm, H. E., Sigler, P. B. (1993). The 2.2 Å crystal structure of transducin-alpha complexed with GTP gamma S. *Nature* 366:654-63.

Norton, A. W., Hosier, S., Terew, J. M., Li, N., Dhingra, A., Vardi, N., Baehr, W., Cote, R. H. (2004). Evaluation of the 17 kDa prenyl binding protein as a regulatory protein for phototransduction in retinal photoreceptors. *J Biol Chem* 2:1248-56.

Renault, L., Hanzal-Bayer, M., Hillig, R. C. (2001). Coexpression, copurification, crystallization and preliminary X-ray analysis of a complex of ARL2-GTP and PDE delta. *Acta Crystallogr D Biol Crystallogr* 57:1167-1170.

Stamm, M., Zhang, H., Irwin, M., Ying, G., Lucero, M., Baehr, W. (2011). The Prenyl Binding Protein PrBP/ä Enables Trafficking of G_{olf} to Olfactory Cilia. *Proc Natl Acad Sci USA*, under review.

van Heel, M., Schatz, M. (2005). Fourier shell correlation threshold criteria. *J Struct Biol* 151:250-262.

Wilson, S. J., Smyth, E. M. (2006). Internalization and Recycling of the Human Prostacyclin Receptor Is Modulated through Its Isoprenylation-dependent Interaction with the δ Subunit of cGMP Phosphodiesterase 6. *J Biol Chem* 281:11780-11786.

Zhang, H., Hosier, S., Terew, J. M., Zhang, K., Cote, R. H., Baehr, W. (2005). Assay and functional properties of PrBP (PDEdelta), a prenyl-binding protein interacting with multiple partners. *Methods Enzymol* 403:42-56.

Zhang, H., Li, S., Doan, T., Rieke, F., Detwiler, P. B., Frederick, J. M., Baehr, W. (2007). Deletion of PrBP/δ impedes transport of GRK1 and PDE6 catalytic subunits to photoreceptor outer segments. *Proc Natl Acad Sci USA* 104:8857-8862.

Zhang, H., Liu, X. H., Zhang, K., Chen, C. K., Frederick, J. M., Prestwich, G. D., Baehr, W. (2004). Photoreceptor cGMP phosphodiesterase delta subunit (PDEdelta) functions as a prenyl-binding protein. *J Biol Chem* 279:407-413.

Zhang, H., Constantine, R., Vorobiev, S., Chen, Y., Seetharaman, J., Huang, Y. J., Xie, G., Montelione, G. T., Gerstner, C. D., Davis, M. W., Inana, G., Whitby, F. G., Jorgensen, E. M., Hill, C. P., Tong, L., Baehr, W. (2011) UNC119 regulates G protein trafficking in sensory neurons. *Nature Neuroscience* 14:874-880.

CHAPTER 4

CONCLUSIONS AND FUTURE DIRECTIONS

Photoreceptor cells are an ideal model system for studying membrane-associated protein transport for multiple reasons. These cells are polarized, consisting of an inner segment in which protein biosynthesis takes place and an outer segment to which, protein components of the phototransduction cascade must be accurately and efficiently delivered. Outer segments, which are renewed every 10 days, consist of numerous membranous discs that house the phototransduction components (Young, 1967). As a result of the continuous turnover of outer segment discs, protein biosynthesis and transport takes place at an exceedingly high rate in order to maintain and deliver the phototransduction machinery to these discs. The membranous nature of the outer segment discs necessitates protein-membrane interactions that are mediated by lipid modifications found on many of the proteins involved in phototransduction. In addition to postbiosynthesis protein transport, massive quantities of transducin molecules are translocated from the outer segment to the inner segment in response to light, a process that reverses itself upon returning to the dark, enabling transducin to continually function in the phototransduction cascade (Calvert *et al*., 2006).

The majority of the work in this dissertation focuses on elucidating the function of the protein UNC119. Previous work in our laboratory generated data showing that the prenyl binding protein, PrBP/δ was in part responsible for the postbiosynthesis transport of prenylated proteins GRK1, PDE6α', and Tγ (Zhang *et al*., 2007). However, other prenylated phototransduction components were delivered to the outer segments as expected, leading us to search for another prenyl binding protein. UNC119 was an obvious candidate as it is biologically related to PrBP/δ, conserved in both vertebrates and invertebrates throughout evolution, and its C-terminal region is 40% similar to

PrBP/δ. By using a number of biochemical approaches, solving the co-crystal structure of UNC119 in complex with a synthetic peptide mimicking the N-terminus of Tα, and using both *C. elegans* and mouse models, we were able to identify UNC119 as an acyl-binding protein that specifically interacts with G protein α-subunits. Pulldown experiments identified Tα as an interacting partner with UNC119 and demonstrated that UNC119 is capable of extracting $T\alpha^{GTP}$ from ROS membranes. Isothermal titration calorimetry provided quantitative binding data between UNC119 and peptide mimics of both Tα and ODR-3, GTPase assays showed that UNC119 inhibits the intrinsic GTPase activity of Tα, and the co-crystal structure of UNC119 and a lauroylated Tα peptide provided details at the molecular level of a predominantly Van der Waals mediated interaction. UNC119 deletion in *C. elegans* resulted in ODR-3 and GPA-13 mislocalization and in an *UNC119*$^{-/-}$ mouse model Tα was partially retained in the inner segments. These data provide direct evidence that extends beyond photoreceptors, showing that that UNC119 functions as an acyl-binding protein that interacts with G protein α-subunits and affects their trafficking. Furthermore, we show that the UNC119-Tα interaction is responsible for the slow return of transducin to the outer segments following light-induced translocation and provide a mechanism explaining why complete dark adaptation is a long process. Until now, this has been a long-standing question in photoreceptor biology.

The molecular details of how UNC119 inhibits the intrinsic GTPase activity of Tα have eluded us. Our efforts at generating an UNC119-Tα-GMP•PNP complex have been fruitful, but growing protein crystals has proven challenging. Future efforts at elucidating the mechanism by which UNC119 inhibits Tα GTPase activity would seemingly reach

farther than the retina, as previous work has shown that UNC119 is able to inhibit the GTPase activity of dynamin, resulting in the regulation of various endocytic pathways (Karim *et al*., 2010).

We also spent time looking into the assembly of a PDE6-PrPB/δ complex. Much like the UNC119-Tα-GMP•PNP complex, we were able to purify pure PDE6-PrBP/δ complex, but struggled to generate protein crystals. However, we obtained a sufficient amount of data using soluble PDE6-PrBP/δ complex to produce a low-resolution cryo-EM reconstruction. Based on our data, we are presently unable to provide new and improved information about the overall assembly of the complex. However, our model accurately supports previous work as we have shown that the stoichiometry of PrBP/δ subunits relative to the PDE6αβγγ complex is 2:1 (Goc *et al*., 2010). Gaining a complete molecular understanding of this complex warrants continued effort as a multitude of mutations in PDE6α and PDE6β subunits have been found in patients with retinal degeneration and retinitis pigmentosa (for review see Conti and Beavo, 2007).

PDEs are well known and already highly targeted therapeutically in the clinical setting. Animal models in which UNC119 or PrBP/δ have been knocked out exhibit visual defects and in the case of UNC119; a human patient with late onset cone dystrophy has been identified (Kobayashi *et al*., 2000). As the function of both UNC119 and PrBP/δ become better understood, the likelihood of deciphering their clinical relevance increases, which in time we hope will have a positive impact on improving vision.

References

Calvert P. D., Strissel K. J., Schiesser W. E., Pugh E. N., Jr., Arshavsky V. Y. (2006). Light-driven translocation of signaling proteins in vertebrate photoreceptors. *Trends Cell Biol* 16:560-568.

Conti, M., Beavo, J. (2007). Biochemistry and Physiology of Cyclic Nucleotide Phosphodiesterases: Essential Components of Cyclic Nucleotide Signaling. *Annu. Rev. Biochem.* 76:481-511.

Goc, A., Chami, M., Lodowski, D. T., Bosshart, P., Moiseenkova-Bell, V., Baehr, W., Engel, A., and Palczewski, K. (2010). Structural characterization of the rod cGMP phosphodiesterase 6. *J. Mol. Biol.* 401**,** 363-373

Karim Z, Vepachedu R, Gorska M, Alam R. (2010). UNC119 inhibits dynamin and dynamin-dependent endocytic processes. *Cell Signal* 22:128-137.

Young R. W. (1967). The renewal of photoreceptor cell outer segments. *J Cell Biol* 33:61-72.

Zhang H, Li S, Doan T, Rieke F, Detwiler P. B., Frederick J. M., Baehr W (2007). Deletion of PrBP/{delta} impedes transport of GRK1 and PDE6 catalytic subunits to photoreceptor outer segments. *Proc Natl Acad Sci USA* 104:8857-8862.